NASA SP-8091

SPACE VEHICLE DESIGN CRITERIA (ENVIRONMENT)

THE PLANET SATURN (1970)

JUNE 1972

NATIONAL AERONAUTICS AND SPACE ADMINISTRATION

FOREWORD

NASA experience has indicated a need for uniform criteria for the design of space vehicles. Accordingly, criteria are being developed in the following areas of technology:

Environment
Structures
Guidance and Control
Chemical Propulsion

Individual components of this work are issued as separate monographs as soon as they are completed. A list of all previously issued monographs in this series can be found on the last page of this monograph.

These monographs are to be regarded as guides to design and not as NASA requirements except as may be specified in formal project specifications. It is expected, however, that the monographs will be used to develop requirements for specific projects and be cited as the applicable documents in mission studies or in contracts for the design and development of space vehicle systems.

This monograph was prepared under the cognizance of the Goddard Space Flight Center with Scott A. Mills and Mason T. Charak as program coordinators. The principal author was Frank Don Palluconi of the Jet Propulsion Laboratory. Valuable contributions were made by A. J. Beck, T. N. Divine, and C. A. Haudenschild of the Jet Propulsion Laboratory. A. F. Cook and F. A. Franklin of the Smithsonian Astrophysical Observatory and Harvard College Observatory served as consultants in the preparation of the Saturn Ring sections.

Comments concerning the technical content of these monographs will be welcomed by the National Aeronautics and Space Administration, Goddard Space Flight Center, Systems Reliability Directorate, Greenbelt, Maryland 20771.

June 1972

CONTENTS

Page

1. INTRODUCTION 1

2. STATE OF THE ART 3

2.1 General Physical Properties 3
2.1.1 Mass 3
2.1.2 Dimensions and Mean Density 4
2.1.3 Rotation Period, Pole Location and Orbital Quantities 5

2.2 Gravitational Field 6

2.3 Magnetic and Electric Fields 7

2.3.1 Magnetic Field 7
2.3.1.1 Radio Frequency Observations 8
2.3.1.2 Jupiter Analogy 8
2.3.2 Electric Fields 9

2.4 Electromagnetic Radiation 10

2.4.1 Direct and Reflected Solar Radiation 10
2.4.2 Reflected Solar Radiation from Saturn's Rings 13
2.4.3 Visual Magnitude of Saturn and Rings 15
2.4.4 Reflected Radiation from Saturn's Satellites 15
2.4.5 Thermal and Nonthermal Radiation from Saturn 15
2.4.6 Thermal Radiation from Saturn's Rings and Satellites 19

2.5 Satellites and Meteoroids 21

2.5.1 Satellites 22
2.5.2 Meteoroids 24

2.6 Saturn's Ring System 25

2.6.1 Dimensions of the Ring System 25
2.6.1.1 Radial Extent 25
2.6.1.2 Ring Thickness 27
2.6.2 The Ring Particles 27
2.6.3 An Upper Limit Saturn Ring Model 29

2.7 Charged Particles 33

2.7.1 Galactic Cosmic Rays 33
2.7.2 Solar Protons 33
2.7.3 Solar Wind 33

2.7.4 Trapped Radiation Belts 34
2.7.4.1 Background 34
2.7.4.2 Radiation Belt Characteristics 37
2.7.5 Magnetospheric Plasma 38
2.7.6 Ionosphere 38

2.8 Atmospheric Composition and Structure 39

2.8.1 Composition 39
2.8.2 Structure 40
2.8.3 Atmosphere Models 41
2.8.3.1 Existing Models 41
2.8.3.2 Basis for Design Models 42
2.8.3.3 Presentation of Design Models 42

2.9 Clouds and Atmospheric Motions 47

2.9.1 Clouds 47
2.9.2 Atmospheric Motions 48
2.9.2.1 Rotation 48
2.9.2.2 Winds 49

3. CRITERIA 49

3.1 General Physical Properties 49
3.2 Gravitational Field 49
3.3 Magnetic and Electric Fields 51
3.4 Electromagnetic Radiation 52
3.5 Satellites and Meteoroids 58
3.6 Saturn's Ring System 61
3.6.1 Dimensions 61
3.6.2 Composition 64
3.6.3 Thickness and Particle Orbits 64
3.6.4 Particles 66
3.6.4.1 Size and Density 66
3.6.4.2 Computation of Impacts 66
3.7 Charged Particles 68
3.8 Atmospheric Composition and Structure 68
3.9 Clouds and Atmospheric Motions 68

REFERENCES 77

APPENDIX A. Definition of Symbols 87

APPENDIX B. Atmosphere and Clouds (Mathematical Basis) 91

APPENDIX C. Glossary 93

NASA SPACE VEHICLE DESIGN CRITERIA MONOGRAPHS 97

THE PLANET SATURN (1970)

1. INTRODUCTION

The design of space vehicles which are to encounter and investigate the planet Saturn requires both qualitative and quantitative descriptions of the expected environment. Although somewhat different data sets are required for the design of fly-by, orbiter, and atmospheric entry spacecraft, present understanding of the Saturn system (planet and surrounding fields and particles) warrants the inclusion of summaries of almost all pertinent system properties in one document. The information presented here reflects published information available in mid-1970. Some information being prepared for publication and available for evaluation in the latter half of 1970, also has been used.

Observations of Saturn have been made by instruments based on the Earth or carried on aircraft, rockets, and balloons. For topics for which no such data is available, analogy with Jupiter conditions has been made if appropriate. A separate design criteria monograph on Jupiter is available in this series.

In the process of evaluating Saturn information, assessments were made of the potential effects of environmental properties on vehicle performance so that appropriate descriptions for vehicle and subsystem design could be formulated. Several of the environments presented, i.e., the gravity field, charged particles, ring particles, and atmospheric structure and composition, will have important implications for mission planning as well as for spacecraft design.

For fly-by and orbiter spacecraft, the electric and magnetic fields, electromagnetic radiation, ring particles and charged particles will be of primary importance in the design of electronic components and subsystems and exposed working surfaces. The cumulative effects of prolonged or repeated exposure to these environments have a direct effect on the useful lifetime of an orbiting spacecraft. The potential hazards of passage through Saturn's rings are sufficient to require a close connection between spacecraft design and mission planning.

For atmosphere entry spacecraft knowledge of the structure, composition, and motion of Saturn's atmosphere are of primary importance. Table I provides a qualitative indication of the relative importance of environments of the Saturn system to the design of various spacecraft subsystems for an atmospheric entry spacecraft. In this table the interaction with Saturn's rings is shown as possible under the assumption direct ring crossing is not attempted. For a ring crossing, the importance of ring particles would increase for all subsystems.

TABLE I

ENVIRONMENT-DESIGN INTERACTION FOR A SATURN ATMOSPHERIC ENTRY SPACECRAFT*

ENVIRONMENT**	SUBSYSTEMS									
	Structure	Propulsion (Acceleration and Deceleration)	Guidance	Attitude Control	Power Supply	Aero Shell	Thermal Control	Radio Frequency	Data Handling and Command	Scientific Instruments
Gravity Field	W	S	W	W	W	S	S	O	O	S
Magnetic Field and Magnetosphere	O	W	W	S	O	O	O	S	W	W
Electric Fields	O	W	W	W	W	O	O	W	W	S
Electromagnetic Radiation	O	W	W	S	W	O	S	S	O	S
Satellites	O	O	S	W	O	O	W	W	O	W
Ring Particles	W	W	W	W	W	W	W	W	W	W
Charged Particles	O	W	W	W	S	O	S	S	S	S
Atmospheric Composition and Structure	S	S	S	S	W	S	S	S	W	S
Atmospheric Motions and Clouds	S	S	S	S	W	S	S	S	W	S

*Introduction discusses impact of environments on design of fly-by and orbiting spacecraft.
**S means strong, probable, or direct design impact.
W means weak, possible, or indirect design impact.
O means no design impact.

2. STATE OF THE ART

The discussion of observation and theory presented in the following state-of-the-art description of Saturn's environment uses the notation, symbols, mathematical formulations, and definitions given in appendices A, B and C.

2.1 General Physical Properties

The physical properties considered in this section are the mass of Saturn, its dimensions, mean density, rotation rate, rotational pole location, and mean orbital elements.

The orbit of Saturn is perturbed by the other planets in the solar system so it is not strictly elliptical. The position of Saturn can be determined from tabulations given in the appropriate year of the *American Ephemeris and Nautical Almanac* or by reference to the mean orbital elements provided by Melbourne et al. (ref. 1) and Sturms (ref. 2).

The reflected and intrinsic energy from the planet and satellites are presented in section 2.4, the physical properties of the satellites in section 2.5, and rings in section 2.6.

2.1.1 Mass

A number of methods have been used to determine the mass of the Saturn system, M_{ss}, i.e., the mass of the planet, atmosphere, satellites and rings. The results are expressed as a mass ratio, the mass of the Sun $M_{\odot}$ divided by the mass of the system. Mass ratios obtained from four recent studies and two summaries are presented in table II.

The mean, $M_{\odot}/M_{ss} = 3498.5 \pm 1.5$, given by Kovalevsky (ref. 7), is in reasonable accord with the average of the first four values of table II, and the associated uncertainty is realistic on the basis of current knowledge. Therefore, both values are adopted here.

To convert the mass ratio $M_{\odot}/M_{ss}$ to the mass of Saturn M_s, it is necessary to know the mass of Saturn's satellites and rings and the mass of the Sun. Titan, the major satellite in the system, is an order of magnitude more massive than the other satellites (section 2.5). The mass of the rings is not well known (section 2.6) and no attempt will be made here to remove their effect. The mass ratio given by Jeffreys (ref. 8) for the mass of Titan M_T to the mass of Saturn is $M_T/M_s = (2.411 \pm 0.013) \times 10^{-4}$. This value coupled with the foregoing mass ratio adopted for the Saturn system gives $M_{\odot}/M_s = 3499.3 \pm 1.5$.

For some purposes such as trajectory analysis, it is appropriate to use the chronocentric gravitational constant GM_s, which can be found from the foregoing mass ratio $M_{\odot}/M_s$ and the heliocentric gravitational constant, $GM_{\odot} = (132712499 \pm 15) \times 10^{18}$ cm^3 sec^{-2}, given by Melbourne et al. (ref. 1). Then, $GM_s = (3.7925 \pm 0.0016) \times 10^{22}$ cm^3 sec^{-2} and $GM_{ss} = (3.7934 \pm 0.0016) \times 10^{22}$ cm^3 sec^{-2}. The gravitational constant, $G = (6.6732 \pm 0.0031) \times 10^{-8}$ dyn cm^2 g^{-2} given by Mechtly (ref. 9), can be used to

TABLE II

RECENT ESTIMATES OF THE SATURN SYSTEM MASS RATIO, $M_{\odot}/M_{ss}$

Author	Mass Ratio $M_{\odot}/M_{ss}$	Object/Method Used
Klepczynski et al. (ref. 3)	3498.7 ± 0.2	Jupiter (1913-1968)
Marsden (ref. 4)	3498.5 ± 0.3	Minor Planet Hildago (1920-1964)
Herget (1970), from Klepczynski et al. (ref. 5)	3497.6 ± 0.2	Comet P/Schwassman-Wachmann 1 (1927-1966)
Lieske et al. (ref. 6)	3499.7 ± 0.2	Preliminary analysis of optical, photographic, radar, and spacecraft (Mariner V) data from the nine planets (1910-1969)
Klepczynski et al. (ref. 5)	3498.1 ± 0.3	Weighted Mean
Kovalevsky (ref. 7)	3498.5 ± 1.5	Rounded Mean

convert these values to the mass in grams as follows, $M_s = (5.683 \pm 0.004) \times 10^{29}$ g and $M_{ss} = (5.685 \pm 0.004) \times 10^{29}$ g.

2.1.2 Dimensions and Mean Density

The equatorial and polar radii of Saturn have been determined by direct visual observation with the aid of filar and double image micrometers or inferred from satellite orbit and eclipse observations. An analysis of these approaches by Cook et al. (ref. 10) leads to the values at 9.5388 AU of 17.″29 ± 0.1 for the angular equatorial and 15.″47 ± 0.1 for the polar diameter. The foregoing equatorial and polar values apply in the visual spectral region centered at approximately 5100Å.

Use of the ratio 149597893 ± 5 km $(AU)^{-1}$ for the astronomical unit (AU) (ref. 1) and the foregoing angular dimensions leads to a value of 59,800 ± 350 km for the equatorial radius R_s and 53,500 ± 350 km for the polar radius R_p. The optical flattening or oblateness, ϵ, expressed as the difference between the equatorial and polar radius divided by the equatorial radius is 0.105 ± 0.008. A dynamic value of flattening can be obtained from gravitational theory with the potential form given in section 2.2 and the values of GM_s, R_s, T_o (the rotation period), and J_2 and J_4 (zonal harmonics), given in sections 2.1 and 2.2. Such computation yields a dynamic flattening of 0.097 ± 0.005. The percent uncertainty in each of the flattening values is large; the difference shows current inadequacies of observation and theory. Either value indicates Saturn is more flattened than any other solar system planet yet measured. The optical value of flattening $\epsilon = 0.105$ will be adopted herein to provide a consistent relationship between the measured values of equatorial and polar radius.

The radius of the visible disk of Saturn R_o, at any chronocentric latitude can be written to first order in ϵ as $R_o(\phi) = R_s[1-\epsilon(\sin\phi)^2]$. The radius R_o given by this formula refers to the atmospheric level which determines the limb in visual observations and should be associated with the NH_3 cloud bottoms given by the model atmospheres of section 2.8.

The mean density is given by $\bar{\rho} = 3M_s/4\pi R_s^2 R_p$ which with the adopted values leads to $\bar{\rho} = 0.71 \pm 0.01$ g cm^{-3}. This is approximately half the mean density of the Sun and 54 percent of the mean density of Jupiter.

2.1.3 Rotation Period, Pole Location, and Orbital Quantities

The rotation period has been determined from spectral line inclinations and visual observation of spots and features. The results are presented in section 2.9. The rotation period T_o indicated in that section is $10^h\ 26^m \pm 14^m$ which corresponds to an angular rate $\omega_o = (1.67 \pm 0.04) \times 10^{-4}$ radians sec^{-1}.

Saturn's equatorial plane is taken to coincide with the plane of Saturns rings. Observations of the rings permit location of the rotational pole in the right ascension (α) declination (δ) coordinate system. For the North rotation pole, the following right ascension and declination with respect to the mean Earth equator and equinox were computed on the basis of values for the ring plane from Gurnette and Woolley (ref. 11).

$$\alpha_p = 39\overset{\circ}{.}5586 + 1\overset{\circ}{.}180 \times 10^{-4}\,(\text{JD-2443000.5})$$

$$\delta_p = 83\overset{\circ}{.}4255 + 1\overset{\circ}{.}182 \times 10^{-5}\,(\text{JD-2443000.5})$$

This result includes the effects of precession of the Earth's rotational axis when the Julian Date, JD of interest is selected. The North rotational pole of Saturn is taken to lie in the direction of the positive angular momentun vector and as such it lies in the same hemisphere as Saturn's North orbital pole and the North rotation and orbital poles of the Earth. A paper in 1898 by H. Struve is quoted by Gurnette and Woolley (ref. 11) as obtaining a precessional motion for Saturn's own rotational axis under the influence of the Sun and Titan.

This precession, which is not included in the foregoing computation for α_p and δ_p, would have a period of 2.8×10^6 years.

The orbital elements for Saturn are functions of time, and the planet's position can best be computed from the references given in section 2.1. Thus, on the basis of reference 11, at 12 hours Ephemeris time January 1, 1960 the inclination of orbital plane to ecliptic plane was 2.° 48991 = 2° 29′ 23″.7, the eccentricity was 0.055682, the mean distance 9.538843 AU, sidereal period 29.45772 tropical years, synodic period 378.09 days, mean daily motion 0°.033460, and the inclination of ring plane and equator to orbit was 26° 44′. From these values and $GM_\odot$ (sec. 2.1.1), it can be determined that Saturn moves in a region 9.0 to 10.1 AU from the Sun with an heliocentric orbital velocity between 9.1 and 10.2 km sec^{-1}.

2.2 Gravitational Field

The gravitational field of Saturn can be conveniently obtained from a potential function U which for Saturn can be approximated by several terms in an infinite series expansion (ref. 1).

$$U = \frac{-GM_s}{R_s}\left[\frac{R_s}{R} + \frac{\sigma}{2}\left(\frac{R}{R_s}\cos\phi\right)^2 - J_2\left(\frac{R_s}{R}\right)^3 P_2(\sin\phi) + J_4\left(\frac{R_s}{R}\right)^5 P_4(\sin\phi)\right]$$

The force per unit mass can be obtained from the gradient of U. The term involving σ accounts for rotation where $\sigma = \frac{\omega_o^2 R_s^3}{GM_s}$, which is equal to 0.158 ± 0.006 with the values selected in section 2.1. This value should be used when the coordinate system of interest corotates with Saturn at the rate ω_o. When a non-rotating coordinate system is used, σ should be set equal to zero.

Gravitational forces arising from the Sun, other planets and Saturn's satellites are not included in the potential U and must be evaluated separately. The positions of Saturn, other planets, and Saturn's satellites can be obtained from orbital information tabulated in the appropriate year of the *American Ephemeris and Nautical Almanac*. The masses of Saturn's satellites are given in section 2.5.1.

Apart from the centripetal term, the dependence of the gravity field on chronocentric latitude is contained in the Legendre polynomials P_2 and P_4. The potential expression is independent of longitude and is also symmetric about the equator because the polynomials contain only even powers of sin ϕ. Values for the zonal harmonics J_2 and J_4 have been obtained from the reduction of Saturn satellite observations by Jeffreys (ref. 8) and Kozai (ref. 12). Use of the combined results of these authors with an allowance for the uncertainty in R_s gives J_2 = 0.01665 ± 0.00020 and J_4 = 0.00096 ± 0.00010. The satellite observations and reduction which lead to these values for J_2 and J_4 cannot distinguish between effects arising from the mass distribution of the planet and the mass distribution of the rings. The radial distribution of mass in Saturn's rings is given in section 2.6 which will

serve as an upper limit from which the gravitational field from the rings alone can be computed.

As indicated, when the coordinate system of interest does not rotate, σ should be set equal to zero. In this case the terms involving J_2 and J_4 contribute at maximum 1.7 percent to the potential function. With the values given for GM_s and R_s in section 2.1, a simple expression can then be written for the external potential in which the uncertainty reflects the neglected ϕ dependence as follows, $U = -(634 \pm 12)(R_s/R)\ km^2\ sec^{-2}$.

For coordinate systems which corotate with the planet at ω_o, the foregoing numerical value given for σ should be used in the full expression for the potential. The non-spherical nature of this potential implies that the direction of the acceleration of gravity which defines the local vertical will not coincide with the radial direction except at the pole and equator. The chronographic latitude ϕ' is then defined as the angle between the direction of the acceleration of gravity and the equatorial plane. An approximate expression to first order in ϵ can be given for the difference between the chronographic latitude and chronocentric latitude as follows:

$$\phi' - \phi = \epsilon \sin 2\phi$$

which is maximum at $\phi = 45°$. The altitude z is defined in section 2.8.3 as the distance from the level where the pressure equals one atmosphere (for a particular model atmosphere). The distance from the center of the planet R in terms of z can be written as

$$R = R_s [1 - \epsilon (\sin\phi)^2 + (z-z_o)/R_s]$$

where z_o is the altitude of the NH_3 cloud bottom. Atmospheric quantities are given in section 2.8.3 as a function of z. A simplified expression for the gravitational acceleration g can be obtained from the potential by neglecting the term containing J_4 (because of its small value) and using the expression for R. Retaining only terms first order in J_2, ϵ, σ, and z/R_s the result is:

$$g = \frac{GM_s}{R_s^2}\left[1 + \frac{3}{2}J_2 - \sigma - \frac{2(z-z_o)}{R_s} + (\sigma + 2\epsilon - \frac{9}{2}J_2)\sin^2\phi\right]$$

From the values given in this and section 2.1, $g = 1050 \pm 200\ cm\ sec^{-2}$ at the level R_o (radius at the visible disk of Saturn). The large range reflects the difference between the equatorial and polar field and the uncertainties in GM_s, R_s, R_p, J_2, and σ.

2.3 Magnetic and Electric Fields

2.3.1 Magnetic Field

The existence of a general Saturn magnetic field has not been established. Of the major bodies in the solar system, information about the magnetic flux density is available for six. The Earth's field can be directly measured and Zeeman splitting of spectral lines permits

local and general solar fields to be measured. Limits to the fields associated with Mars, Venus, and the moon have been established through direct space flight. Deductions based on the characteristics of electromagnetic radiation in the range 60 meters (5 MHz) to 1 millimeter (300 GHz) have established the strength and some properties of Jupiter's magnetic field.

In considering the possibility of a Saturn magnetic field, the same techniques used to establish the magnetic field of Jupiter are applicable. Two extensive discussions of the character and origin of electromagnetic radiation from Jupiter can be found in Carr and Gulkis (ref. 13) and Warwick (ref. 14).

2.3.1.1 Radio Frequency Observations

Estimates of the magnetic field of Jupiter are based on observations of non-thermal radiation in two distinct spectral regions, the decametric (wavelengths tens of meters) and decimetric (wavelengths tens of centimeters). Extensive analysis of these observations have led to estimates of the dipole moment of Jupiter of approximately 4×10^{27} A m^2 (4×10^{30} gauss cm^3) (ref. 14). Repeated attempts to detect decametric emission from Saturn have not been successful although weak brief emissions have been observed (refs. 15, 16, 17, 18). The failure of these attempts to establish Saturn as a decametric source rules out at present this means of estimating the magnetic flux density.

The characteristics of decimeter radiation from Jupiter are given in section 2.7.4 as well as a comparison with Saturn observations in table VII. In this paragraph, aspects of decimetric comparisons with Jupiter that directly relate to the existence of a Saturn magnetic field are considered. Foremost among these are the linear polarization measurements obtained for Saturn by Rose et al. (ref. 19), Davis et al. (ref. 20), Kellermann (ref. 21), Berge and Read (ref. 22), Berge (ref. 23), and Gerard (ref. 24). All but reference 19 place the degree of linear polarization at less than 10 percent. For observations at 9.4 cm during 1962, Rose et al. (ref. 19) give 20 ± 8 percent as the degree of linear polarization with the position angle of maximum polarization nearly parallel to the rotational axis. The degree of linear polarization reported by reference 19 is comparable to that of Jupiter at the same frequency (ref. 13) whereas the position angle of polarization maximum differs from that of Jupiter by $\sim 90°$. Subsequent observers at nearby frequencies have not confirmed the polarization results of reference 19. Taken as a whole, the polarization measurements do not yet provide sufficient information to estimate the magnetic flux density.

The total flux density and source extent measurements discussed in section 2.7.4 indicate that a non-thermal source for Saturn decimetric radiation is not excluded, but alternate explanations are possible and likely.

At present, neither the decametric or decimetric observations of Saturn provide a sound method of estimating its magnetic field.

2.3.1.2 Jupiter Analogy

For the purpose of estimating the magnetic flux density, only Jupiter analogy remains. The two planets are similar in size and rotation rate (Allen, ref. 25) and are formed principally of

hydrogen and helium (sec. 2.8). Although theories of magnetic field generation in rotating bodies are incomplete, the similarities between Jupiter and Saturn suggest the same process could operate for both. Jupiter analogy and the estimates of dipole moment given by Warwick (ref. 14) suggest the range 0 to 10^{29} A m^2 (0 to 10^{32} gauss cm^3) for the dipole moment M of Saturn. This range includes the estimates for Jupiter (refs. 13 and 14) and is not excluded by any measurement of the Saturn system. Warwick (ref. 14) points out that, if it is assumed that the dipole moment of a body is proportional to its rotational angular momentum, reasonable accord can be obtained between the observed dipole moment of the Sun and Jupiter and the dipole moment computed with this assumption using the Earth as a base. This technique leads to a value of approximately 1×10^{27} A m^2 (1×10^{30} gauss cm^3) for the dipole moment of Saturn. Although not based on any substantiated theory of magnetic field generation, this technique serves as a reference point in the foregoing broad range suggested for Saturn's dipole moment M.

The magnetic dipole fields of the Earth and Jupiter are inclined by less than 20° to the rotational axes (refs. 13 and 25). For Jupiter both large and small displacements, 0.75 Jupiter radii (ref. 14) and less than 0.3 Jupiter radii (ref. 26), of the dipole center from the geometric center of the planet have been suggested. Both of these possibilities exist for Saturn. Because no evidence is available, any dipole inclination should be considered possible and a geometrically centered dipole should be assumed with a sufficient range of dipole moment to cover the possibility of dipole displacement. The magnetic flux density $\mathcal{B}$ and dipole moment M are related by the following equation for a centered dipole with M in (A m^2) and $\mathcal{B}$ in (T);

$$\mathcal{B} = (10^{-7}) \frac{M}{R^3} (1 + 3\sin^2 \phi_m)^{1/2}$$

where ϕ_m is the magnetic latitude. Use of the foregoing range of 0 to 10^{29} A m^2 (0 to 10^{32} gauss cm^3) for the magnetic moment, R as equal to R_s, and ϕ_m as equal to 0 leads to the range of 0 to 4.7×10^{-2} T (0 to 470 gauss) for the magnetic flux density at one equatorial radius from the dipole origin.

After the polarization measurements of Rose et al. (ref. 19), two authors, Zheleznyakov (ref. 27) and Zlotnik (ref. 28), presented arguments based on the synchrotron emission mechanism to explain the polarization and the alignment of the polarization plane to the rotational axis. Both authors assume a general, rotationally-aligned dipole field for the planet and demonstrate the possibility of distortion in the region of the rings by interaction of the general magnetic field with Saturn's ring particles and associated gas. Zheleznyakov (ref. 27) finds the magnetic field parallel to the equator near the rings, whereas Zlotnik (ref. 28) places the magnetic field perpendicular to the ring plane but stronger than the field in the absence of rings with the result of high latitude particle traps. Although neither idea can be confirmed, they pose the possibility of magnetic field distortion from ring interactions.

2.3.2 Electric Fields

There has been no discussion in the literature of static electric fields in the vicinity of Saturn. This results from our limited understanding of the magnetic field (section 2.3.1) and charged particles (section 2.7). Two sources of a static electric field, however, are postulated in the following discussion.

An induced electric field can result from motion through a magnetic field. For an object near Saturn but not rotating with it, the magnitude of this field is given by

$$\mathcal{E} = (\omega_o R)(M/R^3)$$

when it is assumed that the relative motion is perpendicular to the field lines and latitude dependence is neglected. Substitution of the values of ω_o from section 2.1 and the range of M from section 2.3.1.2 yields $\mathcal{E} \leq 470\ (R_s/R)^2$ volts meter^{-1}. This value is more than an order of magnitude larger than the fields postulated by Goldreich and Lyden-Bell (ref. 29) in discussing the source of Jupiter's decametric radiation. The foregoing larger value results from the range assumed for the dipole moment in section 2.3.1.2. In the absence of other estimates, 470 $(R_s/R)^2$ volts meter^{-1} will be taken as an upper limit for distances from the planet greater than R_o.

Below the reference level R_o and in the cloud-forming region of the atmosphere, convective activity can be expected to result in charge separation and randomly-oriented electric fields as is the case for Earth. For the Earth, fields within clouds on the order of 10^4 to 10^5 volts meter^{-1} are indicated (ref. 30) with the maximum field of 10^6 volts meter^{-1}, corresponding to electrical breakdown of the atmosphere (ref. 25). Similar values can be expected for the atmosphere of Saturn with fields of 10^4 to 10^5 volts meter^{-1} extending over kilometers and fields up to 10^6 volts meter^{-1} over short distances and times (centimeters and seconds).

2.4 Electromagnetic Radiation

This section discusses direct solar radiation; its reflections from Saturn's body, satellites, and rings; thermal radiation from the planet, satellites, and rings; and nonthermal radiation from a possible radiation belt.

2.4.1 Direct and Reflected Solar Radiation

When unshadowed, the Sun is the dominant natural electromagnetic radiation source above Saturn's atmosphere in the wavelength interval 1 Å to 7 μm. Values for the solar spectral irradiance H_λ (power per unit area and per unit wavelength interval) and the integrated spectral irradiance or solar constant $H_\odot$ (power per unit area) are given in NASA SP-8005 (ref. 31) and apply at 1 AU outside the Earth's atmosphere. The solar constant recommended by reference 31 is $H_\odot = 0.135 \pm 0.002$ watts cm^{-2} and this value is adopted here.

At wavelengths less than 3000 Å, the spectral irradiance increases with solar activity. At wavelengths longer than 1 mm, the spectral irradiance also increases with solar activity and at wavelengths longer than three meters an individual radio burst can exceed the quiet solar level by five orders of magnitude.

With values of spectral irradiance and the solar constant at 1 AU, the spectral intensity I_λ (power per unit area and per unit wavelength interval and per steradian), spectral flux F_λ

(power per unit area and per unit wavelength interval), and integrated flux F (power per unit area) can be computed from the following equations:

$$I_\lambda = H_\lambda/\Omega_\odot$$

$$F_\lambda = H_\lambda/S^2$$

$$F = H_\odot/S^2$$

where $\Omega_\odot$ is the solid angle subtended by the photosphere of the Sun at 1 AU ($\Omega_\odot = 6.8 \times 10^{-5}$ steradians from reference 25) and S is the distance from the Sun in AU to the observer. When the observer is shadowed by Saturn's rings, the foregoing expressions should be multiplied by exp $(-\tau/\sin B'_\odot)$ where $B'_\odot$ is the elevation angle of the Sun from the ring plane and τ is the optical thickness at the radial distance from Saturn where a line from the Sun to the observer crosses the ring plane. $B'_\odot$ will never exceed 29°, and τ can be obtained from the ring model in section 2.6.3.

Next in importance to direct solar illumination is radiation reflected from Saturn and its rings. Solar radiation reflected from the planet depends on the properties of its atmosphere and clouds as well as the Sun-Saturn-observer geometry. All observations of Saturn have been made from the vicinity of the Earth where the phase angle Ψ does not exceed 6°. Therefore, estimates of the change in reflecting ability with phase are uncertain. In addition, the presence of several bright rings with a known phase dependence (refs. 32 and 33) complicates reduction to the no ring situation. Here the geometric albedo p_λ is used to establish upper limits for the intensity and flux. Values for the geometric albedo are given by Bless et al. (ref. 34), Harris (ref. 35), and Walker (ref. 36) as listed in table III. The UV measurements of Bless et al. are uncertain as the ring albedo is not known, and Walker's results represent a single night's observation. These results were used to construct figure 6 which shows the possible range of geometric albedo. The reflected intensity and flux from Saturn can be estimated by

$$I_\lambda = \frac{p_\lambda H_\lambda}{\pi R^2_{s_\odot}}$$

$$F_\lambda = \frac{p_\lambda H_\lambda}{R^2_{s_\odot} (R/Rs)^2}$$

$$F = \frac{p_g H_\odot}{R^2_{s_\odot} (R/Rs)^2}$$

where $R^2_{s_\odot}$ is the Saturn-Sun distance in AU (the range of $R^2_{s_\odot}$ is 91± 11 AU^2), R_s and R (the distance to the planet) must be in the same units, and p_g is the integrated geometric albedo for which the value 0.37 has been given by Walker (ref. 36). The foregoing expres-

TABLE III

MEASURED VALUES OF GEOMETRIC ALBEDO FOR SATURN

Effective Wavelength λ (μm)	Photometric Passband*	Geometric Albedo (P_λ)	Source
0.245	–	$0.44^{+0.14}_{-0.30}$	Bless et al. (ref. 34)
0.280	–	$0.40^{+0.14}_{-0.30}$	Bless et al. (ref. 34)
0.295	–	$0.34^{+0.14}_{-0.30}$	Bless et al. (ref. 34)
0.353	U	0.21 ± 0.03	Harris (ref. 35)
0.448	B	0.32 ± 0.03	Harris (ref. 35)
0.554	V	0.46 ± 0.03	Harris (ref. 35)
1.06	W	0.37 ± 0.05	Walker (ref. 36)
1.13	X	0.17 ± 0.03	Walker (ref. 36)
1.63	Y	0.16 ± 0.03	Walker (ref. 36)
2.21	Z	0.04 ± 0.01	Walker (ref. 36)

*See appendix C, Glossary.

sions refer to zero phase, and as such they may be regarded as upper limits for other phase angles.

The visual magnitude of Saturn at zero phase is given by

$$M_v = (V_v \pm 0.2) + 5 \log (R_{s_\odot} R)$$

where V_v is the absolute visual magnitude. For mean opposition, i.e., $R_{s_\odot} = 9.5388$ AU and $R = 8.5388$ AU, $5 \log (R_{s_\odot} R)$ equals 9.55. V_v and color differences taken from Harris

(ref. 35) and Walker (ref. 36) are given in table XIII. The variation of magnitude with phase is not known (ref. 35). It is certainly less than that of the rings which is 0.036 magnitude per degree according to Franklin and Cook (ref. 32).

2.4.2 Reflected Solar Radiation from Saturn's Rings

The amount of light reflected toward an observer from Saturn's rings depends on three angles; $B'_{\odot}$ (the chronocentric elevation angle of the Sun above the ring plane), B_0 (the chronocentric elevation angle of the observer above the ring plane), and Ψ (the angular distance between these two directions viewed from Saturn) as well as on the reflecting properties of the individual ring particles and their distribution in size and position. For observation from the Earth, Ψ never exceeds 6° and $B'_{\odot}$ and B_0 do not exceed 29° and differ from one another at most by a few degrees. Thus the range of values for $B'_{\odot}$, B_0, and Ψ which can be sampled from Earth is very limited.

Summaries of A and B ring brightness observations and references to earlier work can be found in references 10, 32, and 37. For the A and B rings, the brightness in the visual (V) and blue (B) increases nonlinearly with phase angle for phase angles Ψ less than 1.5°. For observations in 1959 with $B'_{\odot}$ and B_0 near 26°, reported by Cook et al. (ref. 10) and Franklin and Cook (ref. 32), the brightness of the outer third of the B ring (the brightest region of the entire ring system) was within a factor of two of the normal brightness expected of isotropic total reflection from a screen at Saturn's distance from the Sun. The results given by Focas and Dollfus (ref. 37) indicate that, with respect to the dependence of brightness on the elevation angles $B'_{\odot}$ and B_0, the A and B rings are near maximum at 28°. The decrease in brightness for elevation angles less than this value is less rapid than would be expected from a Lambert surface.

On the basis of the photometric properties of the A and B rings, a number of theories and models have been proposed by Bobrov (ref. 33), Franklin and Cook (ref. 32), Hämeen-Anttila (ref. 38), and Lumme (ref. 39). The models of Bobrov and Franklin and Cook emphasize the brightness variation with phase angle Ψ, whereas Hämeen-Anttila and Lumme consider the change in brightness with the elevation angles $B'_{\odot}$ and B_0. Although each of the models presented by these authors is successful in providing an explanation for some of the observed A and B ring photometric properties, none are suitable for a simple description of ring intensity and flux over the full range of values for $B'_{\odot}$, B_0, and Ψ. For the C, D, and D′ rings*, only a few estimates of brightness are available (refs. 40, 41, 42, and 43) and there is no observation or discussion of elevation and phase angle dependences.

In view of the foregoing situation, only an upper limit to the intensity of light reflected from Saturn's five rings will be estimated. The upper limits for the spectral intensity I_λ are plotted in figure 7 as the ratio $k_R = I_\lambda/H_\lambda$. For the A and B rings the intensity was obtained from the brightness measured for these rings by Franklin and Cook (ref. 32) and Cook et al. (ref. 10). These authors give the brightness for several regions of each ring and the brightest region in each case was selected. The D ring brightness estimates given by

*Section 2.6.2 defines the D and D′ ring notations.

Guerin (ref. 42) (1/20 of the maximum B ring brightness) were used for that ring. This estimate was also used for the center of Cassinis division and the part of the D′ring from the outer edge of the A ring to 3.0 R_s. From 3.0 R_s the brightness was assumed to decrease linearly to zero at 4.0 R_s. Feibelman (ref. 43), the only observer to even detect the D′ ring at this distance, indicates that it is extremely faint. The C ring brightness was obtained by a logarithmic interpolation between the B ring and D ring brightnesses in accordance with figure 7. The dimensions of the five rings were taken from table XVIII and section 2.6.1.

With figure 7 and H_λ, the maximum spectral flux and integrated flux from any area of the ring can be found with the following formulas.

$$F_\lambda = \int_{\Omega_R} I_\lambda \cos\theta \, d\Omega$$

$$F = H_\odot \int_{\Omega_R} k_R \cos\theta \, d\Omega$$

Both integrals are over the solid angle Ω_R subtended by the region of the ring of interest, and θ is the polar angle between the normal to spacecraft area of interest and the direction of the incident energy.

For a spacecraft farther than 5R_s from Saturn, the above expressions can be simplified.

$$F_\lambda = I_\lambda \Omega_R \quad \Omega_R = \frac{A_R \sin B_0}{R^2}$$

$$F = H_\odot k_R \Omega_R$$

where Ω_R is the solid angle subtended by the ring region of interest whose area is A_R.

Several special situations can occur which require separate comment. Since the passage of the Earth and Sun through the ring plane in 1966, the southern face of the ring system has been exposed to view. This situation will continue until the next ring-plane passage in 1980. As a result of the changing elevation angle $B'_\odot$ of the Sun, the shadow cast by Saturn on the rings varies with time. At maximum the shadow can cover about 17 percent of the A and B ring area. In addition, the disk of Saturn can occult up to 100 percent* of the ring system area depending on the elevation angle of the observer and the distance from the center of the planet. This occulted area can be entirely separate from the shadowed area. In the worst case, the formulas given above for distances greater than 5R_s will overestimate the flux from the A and B rings by 34%. For approaches closer than 5R_s, the integral expression for F_λ should be used, excluding the occulted ring area, and treating the intensity over the shadowed area as zero. For passage within a few minutes of arc of the ring plane, the contribution from the edge of the ring system (see section 2.6.2 for a discussion of ring thickness) may be greater than that of the ring area (A_R) of interest. An upper limit to the flux from the edge can be computed by assuming: a thickness of 5 km; an intensity equal to

*The 100 percent occultation would occur in the case of a descending polar probe.

that given for ring B; and location of the edge at 2.29 R_s from the center of Saturn. From greater than 5 R_s, the flux from the edge computed with these assumptions will not approach the total from the A and B ring unless the spacecraft is within one minute of arc of the ring plane.

2.4.3 Visual Magnitude of Saturn and Rings

An empirical formula for the magnitude of Saturn and rings in the visual (V) has been given by Müller, quoted in Sharonov (ref. 44) as

$$M_v = (V_v \pm 0.3) + 5 \log (R_{s_\odot} R) - 2.60 \sin B_0 + 1.25 \sin^2 B_0 + 0.044\Psi$$

This formula was developed from Earth-based observations and can be used with confidence only under the restrictions implicit in such observations, i.e.; Ψ should not exceed 6°, $B'_\odot$ and B_0 should be within 3° of one another, and the observer and Sun should be on the same side of the ring plane.

2.4.4 Reflected Radiation from Saturn's Satellites

Harris (ref. 35) and the *Handbook of the British Astronomical Association*, 1971 provide summaries of the available information on the magnitude and color of Saturn's satellites, and these results are tabulated in table XIV.

The variation with phase is not established even over the 6° interval permitted for observation from the Earth. Except for Titan, the geometric albedo is not known because of uncertainty in the satellites' radii (sec. 2.5.1). The visual magnitude of the satellites can be given by

$$M_v = (V_v \pm 0.3) + 5 \log (R_{s_\odot} \Delta) + (0.03 \pm 0.02)\Psi$$

with Ψ in degrees. The range of phase variation shown covers the range expected for objects with or without an atmosphere (ref. 25). The uncertainty of ±0.3 given for V_v should be increased to ±0.5 for Mimas and ±1.0 for Janus and Phoebe as the magnitude of these satellites is not well known. For Iapetus, which shows a large regular variation in brightness, the smallest V_v given in table XIV should be used when this satellite is at western elongation* and the largest value of V_v when at eastern elongation. It is likely that Iapetus rotates in a synchronous manner (sec. 2.5.1). For satellites other than Janus, Mimas, Phoebe, and Iapetus, the uncertainty ±0.3 adequately covers the variation expected with orbital position.

2.4.5 Thermal and Nonthermal Radiation from Saturn

The brightness temperature of Saturn has been measured in the wavelength range from 8 μm to 74 cm. These results are listed in table IV. Observation throughout this wavelength interval is hampered by molecular absorption in the Earth's atmosphere; limitations of

*Defined in Glossary (app. C).

receiver system sensitivity and calibration; variations in background radiation at the longest wavelengths, and an unknown contribution from the rings and nonthermal sources.

It is likely that the increase in brightness temperature with increasing wavelength indicated in table IV, results entirely from the thermal radiation of Saturn's atmosphere (sec. 2.7.4). It is then reasonable to interpret all these measurements as disk brightness temperatures T_D. On the basis of the foregoing sources, the range of disk brightness temperature T_D was estimated and is given in figures 4 and 5 with liberal uncertainty and reasonable extrapolation in regions where no observations have been made. The range is broad enough to include the likely 1.25 cm ammonia absorption reported by Wrixon and Welch (ref. 58). The effective temperature $T_e = 97 \pm 4°K$ (1.5 to 350μm) determined for Saturn by Aumann et al. (ref. 51) and their discussion indicate that Saturn is radiating more energy than it receives from the Sun. The maximum in thermal radiation will occur near 40μm. Spectral flux computations based on the disk brightness temperatures of figures 4 and 5 need not consider the Sun-Saturn-spacecraft geometry. With the disk brightness temperatures from these figures, the spectral intensity and flux can be found by

$$I_\lambda = B_\lambda (T_D)$$

$$F_\lambda = B_\lambda (T_D)\, \Omega_s$$

$$\Omega_s = \pi R_s^2 / R^2$$

where the Planck function $B_\lambda(T_D)$ (in intensity units) can be found in analytic and tabular form in Allen (ref. 25) and elsewhere. The effective temperature of $97 \pm 4°K$ found by Aumann et al. (ref. 51) can be used to compute the integrated flux F by

$$F = \frac{(5.0 \pm 1.5)}{(R_s/R)^2} \text{ watts m}^{-2}$$

where the uncertainity in the effective temperature has been increased to $\pm 6°K$ to account for possible variability and give some weight to the other brightness temperature measurements in the 8 to 25 μm range (table IV).

Section 2.7.4 indicates that Saturn may have a trapped radiation belt, and it is worth considering the spectral flux and brightness temperature expected from the synchrotron radiation such a belt would produce. A reasonable approach is to consider the synchrotron brightness temperature T_{sy} from Jupiter. Use of the innermost contour (largest brightness temperatures) from the Jupiter brightness temperature maps of Berge (ref. 69) at 10 cm and Branson (ref. 70) at 21 cm leads to the relationship $T_{sy} \simeq 1.5\lambda^2\,°K$ for λ in cm. It is shown in section 2.7.4 that if the Jupiter decimetric flux is scaled to Saturn, the flux would be $\sim 0.9 \times 10^{-26}$ watts $m^{-2} Hz^{-1}$. At the longest wavelength of measurement for Saturn

TABLE IV

MEASURED BRIGHTNESS TEMPERATURES FOR SATURN IN THE SPECTRAL RANGE FROM 8 μm TO 73.5 cm

Brightness Temperature (°K)	Wavelength	Source
~120	5 μm	Low and Davidson (ref. 45)
<105	8–14 μm	Murray and Wildey (ref. 46)
93±3	8–14 μm	Low (ref. 47)
103^{+5}_{-10}	7.5–13.5 μm	Low (ref. 48)
93–102	10 μm	McElroy (ref. 49) from Low
95±3	17.25–25 μm	Low (ref. 50)
93±3	22 μm	McElroy (ref. 49) from Low
<100	25–50 μm	Aumann et al. (ref. 51)
140±15	1200 μm	Low and Davidson (ref. 52)
97^{+52}_{-42}	3.2 mm	Tolbert (ref. 53)
125±13	3.3 mm	Epstein et al. (ref. 54)
130±15	3.4 mm	Epstein (ref. 55)
103^{+70}_{-64}	4.3 mm	Tolbert (ref. 53)
133±24	4.3 mm	Kellerman (ref. 56) from Hobbs
132±9	8 mm	Kutuza et al. (ref. 57)
151.1±7.0	8.45 mm	Wrixon and Welch (ref. 58)
116±30	8.6 mm	Tolbert (ref. 53)
96±20	8.6 mm	Braun and Yen (ref. 59)
118±20	9.55 mm	Epstein (ref. 55) from Hobbs
133±20	9.55 mm	Kellermann (ref. 56) from Hobbs
138.1±6.0	9.84 mm	Wrixon and Welch (ref. 58)
130.8±5.0	1.18 cm	Wrixon and Welch (ref. 58)

TABLE IV (Continued)

Brightness Temperature (°K)	Wavelength	Source
127.2±5.5	1.27 cm	Wrixon and Welch (ref. 58)
133.2±7.5	1.46 cm	Wrixon and Welch (ref. 58)
141±15	1.53 cm	Welch et al. (ref. 60)
140±15	1.9 cm	Kellermann (ref. 56) from Kellermann and Pauliny-Toth
200±30	1.9 cm	Kellermann and Pauliny-Toth (ref. 61)
137±12	3.12 cm	Berge (ref. 23)
144±30	3.45 cm	Cook et al. (ref. 62) corrected by Seling (ref. 63)
106±21	3.45 cm	Cook et al. (ref. 62)
168±11	3.75 cm	Seling (ref. 63)
190±45	6 cm	Hughes (ref. 64)
179±19	6 cm	Kellermann (ref. 21)
165±25	9 cm	Berge and Read (ref. 22)
177±30	9.4 cm	Rose et al. (ref. 19)
196±44	10 cm	Drake (ref. 65)
172±20	10.7 cm	Berge and Read (ref. 22)
166±13	11.13 cm	Gerard (ref. 24)
196±20	11.3 cm	Kellermann (ref. 21)
182±19	11.3 cm	Davis et al. (ref. 20)
286±37	21.2 cm	Davis and Williams (ref. 66)
303±50	21.3 cm	Kellermann (ref. 21)
<1250	70 cm	Gulkis et al. (ref. 67)
1690±430	73.5 cm	McAdam (ref. 68)

(73.5 cm), the brightness temperature obtained by McAdam (ref. 68) leads to a flux of $\sim 0.05 \times 10^{-26}$ watts m^{-2} Hz^{-1} at mean opposition. Compared on this basis, Saturn radiates 1/18 the spectral flux expected from a scaled Jupiter model. Because the rings probably interfere with the formation of a radiation belt interior to 2.3 R_s, (sec. 2.7.4),a factor of 10 is a more reasonable estimate of the brightness difference. The synchrotron brightness temperature of Saturn can then be given by

$$T_{sy} = (0.2 \pm 0.2)\lambda^2 \ (^\circ K)$$

for λ in cm. The intensity can then be obtained from the Planck function B_υ (T_{sy}). The maximum synchrotron flux should not exceed $0.05 \pm 0.05 \times 10^{-26}$ watts $m^{-2} Hz^{-1}$ at 8.54 AU and should be nearly constant within the source region ($R < 3$ R_s) and proportional to R^{-2} outside the source. An expression which fits these considerations is given by

$$F = \frac{(1.6 \pm 1.6) \times 10^{-19}}{9 + (R/R_s)^2} \quad \text{watts } m^{-2} Hz^{-1}$$

The flux given by this formula is the maximum permitted from the postulated synchroton source for wavelengths less than 100 cm.

For wavelengths longer than 100 cm, there are no confirmed detections of radiation from Saturn. (Section 2.3.1 discusses possible decametric detections.) On the other hand, observations indicate that Jupiter is an intense source of decametric radiation with strong directional characteristics (ref. 14). Such sources could be associated with Saturn and escape detection because observation has been carried out over only about one half of Saturn's orbital period. As a result, the intensity of radiation at wavelengths longer than 100 cm cannot be adequately predicted and equipment sensitive to such radiation should be avoided.

2.4.6 Thermal Radiation from Saturn's Rings and Satellites

To estimate the thermal radiation from the rings and satellites, it is necessary to know the emitting area, its temperature, and emission properties. A temperature of the rings of less than 60°K was estimated by F.J. Low according to Aumann et al. (ref. 51). Kuiper et al. (ref. 71) with reflection spectra in the 1 to 4 μm region obtained a value of 83°K as the best temperature to fit the overall ring spectrum. The uncertainty in this determination is not given, but the method has the advantage of being independent of the amount of material present in the rings. In addition, Kuiper et al. (ref. 71) report that F. J. Low determined the ring temperature as 84° ± 3°K from 10 μm and 20 μm observations. The conflict between the foregoing ring particle temperatures may arise from measurement difficulties, variability of Saturn emission, or a change in ring particle absorption and emission with ring inclination. The equilibrium temperature for a completely black particle of uniform temperature at Saturn's mean distance from the Sun is 91°K. The photometry of Franklin and Cook (ref. 32), Cook et al. (ref. 10), and Lebofsky et al. (ref. 72) indicates that the geometric albedo of the ring particles is high (greater than 0.8 in both the B and V photometric passbands).

Therefore, 91°K is taken as reasonable upper limit for the physical temperature of the ring particles.

Attempts to establish a connection between the brightness temperature of the Saturn system in the radio region $\lambda \geq 0.1$ cm and the inclination of the ring have not met with success (refs. 22 and 60). Epstein et al. (ref. 54) present a series of observations extending from April 1966 through November 1969. Although the solid angle of the A and B rings ranges from 0 to 80 percent of the planetary disk solid angle, no significant trend in brightness temperature is apparent. The absence of a confirmed variation in the Saturn system brightness temperature with ring inclination could result from low particle emissivity, small particle size in relation to the observation wavelength, or a ring optical thickness in the order of 1/10 of those shown in figure 8 and discussed in section 2.6.2 (refs. 22 and 60). Although the presence of water ice in the rings is established, other undetermined compounds or mixtures may also be required to explain the A and B ring color (sec. 2.6.2).

At present it is not possible to choose between the several foregoing alternatives. Therefore, a simple set of assumptions will be made which will lead to an upper limit estimate of the spectral flux and intensity. The particle temperature will be taken as 91°K, and the particle emissivity as unity. The fraction of projected area occupied by particles will be taken as being proportional to

$$[\ 1\text{-}\exp(-\tau(R)/\sin B_R)\ ]$$

where τ (R) is to be taken from figure 8 and B_R is the elevation angle of the observer above the ring plane measured from the ring section of interest. The spectral flux and intensity will then be given by

$$I_\lambda = B_\lambda(91°K)\,[1 - \exp(-\lambda(R)/\sin B_R\,]$$

$$F_\lambda = \int_{\Omega_R} I_\lambda \cos\theta\, d\Omega$$

where θ is a polar angle measured between the normal to the spacecraft area of interest and the direction of incident radiation. The integral is to be taken over the ring section of interest.

For observation from greater than 5 R_s the spectral flux can be written as

$$I = B_\lambda\,(91°K)\,[1 - \exp(-\bar{\tau}/\sin B_o)]$$

$$F_\lambda = I_\lambda \Omega_R$$

$$\Omega_R = \frac{A_R \sin B_o}{R^2}$$

where A_R is the area of the ring segment of interest, $\bar{\tau}$ is the average optical thickness over this area, and B_0 is the elevation angle of the observer above the ring plane. The A and B rings will be of primary importance in most situations and the following values combined with the foregoing formulas will provide correct upper limits. For B ring, $A_R = 4.6R_s^2 = 1.8 \times 10^{10}$ km^2 and $\bar{\tau} = 1.0$; for A ring, $A_R = 3.5R_s^2 = 1.3 \times 10^{10}$ km^2 and $\bar{\tau} = 0.45$. Before any of these formulas are used, it should be determined that in the worst case (near a large ring particle) this radiation is important. For this situation the intensity, spectral flux, and integrated flux are given by

$$I = B_\lambda (91°K)$$

$$F_\lambda = \pi B_\lambda (91°K)$$

$$F = 4 \text{ watts m}^{-2}$$

Titan is the only one of Saturn's satellites whose brightness temperature has been measured. Low (ref. 50) gives the value 132± 5°K from measurements in the region from 7.5 to 13.5 μm. This value is a few degrees larger than the 128°K subsolar point temperature expected for a non-conducting, non-rotating, black object at Saturn's mean distance from the Sun. The Low (ref. 50) measurement may be related to the presence of a Titan atmosphere (sec. 2.5.1). For the remaining satellites, no brightness temperature measurements exist and the satellite radius is uncertain (sec. 2.5.1) so that albedo computation is difficult. It is unlikely that the brightness temperature for any of the satellites exceeds 128°K by more than a few degrees throughout the 1 μm to 3 meter wavelength range. An upper limit to the spectral intensity, flux, and integrated flux can then be given by

$$I_\lambda = B_\lambda (128°K)$$

$$F_\lambda = \frac{\pi B_\lambda (128°K)}{(\Delta/R_{sat})^2}$$

$$F = \frac{15}{(\Delta/R_{sat})^2} \text{ watts m}^{-2}$$

where Δ is the observer-satellite distance and R_{sat} is the radius of the satellite of interest (table XVII). Approaches to $1.5R_s$ from any Saturn satellite may be made before the contribution to spectral and integrated flux from the satellite has any chance of exceeding that of Saturn itself.

2.5 Satellites and Meteoroids

This section discusses the properties of Saturn's ten satellites which have been derived from observation and the possible meteoroid environment near Saturn. Saturn's rings, which are themselves a collection of satellites, are considered separately in section 2.6.

2.5.1 Satellites

Saturn has ten satellites, the second largest number for any planet in the solar system. Jupiter has twelve. Limits to the photographic magnitude of any as yet undiscovered satellites were established in 1961 by Kuiper (ref. 73). In his survey, Kuiper (ref. 73) detected no new satellites brighter than photographic magnitude 14 near the rings and photographic magnitude 19-20 away from the rings. By assuming a geometric albedo of 0.2, Kuiper (ref. 73) concluded that away from the rings, 40 km may be regarded as an upper limit to the diameter of undiscovered satellites. Because satellites with diameters less than 40 km are known to exist (ref. 25), small undiscovered satellites are a possibility. During the 1966 passage of the Sun and Earth through Saturn's ring plane, Dollfus (ref. 74) reported the photographic detection of a new satellite near, and apparently, in the plane of the rings. This satellite, for which Dollfus has suggested the name Janus, is probably fainter than photographic magnitude 14 (ref. 75) and thus is consistent with foregoing the limits of completeness established by Kuiper (ref. 73).

Table XVII lists some of the orbital and physical properties of Saturn's satellites. The column giving the range of distance from Saturn's center was obtained from the mean distance given by the *Handbook of the British Astronomical Association*, 1971 and the eccentricities given by Gurnette and Woolley (ref. 11) and Kozai (refs. 12 and 76). The ratio of mean distance to Saturn's equatorial radius was computed from the mean distance of column 1 and the equatorial radius 59,800 km in section 2.1.2. The orbital period was taken from the *Handbook of the British Astronomical Association*, 1971 and the orbital speed computed from the mean distance of column 1 and the Saturn mass given in section 2.1.1. The range of chronocentric latitude was obtained from the inclinations given by references 11, 12, and 76. The radius of all the satellites is very uncertain. Direct determinations of the diameter of Tethys, Dione, Rhea and Titan have been made by Kuiper (ref. 77) with a discometer. Sharonov (ref. 44) reported a discometer measurement of the diameter of Rhea by H. Camichel. Dollfus (ref. 41) gives a double image micrometer measurement for Titan and reports a discometer measurement of Titan by H. Camichel. Focas and Dollfus (ref. 37) determined the diameter of Tethys by estimating its albedo after observing a transit of this satellite across the disk of Saturn. Because the diameter of Titan subtends less than a second of arc as viewed from the Earth, the double image micrometer and discometer measurements are difficult. For Tethys, Dione, Rhea, and Titan, the values given in table XVII are those of Kuiper (ref. 77) with uncertainties large enough to include other determinations from the foregoing sources. The radii of the remaining six satellites were estimated from a range for the geometric albedo and from the visual magnitudes given by Harris (ref. 35) and the *Handbook of the British Astronomical Association*, 1971. The mass values in table XVII were obtained from Brouwer and Clemence (ref. 78) and Kozai (refs. 12 and 76) when possible. For Janus, Phoebe and Hyperion, no mass estimates on the basis of satellite perturbations have been published. For these three satellites, the mass of Mimas was adopted as an upper limit because Mimas is approximately two magnitudes brighter visually than Janus and more than two magnitudes brighter than Hyperion or Phoebe.

In terms of distance from Saturn's center, the satellites range from 2.82 R_s for Janus to 254 R_s for Phoebe at apoapsis. The corresponding orbital periods range from 4/5 day to 550

days. Except for Hyperion and Phoebe the orbital eccentricities are less than 0.03, and for these two satellites the eccentricity is less than 0.2. The motion of all the satellites is direct except Phoebe whose motion is retrograde and inclined 30° to the planetary equatorial plane. The orbit of Iapetus is inclined 14.7° to the planetary equatorial plane, whereas the inclination of each of the remaining satellites to this plane is less than 1.6°

Perturbations arising from Saturn's non-spherical gravitational field, gravitational field of the Sun, and other satellites result in secular and periodic changes in the orbital elements of Saturn's satellites. Location of the satellites can be determined by use of the appropriate year of the *American Ephemeris and Nautical Almanac.* Orbital elements given as functions of time for all satellites except Janus can be found in reference 11 and for Mimas, Enceladus, Tethys, Dione, Rhea, and Titan, in references 12 and 76. The ratios of the mean motions of 3 pairs of satellites can be reduced to the ratios of integers. The mean motions of Mimas and Tethys are nearly in the ratio of 2 to 1 as are those of Enceladus and Dione; the mean motions of Titan and to Hyperion are nearly in the ratio of 4 to 3.

The photometric properties of Saturn's satellites are presented in table XIV and discussed in section 2.4.4. Satellite temperatures and thermal radiation are discussed in section 2.4.6. The rotation periods of Saturn's satellites are not known except for Iapetus, which is discussed in the following paragraphs. Dollfus (ref. 41) reported observation of features on the disk of Titan, but the rotation period was not established.

Janus, Titan, and Iapetus require special comment. Janus has been identified in four published photographs, one by Dollfus (ref. 74), two by Texereau (ref. 79), and one from Walker (ref. 80). Other observers such as Rosino and Stagni (ref. 75), who searched for Janus after announcement of its discovery, were unable to detect it at the calculated times of elongation. The faintness of this satellite and its apparent small inclination and nearness to the outer edge of the A ring (2.82 R_s for Janus against 2.29 R_s for the outer radius of ring A) make observation from the Earth difficult other than during passage of the Earth and Sun through the ring plane.

Measurement of Janus' position in photographs published by Dollfus (ref. 74), Texereau (ref. 79), and Walker (ref. 80) showed that if Janus is in direct circular orbit, six different orbital periods seemed to fit the photographic results according to Cook et al. (ref. 10). The orbital periods range from $17^h.701$ to $19^h.565$ with $19^h.565$ being the best fit with the photographic data. None of the six periods agrees well with Dollfus' period of $17^h.965$ (ref. 74) which was used by Rosino and Stagni (ref. 75) in the unsuccessful search for Janus. If Cook et al. (ref. 10) are correct, a search of Saturn plates taken during the 1966 ring plane passage could provide confirmation. At present the period and thus the semimajor axis must be considered uncertain. The period of Janus will be taken herein as $19^h.565^{+0.5}_{-2.0}$ with the uncertainty spanning all present suggestions.

Titan, the largest of Saturn's satellites, has a diameter of 4800 ± 400 km which is greater than the moon (3476 km) and is second in size to Jupiter's satellite Ganymede (diameter 5100 km, ref. 25) among satellites of the solar system. Kuiper (ref. 77) reported methane absorption lines in the reflection spectrum of Titan and concluded that an atmosphere

was present. No other molecular species was detected. Kuiper (ref. 77) computed the methane abundance and an upper limit to the ammonia abundance on the basis of comparison with laboratory spectra produced at a temperature different from that expected for the atmosphere of Titan. Although a re-analysis of the Titan methane abundance has not appeared. Belton (ref. 81) estimated Jupiter's methane abundance as approximately 5 times smaller than that obtained for Jupiter by Kuiper (ref. 77). As a result of the foregoing work, the presence of methane is accepted, but the amount is uncertain. Of Saturn's satellites, only the diameter of Titan is known within about ten percent and thus only for Titan can the geometric albedo values given by Harris (ref. 35) be accepted with reasonable confidence.

The brightness of Iapetus varies in a regular manner, being brightest at western elongation (refs. 82 and 35). The regularity of this variation is taken as an indication of synchronous rotation. The visual magnitude varies by 2.1 magnitudes. A cross section change in the satellite disk of more than a factor of 6 would be required to explain this variation geometrically. The color of this satellite, as measured by the indexes B-V and U-B, does not change by more than 0.04 over the entire orbit. It is possible that a change in both albedo and cross section is necessary to account for the observed brightness variation.

2.5.2 Meteoroids

No direct evidence exists for establishing the distribution of meteoroids near Saturn. The interplanetary and planetary meteoroid environment has been described in another NASA design criteria monograph (ref. 83). This monograph suggests that at the orbit of Saturn meteoroids of asteroidal origin are not likely to be as important as cometary debris and that estimates of cometary meteoroids on the basis of measurements from the inner solar system will carry an additional uncertainty because of the long-term gravitational influence of the four major planets, Jupiter, Saturn, Uranus, and Neptune.

Cook and Franklin (ref. 34) estimate the space density of meteoroids of cometary origin near Saturn's B ring as 1.5×10^{-24} g cm^{-3}. This value is based on a consideration of observed meteoroids in nearly parabolic orbits. These authors point out that this estimate neglects material in nearly circular circular orbits arising from comets whose perihelia lie beyond the orbit of Saturn.

Computation with the formulas given in reference 83 for cometary meteoroids in the mass range 10^{-6} to 10^{2} grams at the mean orbital distance of Saturn results in a space density that is within a factor of two of that given by Cook and Franklin (ref. 84). Two factors, in addition to the interplanetary number density, will affect the flux of meteoroids encountered by a spacecraft near Saturn. First, the Saturn system can be expected to have captured and held interplanetary meteoroids. Second, the gravity of Saturn will enhance the flux of transient meteoroids passing near the planet. These two factors suggest that the formula given in reference 83 for the cumulative number density in the mass range 10^{-6} to 10^{2} grams be increased by a factor of ten. Then

$$\log S_c = -24.6 \pm 2 - 1.2 \log m$$

where S_c is the number of meteoroids per cubic centimeter with mass greater than mass m expected in the mass range 10^{-6} to 10^2 grams within 600 R_s of Saturn. The uncertainty in this expression is an attempt to account for the limitations involved in extrapolation to the orbit of Saturn. The omnidirectional flux F_c can be computed by

$$F_c = S_c (V_s{}^2 + V_c{}^2)^{1/2}/4$$

where V_s is the speed of the spacecraft and V_c is the speed of the meteoroids, both with respect to Saturn. V_c may be approximated by $V_c = 36\ (R_s/R)^{1/2}$ km/sec. In calculations of the impact effect of cometary particles, the particle density, $\rho_c = 0.5 \times 3^{\pm 1}$ grams/cm^3, should be used. For spacecraft crossing the equatorial plane inside the orbit of Enceladus, $\sim 4R_s$, dominance of ring particles is expected (sec. 2.6.3).

2.6 Saturn's Ring System

Saturn's system of rings is unique in the solar system. The following sections treat the dimensions of the ring system and the nature, size, and distribution of the ring particles. A ring model and its associated uncertainties also are given.

2.6.1 Dimensions of the Ring System

2.6.1.1 Radial Extent

It is convenient to designate the principal rings by letters as has been done historically (ref. 40). The two brightest rings are labeled B and A with A being farther from the planet. Dollfus (refs. 41 and 85) gives a qualitative intensity profile for these rings and a drawing by B. Lyot (ref. 41). This profile indicates that the A and B rings decrease rapidly in intensity at their inner and outer edges and are separated by the Cassini division. Inward toward the planet from ring B, the intensity continues to decrease to about 1.21 R_s. This region between $1.21R_s$ and the inner edge of the B ring is called ring C. The Dollfus (ref. 41) profile indicates a gap at the inner edge of the B ring separating it from the C ring. However, Kuiper, quoted by Alexander (ref. 40), used the 200 inch Hale telescope in concluding that only one division, the Cassini division, exists in the region of the A, B, and C rings and that there is no gap between the rings B and C. It is likely that the decrease in brightness at the inner edge of the B ring creates the impression of a gap at this location. Recently Guerin (ref. 42) with corroboration by B. A. Smith has presented photographic evidence for a ring interior to the C ring and separated from it by a distance roughly equivalent to Cassini's division. Guerin's suggestion for calling this ring the D ring is adopted here because it extends the alphabetic-distance relationship established for the A, B, and C rings. In addition to these four rings, there have been several reports of a ring exterior to ring A (refs. 40 and 43). Although this ring originally was designated as the D ring, such a ring external to the A ring will be referred to here as the D′ ring to avoid confusion with the interior D ring discovered by Guerin.

Brightness variations across the A and B rings have been reported by numerous observers (ref. 40) and are reproduced in the intensity profile by Dollfus (refs. 41 and 85). The best

known of these variations is a decrease in intensity in the outer half of ring A and is called Encke's division. Kuiper, quoted by Alexander (ref. 40), found no variation in brightness in A or B ring greater than 10 to 15 percent and suggested that such variations or intensity contrast effects be called ripples.

Cook et al. (ref. 10) determined the dimensions of the A, B, and C rings from the measurements of previous observers including Dollfus (ref. 86). Where appropriate, irradiation corrections were applied to individual measurements; then the results of the different observers were combined to determine the mean values which are given in column 2 of table V. In this table the radii in arc seconds were converted to kilometers with the ratio for the astronomical unit of 1.49597893×10^8 km $(AU)^{-1}$ given by Melbourne et al. (ref. 1) and to a ratio in equatorial radii with the value $R_s = 59{,}800$ km given in section 2.1.2. Except for the radius of inner C and the width of Cassini's division, the uncertainities given are from Cook et al. (ref. 10). The radius of inner C is difficult to define as the change in intensity at this boundary is considerably less than for the boundaries of the A and B ring. The uncertainty given for the inner radius of C is large enough to include the location of the division noted by Guerin (ref. 42) between the C and D rings.

TABLE V

DISTANCE OF SATURN'S RINGS FROM THE CENTER OF SATURN*

Parameter	Arc Seconds at 9.5388 AU	Kilometers	Equatorial Radii
Saturn Equatorial Radius	8.645 ± 0.05	59,800 ± 350	1.00
Radius of Inner C	10.5 ± 0.5	72,000 ± 3,500	1.21
Radius of Inner B	13.21 ± 0.1	91,400 ± 700	1.53
Radius of Outer B	16.87 ± 0.1	116,700 ± 700	1.95
Width of Cassini's Division	$0.7^{+0.2}_{-0.4}$	$4{,}800^{+1{,}400}_{-2{,}800}$	
Radius of Inner A	17.57 ± 0.1	121,600 ± 700	2.03
Radius of Outer A	19.82 ± 0.1	137,100 ± 700	2.29

*From Cook et al. (ref. 10) based principally on the measurements of See (refs. 87 and 88), Lowell and Slipher (refs. 89 and 90), Dollfus (ref. 86), and Cook and Franklin (ref. 82). The D ring discovered by Guerin (ref. 42) lies between the planet and the inner radius of C ring. The D' ring detected by Feibelman (ref. 43) is taken as extending from the outer edge of A ring to 4.0 R_s.

The radius of the outer B ring was given by Dollfus (ref. 86) as 17 ".05 at 9.539 AU which is one of the largest values reported for this feature (refs. 10 and 40). Dollfus (ref. 86) also reports a direct measurement of the width of Cassini's division as 0.4 "at 9.539 AU. These two results were used to set the asymmetric uncertainty limits given in table V for the width of Cassini's division.

2.6.1.2 Ring Thickness

The thickness of the rings, i.e., the distance normal to the ring plane over which the majority of ring material is found, has been determined most directly from observation of the amoung of reflected light near the time of passage of the Earth through the ring plane. Limits to the ring thickness on this basis have decreased with improved observations (ref. 40). The 1966 triple passage of the Earth through the ring plane led to two new determinations. Focas and Dollfus (ref. 91) gave 2.8 ± 1.5 km for the ring thickness, whereas Kiladse (ref. 92) gave 0.92 ± 0.57 km. These results establish an upper limit of about 5 km for the A and B rings. For regions of low particle density (the interior of the C ring, the D, and D′ rings, and Cassini's division), the thickness could be greater. The actual thickness, even for the A and B rings, is not established by these measurements. The thickness for the A and B rings could be less than even the minimum 0.35 km given by Kiladse (ref. 92).

2.6.2 The Ring Particles

In the 360 years since the first telescopic observation of Saturn's rings, a vast amount of observational material has been collected. The number of sound deductions which can be made concerning the ring particles themselves are few, however.

Spectroscopic determination of the inclination of solar absorption lines in light reflected from the A and B rings established that these rings do not rotate as a rigid sheet (ref. 44). Investigation of ring stability, observations of the occultation of stars by the A and B rings, the shadow of the rings on the planet, and the observation of the planet through the rings have established the particle nature of the ring material (refs. 40, 93, 94, 95, and 96).

It has been suggested for some time that the ring particles consist of H_2O ice (refs. 77, 97, and 98). Recently, excellent infrared reflection spectra (1 to 4μm) have been obtained by Kuiper et al. (ref. 99). Subsequent interpretation by Pilcher et al. (ref. 100) and Kuiper et al. (ref. 71) provides convincing evidence of solid H_2O in the rings. However, the color of the rings in the photometric passbands V and B has led Franklin and Cook (ref. 32) to conclude that H_2O ice is not the only ring constituent. Lebofsky et al. (ref. 72) used photometry in the spectral region 0.3 to 1.05μm for the B and A rings to reach similar conclusions. They suggest the possibility of H_2O-frost-covered silicates or H_2O frost mixed with other compounds and modified by ultraviolet or particle radiation.

The optical thickness, τ, i.e. a measure of the attenuation expected when an object is viewed normally through rings, has been determined for the A, B, and C rings. For the C ring and the inner edge of the B ring, the optical thickness was determined by Cook and Franklin (ref. 82) from observations by E. Barnard of the eclipse of Iapetus by the shadow of these

rings. The values range from $\tau = 0.01$ near the inner edge of ring C to $\tau = 0.18$ near ring B and $0.45 \leq \tau \leq 0.58$ at the inner edge of ring B. The optical thickness for the A and B rings has been estimated by Cook and Franklin (ref. 82) and Bobrov (ref. 96) from occultations of stars by these rings. These reductions indicate the B ring optical thickness is likely greater than that of ring A, and Bobrov (ref. 96) gives a range of τ for ring A from 0.4 to 0.9. Analysis of photometric-photographic observation of the brightness of the A and B rings by Franklin and Cook (ref. 32) and Cook et al. (ref. 10) leads to values of from 0.17 to 0.37 for ring A and 0.32 to 1.0 for ring B. In this analysis (ref. 32), the value $\tau = 1.0$ for the outer portion of ring B was not derived but taken from the foregoing occultation and eclipse results. Lumme (ref. 39), in an analysis of the variation of ring brightness with the elevation angle of the Earth and Sun above the ring plane, obtained an optical thickness of 0.3 for ring A and 1.25 for ring B.

A central question in discussing Saturn rings is the size of the particles. Dominance by particles smaller than 0.1 μm and larger than 5 kilometers can be excluded. Particles less than 0.1μm would show Rayleigh scattering and this has not been observed (refs. 32 and 72). The foregoing limit on the maximum size of the ring particles is based on the ring thickness observations of Kiladze (ref. 92) and Focas and Dollfus (ref. 91).

A number of processes can be expected to alter the form of the ring particles, their number density, and amount. These include meteoroidal impact (refs. 84 and 101), sputtering from solar ultraviolet and proton bombardment (ref. 102), thermal evaporation (ref. 103), and angular momentum decay by the Poynting-Robertson effect (ref. 103). Several of these processes remove material from ring particles, but this material does not necessarily leave the ring as it may reaccrete at another location (ref. 84). Loss processes exist which could eliminate small particles from the rings, but collisions and non-conservative interactions arising from perturbations by the satellites are likely to mitigate this loss. The time scale for such loss is not known nor is the age of the ring system known beyond the 360 years of telescope observation.

Although theories of the origin of Saturn's rings are likely to be important in our understanding of cosmic formation processes, they are at present quite diverse and difficult to substantiate (refs. 40, 104, 105 and 106). For this reason, they do not apply directly to the question of ring particle sizes and numbers.

Variation of the brightness of the A and B rings with phase angle (ref. 32), wavelength (refs. 32 and 72), and elevation angle of the Sun and Earth above the ring plane (ref. 91) has led to a number of estimates of particle size, ring thickness, and particle number density. Theories concerning the increase in brightness of the A and B rings for phase angles less than 1° 30′ have been given by Franklin and Cook (ref. 32) and in articles by Bobrov (refs. 33, 107, 108, 109, 110 and 111). These theories rely on Seeliger's shadowing mechanism (ref. 112) according to which the nearest particles cover their own shadows at opposition and cause the ring to appear brightest, whereas away from opposition, the shadows cast by the forward particles fall on interior particles and decrease the ring brightness. The models developed from this mechanism require that the ring be many particles thick. As an example, model II of Franklin and Cook (ref. 32) is 100 to 300 particles thick. The small

particle inclinations implied in this concept would lead to frequent collisions. The ring could then rapidly evolve to a layer one particle thick (ref. 95). Cook et al. (ref. 10) consider a number of mechanisms for maintaining a ring many particles thick, but none of them are satisfactory for particles greater than 0.1 cm in radius. Theories that consider A and B ring brightness as a function of the elevation angle of the Earth and Sun above the ring plane (refs. 38 and 39) also assume a ring many particles thick so the same objection can be applied to them.

If the opposition brightening cannot be explained in terms of shadowing theory for particles greater than 0.1 cm in radius, then it must arise from the properties of the particles. Oetking (ref. 113) and Hapke (ref. 114) found that an opposition brightening was nearly always present for a variety of laboratory samples. Cook et al. (ref. 10) believe that this effect may be exhibited by the ring particles and may account for all or part of the opposition brightening.

Particles smaller than 0.1 cm require separate consideration because they could exist in a layer many particles thick (ref. 10). Bobrov (ref. 111) considered such particles with radii from 0.71 to 5.3 μm and concluded that backscattering would be insufficient to account for the B ring brightness. However, the Mie theory on which the Bobrov conclusion (ref. 111) rests is not adequate for small particles of arbitrary shape; and, as indicated by Franklin and Cook (ref. 32), the backscatter direction is particularly difficult. The question of particles from 0.1 μm to 0.1 cm must await a full treatment by the techniques of scattering theory (ref. 115).

2.6.3 An Upper Limit Saturn Ring Model

At present it is not possible to construct a unique ring model even for the best-studied A and B rings. The approach taken here will be to develop a simple ring model which conservatively estimates the hazard to a spacecraft crossing the ring plane.

In constructing this model, the ring particles will be assumed to lie in a single plane. The quantity $[1 - \exp(-\tau)]$ will then represent the fraction of ring area obscured by particles when the ring is viewed normally and be related to the number of particles per unit area. The selected values of optical thickness τ are plotted in figure 8, and sample values are tabulated in table XIX.

The values for A, B, and C rings were obtained from Cook and Franklin (ref. 82), Cook et al. (ref. 10), and Bobrov (ref. 96). The D ring values were estimated from those given for the interior portion of the C ring by Cook and Franklin (ref. 82). In this region no account was taken of the gap between C and D discovered by Guerin (ref. 42) because its position and width are not well established. In accordance with Feibelman (ref. 43), the D′ ring is extended to a distance of 4 R_s. Other observations of the D′ ring (refs. 40 and 116) place it inside the orbit of Mimas (3.1 R_s) and near the outer edge of ring A. In addition, Cook et al. (ref. 10) indicate that ring particle orbits, stable against perturbations from Saturn's satellites, exist just outside ring A. For these reasons the greatest D′ optical thickness was chosen in the region from the outer edge of A to 2.8 R_s. Beyond 2.8 R_s, the optical

thickness was taken as decreasing linearly to the value 0.01 at 4 R_s. The minimum in the center of Cassini's division was taken as 0.02. Beyond 4 R_s, τ is taken as zero and the only particles expected are meteoroidal (sec. 2.5.2).

For the A, B, and D' rings, the relative number of particles with radius r between r and r + dr is taken from the following power law relation

$$dN_1 = A_1 r^{-2.5}\, dr$$

where $0.1 \leq r \leq 10^5$ cm. The form of this expression was taken from Bobrov (refs. 107 and 108); both the exponent of r and the range of r were chosen to emphasize the possibility of large particles (ref. 10). The constant A_1 is evaluated by requiring that the integral of dN_1 over the range equals 1. Then $A_1 = 4.74 \times 10^{-2}\ cm^{3/2}$.

Cook et al. (ref. 10) suggest that the material in ring C is likely to consist of spalled material from the A and B rings. These authors point out that although the C ring is fainter than the A ring, the optical thickness is comparable in some regions. For these reasons Cook et al. suggest a range of particle sizes in C ring from 10^{-3} to 0.1 cm. This suggestion is adopted for both the C and D rings (with the same form used for expressing the relative number density for rings A, B, and D') and is given by

$$dN_2 = A_2\, r^{-2.5}\, dr$$

where 10^{-3} cm $\leq r \leq 0.1$ cm. The same normalization procedure is used as in the preceding evaluation of A_1. Then $A_2 = 4.75 \times 10^{-5}\ cm^{3/2}$.

A fraction of the particles in rings C and D could be larger than 0.1 cm. For rings C and D, the fraction f of the projected particle area occupied by such particles will be taken as 0.1 (f = 0.1).

With these assumptions, the number of particles can be related to $\tau(R)$ through the use of two intermediate constants k_1 (R) and k_2 (R), defined by

$$\left.\begin{aligned} [1 - \exp(-\tau(R))] &= k_1(R) \int_{0.1}^{10^5} \pi r^2 dN_1 \\ k_2(R) &= 0 \end{aligned}\right\} \text{ for B, A, D'}$$

$$\left.\begin{aligned} f\,[1 - \exp(-\tau(R))] &= k_1(R)\int_{0.1}^{10^5} \pi r^2\, dN_1 \\ (1-f)\,[1 - \exp(-\tau(R))] &= k_2(R)\int_{10^{-3}}^{0.1} \pi r^2\, dN_2 \end{aligned}\right\} \text{ for C, D}$$

Values for k_1 (R) and k_2 (R) at selected distances from the planet are listed in table XIX.

Over the entire region of the rings, the number of particles, $S_r(r > r_i)$, with radius r greater than r_i is given by

$$S_r(r > r_i) = k_1(R)\int_{r_i}^{10^5} dN_1 + k_2(R)\int_{r_i}^{0.1} dN_2$$

where r_i is in centimeters. The first integral is replaced by 1.0 when $r_i \leq 0.1$ cm and the second integral is replaced by 0 for $r \geq 0.1$ cm. The number of particles, $S_m(m > m_i)$, with mass m_i is given by

$$S_m(m > m_i) = S_r[r > r(m_i)]$$

where r (m_i) is the radius of a spherical particle with mass m_i, i.e.,

$$r_i(m_i) = (3\, m_i/4\, \pi\, \rho_p)^{1/3}$$

with ρ_p the individual particle density.

The cumulative mass distribution can then be written as

$$S_m\,(m > m_i) = k_1(R)\underbrace{3.16 \times 10^{-2}\left\{2.05\left(\frac{\rho_P}{m_i}\right)^{1/2} - 3.16 \times 10^{-8}\right\}}_{①}$$

$$+\; k_2(R)\underbrace{3.17 \times 10^{-5}\left\{2.05\left(\frac{\rho_P}{m_i}\right)^{1/2} - 31.6\right\}}_{②}$$

where the underlined expression ① is set equal to 1.0 when $r_i(m_i) \leq 0.1$ cm and the underlined expression ② is set equal to zero when $r_i(m_i) > 0.1$ cm. The particle density and mass must be in the same units. A range of particle densities have been suggested which depend on assumed particle composition and structure (refs. 10 and 84). Because only the presence of H_2O ice is established (section 2.6.2), the range here is taken as $\rho_p = 1 \times 4^{\pm 1}$ gram cm^{-3}. This range includes the densities suggested by Kessler in reference 83 for both cometary and asterodial meteoroids.

For a spacecraft crossing the ring plane inside $4R_s$, the relative velocity (or impact velocity) $\vec{V}_{rel}$ of the particles with respect to the spacecraft is given by

$$\vec{V}_{rel} = \vec{V}_s - \vec{V}_p$$

where $\vec{V}_s$ is the velocity of the spacecraft and $\vec{V}_p$ is the velocity of ring particles both with respect to a Saturn-centered coordinate system. The velocity of the ring particles should be taken as being in the equatorial plane and perpendicular to a radius vector. The speed of the ring particles $|\vec{V}_p|$ is given by

$$|\vec{V}_p| = 25.2\,(R_s/R)^{1/2} \text{ km sec}^{-1} .$$

The actual ring thickness (2.6.1.2) is not known although almost all ring particles are expected to lie within 5 km of the equatorial plane. For the purpose of computing the area swept out in crossing the ring plane, the model developed above should be used as though all particles were in a single plane. The area swept out will then be given by

$$\left| \frac{\vec{A}_s \cdot \vec{V}_{rel}}{V_{sz}} \right|$$

where A_s is the spacecraft area of interest with the direction established from the outward normal to this surface, V_{sz} is the component of the velocity of the spacecraft normal to the ring plane, and the vector dot product $\vec{A}_s \cdot \vec{V}_{rel}$ must be negative.

Taken as a whole, the foregoing model conservatively estimates the hazard to a spacecraft crossing the ring plane. It is unlikely that the optical thickness anywhere in the ring system is a factor of 3 greater than the values plotted in figure 8. Such an increase in optical thickness would span all optical thickness determinations from the sources given in the section 2.6.2. The form for the number distribution and the range of particle radii were selected deliberately to emphasize the possibility of large particles. Particles of the order of 1 km, even if composed entirely of H_2O ice, would be stable anywhere within the ring system (ref. 117).

If the particle radii are considerably less than 0.1 cm, the assumptions made in constructing the foregoing ring model lead to a gross overestimate of the hazard to a spacecraft crossing the ring plane. A ring system composed entirely of small particles is a possibility, but the literature is too incomplete and contradictory to construct such a model with confidence.

Therefore, the model presented herein should be used as an upper limit to the expected hazard.

2.7 Charged Particles

2.7.1 Galactic Cosmic Rays

As observed near the Earth, galactic cosmic ray intensities are modulated by the interplanetary magnetic field. In general, it is expected that this modulation reduces the intensities more severely at lower energies, closer to the Sun, and during intervals of greater solar activity. Quantitative predictions of the intensities near Saturn have not been made on this basis because it is not known whether the solar-interplanetary magnetic field boundary occurs inside or beyond Saturn's orbit. Saturn's own magnetic field also may further reduce the intensities, particularly at low energies and low magnetic latitudes. Therefore, the approach adopted here is to specify fluxes in the energy range observed (0.1 to 10^{10} GeV) between zero and a spectrum extrapolated from the highest energies observed for the most abundant particle kinds at times near minimum solar activity. This spectrum can be approximated for the flux of particles with kinetic energy greater than E by

$$\phi_E = K(E + m_0c^2)^{-1.5}$$

where m_0c^2 is the rest energy of the particle and E is the particle kinetic energy in GeV (both m_0c^2 and E in GeV per nucleon for alpha-particles). The summary given by Haffner (ref. 118, fig. 2-3) specified $K \simeq 2.5$ cm^{-2} sec^{-1} for protons and $K \simeq 0.25$ cm^{-2} sec^{-1} for alpha-particles, whereas Fanselow (ref. 119) specifies $K \simeq 0.02$ cm^{-2} sec^{-1} for electrons.

2.7.2 Solar Protons

Protons of energy >1 MeV constitute an important component of the solar cosmic rays. Their intensity near the Earth varies over several orders of magnitude, has both directional and isotropic components, and is correlated positively with solar flare activity. The intensity variation with heliocentric distance S has not been measured, but simple geometric considerations suggest an S^{-2} dependence, according to Burlaga (ref. 120). In particular, a boundary could exist inside the orbit of Saturn near which some of the protons are reflected or diffused. Because the phenomena are sporadic and incompletely explained, the fluxes adopted here are between 0 and 1.0 times the near-Earth values specified in NASA TR R-169 (ref. 121).

2.7.3 Solar Wind

Properties of the solar wind are summarized by Hundhausen (ref. 122). On the basis of data from Mariner spacecraft at distances S from the Sun in the range 0.8 to 1.5 AU, protons and electrons have observed concentrations of approximately 8 S^{-2} cm^{-3} for S in AU and are streaming radially away from the Sun at speeds near 320 km/sec during quiescent solar conditions. Increased solar activity results in temporary increases up to factors of 10 in the concentration and 3 in the speed. The applicable theory suggests that the extrapolation of

these conditions on the basis of heliocentric distance to the orbit of Saturn is justified in the absence of evidence of a boundary which might terminate the solar wind at less than 9 AU. NASA SP-8017 (ref. 147) specifies a nominal value of 6 nT and a range of 2 to 40 nT for the total interplanetary field at 1 AU from the Sun. Therefore, the parameters given in table VI are adopted where minimums are at zero and the tangential interplanetary field is scaled as S^{-1} and its radial component as S^{-2} with S=9.54 AU.

TABLE VI

PARAMETERS OF THE SOLAR WIND NEAR SATURN

Parameter		Minimum	Nominal	Maximum
Concentrations of electrons and protons (cm^{-3})		0	0.09	0.9
Velocity (directed radially from Sun) (km/sec)		0	320	960
Interplanetary Magnetic Field	Tangential (nT)	0	0.44	3
	Radial (nT)	0	0.047	0.3
	Total (nT)	0	0.045	3

2.7.4 Trapped Radiation Belts

On the basis of observations of non-thermal UHF radiation, Jupiter is known to have extensive trapped radiation belts with relativistic electrons (refs. 13 and 14). Observations of UHF radiation likewise form the basis for discussing trapped radiation belts near Saturn.

2.7.4.1 Background

The sources of information describing Saturn's UHF emission are given in table IV. The available results of polarization, spectrum, and source extent measurements are pertinent here. Table VII compares these characteristics with those for Jupiter. Two questions are fundamental to the problem of associating trapped radiation belts with Saturn UHF observations. Are trapped radiation belts necessary to explain the observed UHF emission characteristics and do the UHF emission characteristics limit the properties of such belts?

Among the source mechanisms suggested for planetary UHF emission, four are appropriate for consideration (ref. 123): (a) thermal radiation from an ionosphere, (b) thermal radiation from the atmosphere, (c) cyclotron radiation from trapped charged particles, (d) synchrotron radiation from trapped charged particles.

TABLE VII

COMPARISON OF SELECTED UHF RADIATION DATA FOR JUPITER AND SATURN

JUPITER			SATURN		
Reference	Wavelength	Characteristic	Characteristic	Wavelength	Reference
Carr & Gulkis (ref. 13)	10-100 cm	22% linear polarization (approx. east-west)	20 ± 8% linear polarization (approx. north-south) <10% linear polarization	9.4 cm —	Rose et al. (ref. 19) Section 2.3.1.1 (refs. 20-24)
Berge (ref. 69)	10.4 cm	Most emission definitely external to disk	Emission confined to disk	11.3 cm	Kellerman (ref. 21)
Branson (ref. 20)	21 cm	Same as above	No more than 10% of emission is external to disk	10.7 cm	Berge & Read (ref. 22)
Gulkis (ref. 124)	74 & 128 cm	Same as above			
Carr & Gulkis (ref. 13)	10-100 cm	Flux at 4.04 AU – $(6.7 \pm 1) \times 10^{-26}$ watts $m^{-2} Hz^{-1}$	Flux at 8.54 AU – 0.26×10^{-26} watts $m^{-2} Hz^{-1}$ $\leqslant 0.05 \times 10^{-26}$ watts $m^{-2} Hz^{-1}$	10.7 cm 73.5 cm	Berge & Read (ref. 22) McAdam (ref. 68) and Gulkis et al. (ref. 67)
Mayer (ref. 125)	3.15 cm 10.3 cm 68 cm	Brightness temperature* 140° K 640° K 50,000° K	Brightness temperature* 137 ± 12° K 172 ± 20° K 1690 ± 430° K	3.12 cm 10.7 cm 73.5 cm	Berge (ref. 23) Berge & Read (ref. 22) McAdam (ref. 68)

* All flux assigned to disk

McAdam (ref. 68) and Gulkis et al. (ref. 67) have considered the ionosphere mechanism and find that a density of 3×10^7 electrons/cm^3 throughout a 1000 km altitude interval would explain the observations, but they exclude the mechanism from further consideration because the required conditions are so extreme as to be very unlikely.

Welch et al. (ref. 60) have considered the atmosphere quantitatively as the UHF source at 1.53 cm. They calculated the saturated ammonia opacity and temperature structure in Kuiper's 1952 model b atmosphere and predicted a brightness temperature of 143°K which agrees well with the observed value of 141 ± 15°K (table IV, sec. 2.4.5). Gulkis et al. (ref. 67) used Kuiper's 1952 model b and various assumptions about the ammonia mixing ratio and opacity in considering the wide wavelength interval 4 to 300 cm. In spite of the uncertainties involved, which are particularly severe at high pressures and long wavelengths, the qualitative agreement between the calculated and observed spectrum was striking. The relevant conclusion is that an atmospheric thermal source could be responsible for all of the characteristics of the UHF radiation with the exception of the polarization reported by Rose et al. (ref. 19) which has not been confirmed by subsequent observations.

Cyclotron radiation requires strong magnetic fields to be responsible for the UHF radiation, namely 10^{-1} T (10^3 gauss) at 10 cm and 10^{-2} T (100 gauss) at 100 cm. Further measurements of source polarization and extent would be required to distinguish it from synchrotron radiation. Because of the high field strengths required and because synchrotron radiation is responsible for Jupiter's UHF emission, cyclotron radiation is not considered further as a source for Saturn's UHF radiation.

The possibility that synchrotron radiation is responsible for Saturn's UHF emission can be discussed comparatively with respect to Jupiter on the basis of table VII and the thorough analyses of the Jupiter situation published by Carr and Gulkis (ref. 13) and Warwick (ref. 14). Strong linear polarization of the UHF emission supports the synchrotron mechanism in Jupiter's case, but for Saturn all polarization measurements (sec. 2.3.1.1) set upper limits of 10 percent except that of Rose et al. (ref. 19) which is discounted here. This neither confirms nor denies the mechanism because the polarization depends on the electron pitch angle distribution which in some circumstances could yield a null polarization measurement for the source as a whole.

Another characteristic of Jupiter's synchrotron emission is that the emission regions do not coincide with the planetary disk. Although polarization and extent measurements have not been reported for Saturn at wavelengths longer than 11.3 cm., the strongly negative results cited in table VII limit the synchrotron emission to a fraction of the total near 10 cm. If that fraction is taken as 10 percent (ref. 22), then the upper limit synchrotron flux from Saturn's trapped radiation belts is 0.03×10^{-26} watts m^{-2} Hz^{-1} at 10.7 cm wavelength and a distance of 8.54 AU. If the radiation from Jupiter is scaled to Saturn's distance and volume, the flux is

$$\left[\frac{4.04}{8.54}\right]^2 \times \left[\frac{5.98}{7.14}\right]^3 6.7 \times 10^{-26} \text{ watts m}^{-2}\text{ Hz}^{-1} = 0.9 \times 10^{-26} \text{ watts m}^{-2}\text{ Hz}^{-1}$$

at 10.7 cm. Thus, even at this wavelength with all of Saturn's UHF emission considered as synchrotron, Saturn is a weaker synchrotron emitter than Jupiter.

At other wavelengths, table VII shows that Saturn's brightness temperature increases only mildly with wavelength if all the flux is ascribed to the disk, whereas Jupiter's brightness temperature increases sharply. However, a flat synchrotron spectrum in terms of flux (like Jupiter's) at 0.03×10^{-26} watts $m^{-2} Hz^{-1}$ from 10 to 100 cm would be consistent with the Saturn observations.

The conclusions adopted herein are (1) that the UHF radiation characteristics observed for Saturn do not require radiation from trapped charged particles for an explanation because thermal radiation from a deep atmosphere suffices and (2) that observed UHF radiation limits the synchrotron emission from any existing radiation belts to approximately 0.05×10^{-26} watts $m^{-2} Hz^{-1}$ at all decimetric wavelengths and at a distance of 8.54 AU from the observer.

2.7.4.2 Radiation Belt Characteristics

To place an upper limit to the possible radiation belts for Saturn, the model developed for Jupiter by Warwick (ref. 14) and Divine in NASA SP-8069 (ref. 126) has been modified. There are various others which might have been used, e.g., Branson (ref. 70) and Carr and Gulkis (ref. 13), but the results would not be an order-of-magnitude different. Numerous authors, e.g., Drake (ref. 65), have suggested that Saturn's rings could effectively depopulate any radiation belts at $L \leq 2.3$ through accretion and Coulomb scattering which would result in pitch angle changes and subsequent loss by collision with atmospheric molecules. Because the peak emission of Jupiter's belts falls at $L < 2$ in the magnetic equatorial plane, it is clear that Saturn's belts, scaled from Jupiter and cut off for $L < 2.3$, would exhibit considerably reduced fluxes compared to Jupiter, in accordance with observations (sec. 2.7.4.1).

The model is described for both protons and electrons by the flux ϕ_E of particles with energy greater than E (for $E \geq 1$ MeV) as follows

$$\phi_E = \phi_0 (1 + E/E_0) \exp(-E/E_0)$$

where the characteristic energy E_0 and flux parameter ϕ_0, appropriate for $L \geq 2.3$, are given in table XX and ϕ_0 should be set equal to zero for $L < 2.3$. The latitude dependence and pitch angle distribution have been omitted from this model because the orientation of a possible Saturn dipole magnetic field is unknown.

Without specific knowledge of the magnetic axis orientation, it is appropriate that the magnetic shell parameter L in the formulas given be interpreted simply as the chronocentric distance in units of Saturn's equatorial radius R_s (sec. 2.1.2). The lower limit concentration is zero.

For Jupiter, the model in NASA SP 8069 (ref. 126) is appropriate only for energies greater than 1 MeV so it is reasonable to accept the same limit for the Saturn. At lower energies the trapped radiation belt concentration is limited by the capacity of the magnetic field to trap the heavy ion (proton) component and force its corotation. That limit, derived from simple energy considerations, is specified by

$$N_E \leq \frac{5.5 \times 10^{15}}{[E + (0.52) L^2] L^6} \text{ cm}^{-3}$$

for E in eV, and is ample because the upper limit magnetic dipole strength (sec. 2.3.1) has been used. In addition, N_E is almost certainly less than 10^7 cm^{-3} everywhere for both electrons and protons. This is an ample ionospheric electron density which is estimated in section 2.7.6.

2.7.5 Magnetospheric Plasma

Because Saturn's magnetic field (sec. 2.3.1) is unknown, few articles dealing with Saturn's magnetosphere have been published. Its sunward boundary could be as near to the planet as the ionosphere (small magnetic field and peak solar wind) or further away than 240 R_s (upper limit magnetic field and nominal solar wind). Thus, broad limits are appropriate for the description of its magnetospheric plasma as well. For the temperature, the limits adopted are 100°K (associated with the ionosphere sec. 2.7.6) and 10^5 °K (a hot plasma estimate for Jupiter by Papadopoulos and Lerche, ref. 127). The lower concentration limit for both electrons and protons is zero (no magnetosphere); the upper limit is 10^7 cm^{-3} (associated with the ionosphere, sec. 2.7.6) or 10^{16} cm^{-3} L^{-8} (the maximum concentration capable of corotation in the upper limit magnetic field per sec. 2.3.1). The two upper limits are equal at L = 13.

2.7.6 Ionosphere

No data observed for Saturn have been related to characteristics of its ionosphere. Theories pertaining to Jupiter's ionosphere have been published, but the conclusions have not been applied to Saturn. Peak electron and proton densities of $10^{6 \pm 1}$ cm^{-3} derived for Jupiter by Gross and Rasool (ref. 128) and Hunten (ref. 129) may be representative for Saturn as well and ionosphere temperatures close to the exospheric values (100 to 200°K) derived by McGovern (ref. 130) for Saturn are also reasonable. If the solar UV radiation responsible for the maintenance of the ionosphere is absorbed principally at the same optical depth at Saturn as at Jupiter, the corresponding pressure level will be 2.5 times smaller (the ratio of the surface gravities). Thus, the 3 dyn/cm^2 level appropriate for Jupiter (ref. 128) suggests 1 dyn/cm^2 as a reasonable gas pressure at the peak of the ion and electron concentration. The ionosphere scale height on Saturn should be 2.5 times that for Jupiter, near 250 km. Therefore, the description adopted herein for Saturn's ionosphere has temperature 150 ± 50°K and equal electron and proton concentrations given by $N_o = 10^{6 \pm 1}$

$\exp\left[-\frac{z - z_1}{250}\right]$ cm^{-3} for $z > z_1 = 450 \pm 200$ km, and $N_0 = 0$ for $z < z_1$. The range of values for z_1 is large enough to include a few different ionospheric layers of local maximum electron density, a situation to be expected on the basis of Earth analogy.

2.8 Atmospheric Composition and Structure

Observations of Saturn have not indicated the presence of a solid surface. In the absence of such a reference level the region considered in this section will be taken to extend outward from the level at which the total pressure equals 10^3 atmospheres to 10^{-7} atmospheres. The following paragraphs will discuss the composition, pressure, temperature, density, and related atmospheric quantities expected in this region and conclude with a presentation of three atmospheric models.

2.8.1 Composition

Two molecules, molecular hydrogen (H_2) and methane (CH_4) have been detected unambiguosly in the atmosphere of Saturn, according to Owen (ref. 131), Bless et al. (ref. 34), Spinrad (ref. 132), and Kuiper (ref. 77). An upper limit on the amount of ammonia (NH_3) was reported by Kuiper (ref. 77). Subsequent investigators, Spinrad (ref. 132), Giver (ref. 133), and Moroz (ref. 134), have not detected spectral features which could be attributed solely to NH_3. Radio brightness temperature observations (refs. 58 and 67) have provided indirect evidence of the existence of NH_3 at levels in the atmosphere which are inaccessible in the visual and photographic infrared. No other molecular or atomic species has been detected in the atmosphere of Saturn.

Summaries of current estimates of the abundance of atoms and molecules in Saturn's atmosphere (refs. 49, 131, and 135) are subject to large uncertainties because of difficulties with the observation and interpretation of the absorption spectra on which the abundance values are based.

Because of the foregoing limitations, the approach here will be to assume that the composition is essentially solar, formed into the simplest molecules expected in a hydrogen-reducing atmosphere. The abundance of elements in the Sun is from the compilation given by Lewis (ref. 136), and the expected number and mass fraction of the atoms and molecules are designated in table VIII as nominal. Account of the uncertainty in atmospheric composition is provided by two additional models given in table VIII (labeled Cool and Warm), derived from the nominal model by considering the mass fraction of helium to be uncertain by a factor of two and the mass fraction of the constituents other than hydrogen and helium to be uncertain by a factor of 3.

Only species whose number is greater than 0.01 percent are considered in table VIII. For some purposes, estimates of constituents present in trace amounts are necessary. Lewis (ref. 136) has provided a study of the compounds expected in the atmosphere of Jupiter which can be applied to Saturn in conjunction with the models presented here without major modification.

2.8.2 Structure

Recent infrared measurements by Aumann et al. (ref. 51) indicate that Saturn radiates more than twice as much energy as it receives from the Sun. In an atmosphere where the opacity is large, energy transport from an internal source by radiation alone is likely to require a temperature gradient favorable to convection. The idea of a convective lower atmosphere is strengthened by the qualified success of models of Saturn's interior by Peebles (ref. 137) and Hubbard (ref. 138) which assume convection to great depth.

For the models constructed here, the lower atmosphere will be assumed to be in convective equilibrium with a near adiabatic gradient. The temperature minimum at the top of the lower atmosphere will be taken near the gray atmosphere radiative equilibrium boundary value given by $(0.5)^{1/4}\ T_e$. The value of effective temperature T_e determined by Aumann et al. (ref. 51) is 97° ± 4°K. This temperature is sufficiently low that NH_3, H_2O, and possibly CH_4 will condense at altitudes below the tropopause. Although the visual appearance of Saturn is considerably more uniform than Jupiter, spots and changes in belts and zones do occur (refs. 40 and 139) which indicate the presence of clouds. The occurence of such condensing material will alter the temperature gradient from its "dry" value. An analysis of the change expected for cloud formation of Jupiter has been given by Lewis (ref. 140). For Saturn, the expected variation in lapse rate from condensates is not significant in comparison to other uncertainties.

The structure of the adopted convective lower atmosphere can be determined if a temperature-pressure correspondence is established at a common point. Absorption spectra used in abundance determinations can be used to yield the pressure and temperature in the region of line formation. These values are even more uncertain than abundance determinations and have been given for H_2 only by Owen (ref. 131). A different approach has been suggested by Gillet et al. (ref. 141) in an analysis of the Jupiter spectrum in which the pressure corresponding to a 12 μm brightness temperature is calculated by assuming H_2 is the sole source of opacity. This suggestion is adopted herein and is strengthened by the work of Trafton and Münch (ref. 142) which indicates that NH_3, the other possible opacity source at wavelengths longer than 12 μm, will produce negligible absorption at temperatures less than 115°K. The brightness temperatures measured by Low (refs. 47, 48 and 50) and Aumann et al. (ref. 51) in the range from 7.5 to 50 μm indicate a temperature near 95°K which is adopted herein. The pressure corresponding to optical depth unity at 14 μm is computed by using the H_2 pressure-induced dipole absorption coefficients given by Trafton and Münch (ref. 142) and the nominal model composition of table VIII. This leads to a pressure of $0.3 \times 2^{\pm 1}$ atm. The uncertainty arises from an assumed uncertainty factor of two in both the absorption coefficient and pressure scale height with the pressure being inversely proportional to the square root of the product of the absorption coefficient and scale height. This range, 0.15 to 0.6 atm, is used to establish the correspondence level pressure for the limiting models shown in table VIII.

No measurements which lead to a definition of the temperature and pressure structure above the tropopause have been published. Considerable analysis of this region has been carried out for Jupiter by Gross and Rasool (ref. 128), Hunten (ref. 129), and Lewis and

Prinn (ref. 143); and the main features of their arguments are relevant to Saturn. In this region, only H_2, He, CH_4, and their photochemical products are likely to be important; H_2O and NH_3 have been removed by condensation below the tropopause. If only H_2 and He are important opacity sources, Trafton's 1967 non-gray model atmospheres (ref. 144) indicate that this region will be nearly isothermal. When CH_4 is added and consideration is given to photo-chemical processes and energy deposition by solar heating at wavelengths shorter than 2000 Å, there is a possibility of a positive temperature gradient at some level above the tropopause. This level, called the mesopause, is marked by a change in the dominant energy transport process from radiation immediately below the mesopause to conduction above. Hunten (ref. 129) indicates that there is observational and theoretical evidence for a temperature inversion in the upper atmosphere of Jupiter. McGovern (ref. 130) indicates a range of values in the upper atmosphere of Saturn from 109 to 172°K which depend on mesopause composition and solar cycle. Although McGovern does not establish an upper atmosphere temperature-pressure correspondence or temperature gradient, a mesopause density of 1×10^{14} molecules per cm^{-3} is given. From the foregoing studies, a temperature inversion in Saturn's upper atmosphere is considered possible. Therefore, two of the models adopted herein incorporate an upper atmosphere temperature inversion.

2.8.3 Atmosphere Models

2.8.3.1 Existing Models

Two sets of atmospheric models for Saturn exist in the literature, a pair by Kuiper (ref. 77) and trio by Trafton (ref. 144). These sets differ in basic assumptions and method of construction. When Kuiper's models were constructed in 1952, the dominant source of thermal opacity H_2 had not been identified and its abundance was unknown. The lower atmosphere was assumed convective with an adiabatic gradient to the tropopause above which the atmosphere was taken as isothermal. These models consisted basically of H_2 and He and the temperature-pressure correspondence in the lower atmosphere was obtained from the existing abundance measurements of NH_3 and CH_4. The stratosphere temperature was set at 64°K on the basis of a 76°K theoretical estimate of the effective temperature. Although the basic features of Kuiper's models are still valid, the intervening 18 years have produced questions about the NH_3 and CH_4 abundance measures. In addition, recent improvements in infrared techniques have lead to the Aumann et al. (ref. 51) effective temperature estimate of 97°K which is considerably larger than Kuiper's estimate of 76°K.

Trafton (ref. 144) constructed three non-gray model atmospheres for Saturn with H_2 as the dominant source of thermal opacity. The effective temperatures of the three models were taken as 80°K, 90°K, and 100°K. Convection was indicated in the lower atmosphere and this was added as a correction to Trafton models. The stratosphere in these models is nearly isothermal as no additional source of opacity was assumed for this region. These models incorporate the only radiative analysis of the transition region from lower to upper atmosphere.

2.8.3.2 Basis for Design Models

No complete tabulation of the composition, pressure, temperature, density, scale height, and other atmospheric parameters exists which indicates the range of values possible for the Saturn atmosphere. Therefore, new models of Saturn's atmosphere were constructed. Table VIII lists the composition and other parameters used in model development. Hydrostatic equilibrium and the ideal gas law were assumed. Clouds and cloud properties obtained from these models are discussed separately in section 2.9. The lower atmosphere is assumed convective with a lapse rate dependent on composition without taking into account changes from condensation or radiative effects near the tropopause. With the foregoing assumptions, the temperature and pressure in the lower atmosphere are related by $(P/T)\,(dT/dP) = \beta$. The lapse rate β depends on temperature through the specific heat of the atmosphere's constituents. For hydrogen-rich atmospheres at low temperatures, this change is important and was incorporated in the models by representing β with a simple analytic form $\beta = \beta_o\,(T + K_1)/(T + K_2)$. For the nominal model, the specific heats of hydrogen as a function of temperature provided by Trafton (ref. 144) and the *Handbook of Chemistry and Physics* 1958-59 were used to evaluate the three constsnts β_o, K_1, K_2. For the cool and warm models these constants were selected to provide a range of β.

2.8.3.3 Presentation of Design Models

The values for pressure, temperature, density, β, dT/dz, pressure scale height, and density scale height for each model are given in tables XXII, XXIII, and XXIV. Plots of pressure versus temperature, pressure versus density, and altitude versus pressure are given in figures 1, 2, and 3. Interpolation between values given in the tables should be made with the aid of the equations given in appendix B-1. The full set of equations relating atmospheric quantities can be found in appendix B-1.

The nominal model is characterized by solar type composition, mean molecular weight of 2.27 gm mole $^{-1}$, acceleration of gravity of 1050 cm/sec^2, and effective temperature of 97°K. The lower atmosphere ends at the tropopause whose temperature is taken as 77°K. Above the tropopause, the atmosphere is taken as isothermal upward for two pressure scale heights above which a constant lapse rate is assumed that is compatible with a temperature of 109.7°K at the 10^{-6} atm pressure level.

The cool and warm models are constructed as limiting cases. The labels were chosen to indicate that at a given pressure, the cool model possesses the lowest temperature and the warm model the highest. The molecular weight and acceleration of gravity were chosen to provide the maximum range in pressure scale height, being smallest for the cool and largest for the warm. The correspondence level pressure and temperature reflect the uncertainties in the model construction and preserve the cool, warm sense of the limiting models. Above the tropopause, the cool model is assumed isothermal and the warm model temperature increases to 170°K at the 10^{-6} atm pressure level. For all three models the tropopause temperature is taken a few degrees below the value obtained from $(0.5)^{1/4}\,T_e$ as suggested by Trafton's (ref. 144) non-gray atmosphere solutions. The zero of altitude is taken at a pressure of 1 atm for all models.

TABLE VIII

PHYSICAL PARAMETERS FOR SATURN MODEL ATMOSPHERES

Parameter		Cool Model	Nominal Model	Warm Model	Units
Fraction by Mass	H_2	0.55279	0.78514	0.89550	
	He	0.39474	0.19737	0.09868	
	H_2O	0.02484	0.00828	0.00276	
	CH_4	0.01332	0.00444	0.00148	
	Ne	0.00360	0.00120	0.00040	
	NH_3	0.00339	0.00113	0.00037	
	Others	0.00732	0.00244	0.00081	
		1.00000	1.00000	1.00000	
Fraction by Number	H_2	0.72996	0.88572	0.94679	
	He	0.26251	0.11213	0.05254	
	H_2O	0.00367	0.00105	0.00033	
	CH_4	0.00221	0.00063	0.00020	
	Ne	0.00047	0.00013	0.00004	
	NH_3	0.00053	0.00015	0.00005	
	Others	0.00065	0.00019	0.00005	
		1,00000	1.00000	1.00000	
Mean Molecular Weight μ		2.66	2.27	2.13	grams/mole
Acceleration of Gravity g		1250	1050	850	cm/sec^2
Effective Temperature Te		91	97	103	°K
Troposphere					
$(P/T)(dT/dP)=\beta_0(T+K_1)/(T+K_2)$					
	β_0	0.220	0.234	0.288	
	K_1	97	484	450	°K
	K_2	71	282	324	°K
Correspondence Level Temperature		95	95	95	°K
Correspondence Level Pressure		0.6	0.3	0.15	atm
Tropopause Temperature		72	77	82	°K
Stratosphere Extent		∞	2	0	pressure scale height (H_p)

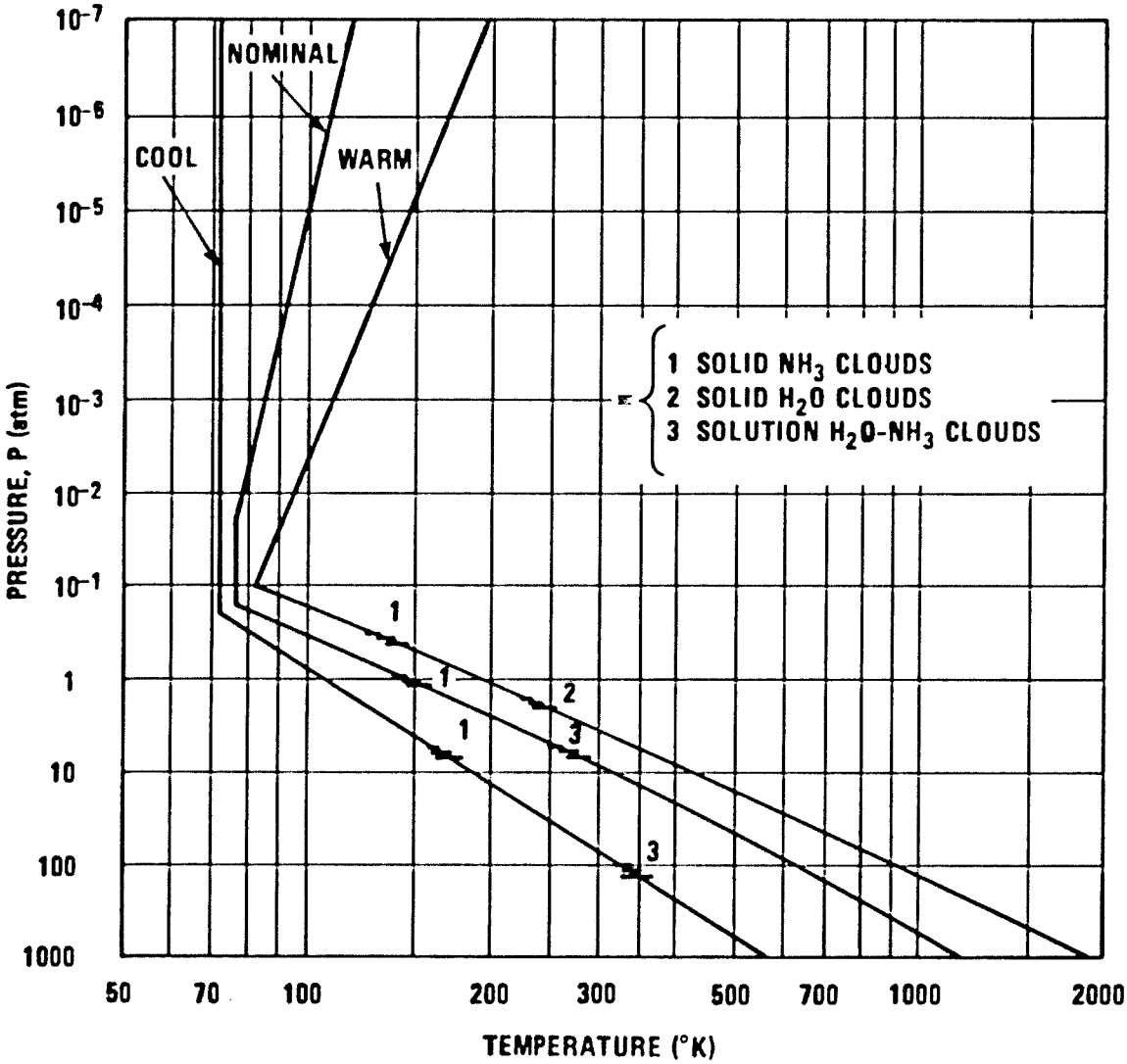

Figure 1.—Pressure vs temperature and cloud levels for Saturn Model Atmospheres.

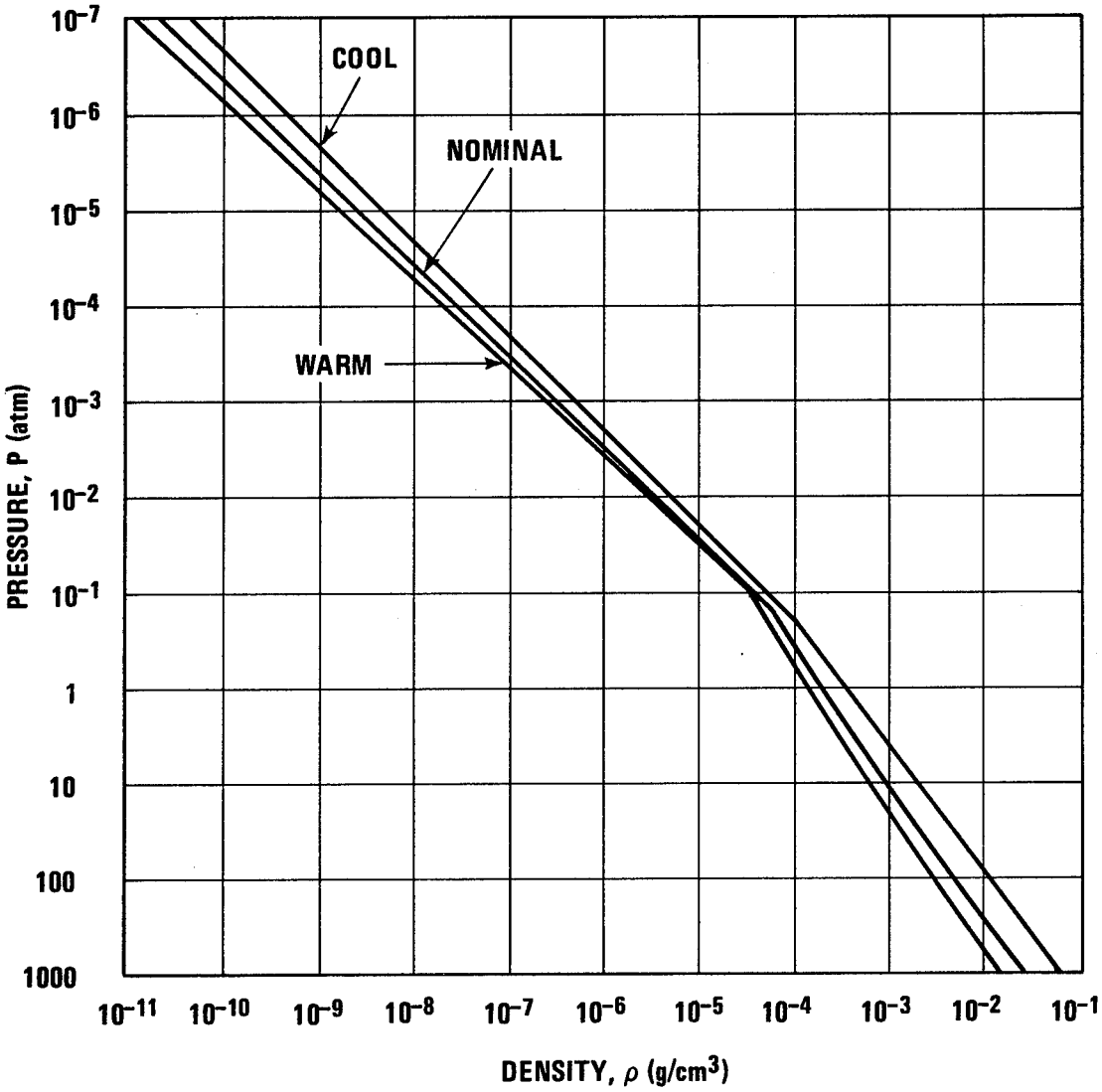

Figure 2.—Pressure vs density for Saturn Model Atmospheres.

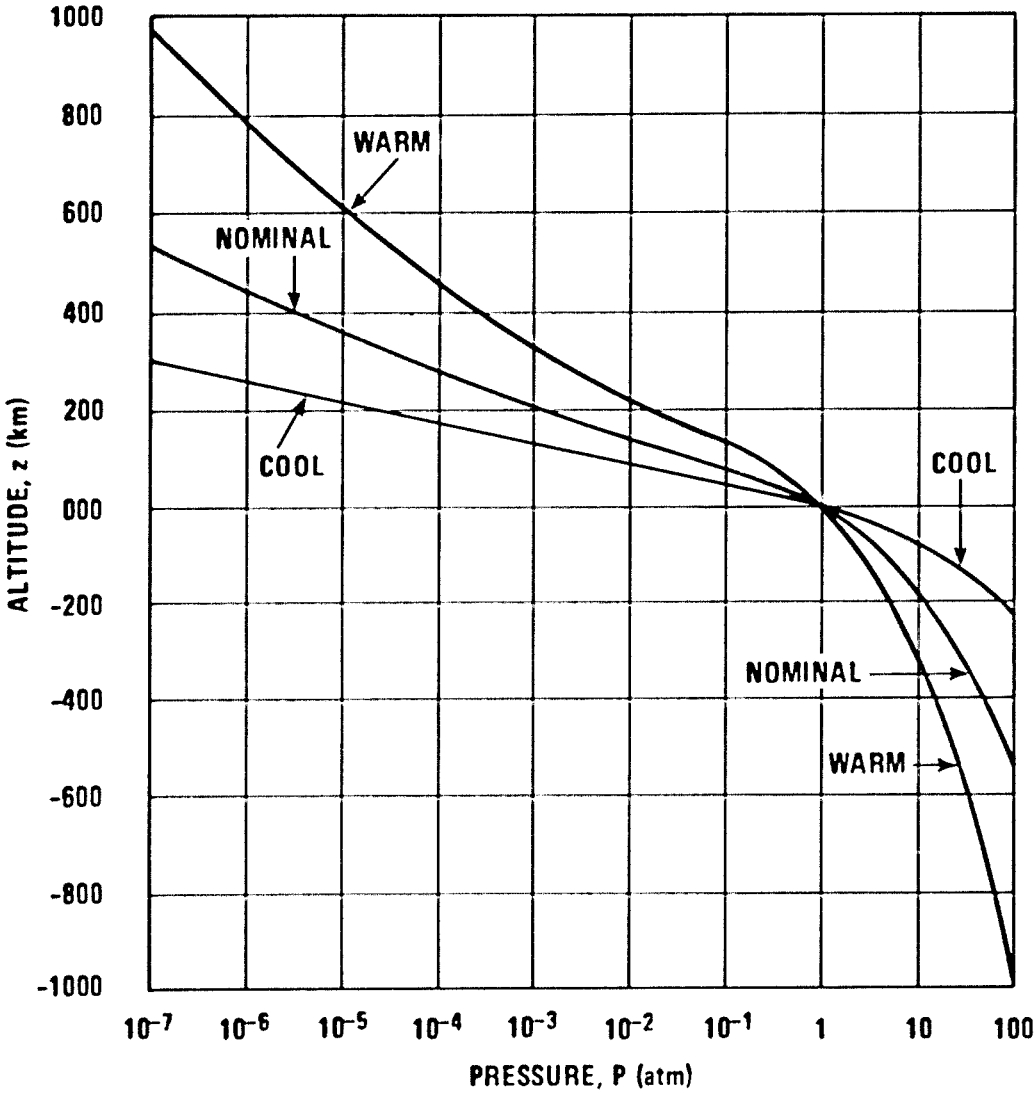

Figure 3.—Pressure vs altitude for Saturn Model Atmospheres.

The limiting high pressure for all models is taken as 10^3 atm; higher pressures would require modification of the ideal gas law. The limiting low pressure is 10^{-7} atm for all models. At still lower pressures the temperature at the 10^{-7} atm level should be used, diffusive separation of H_2 and H_e is likely, and atomic hydrogen will become increasingly important.

The radial distance from the center of the planet R can be related to the altitude z by the following equation:

$$R = R_s [1 + (z-z_o)/R_s - 0.105 (\sin \phi)^2]$$

where z_o is the altitude of the NH_3 cloud bottom which is treated separately for each model atmosphere. The uncertainty in atmospheric quantities plotted as a function of radial distance is primarily the result of the ± 350 km uncertainty in the equatorial radius of Saturn. The ranges permitted by the limiting model atmospheres for density, pressure, and temperature as a function of radial distance are shown in figures 9, 10, and 11.

2.9 Clouds and Atmospheric Motions

2.9.1 Clouds

Saturn's cloud phenomena are similar to Jupiter's although clouds are observed less frequently and contrast less with the planetary disk. Numerous photographs confirm that Saturn's bland appearance is real and not a result of its being observed less regularly and at lower resolutions than Jupiter (ref. 139). This appearance could result from lower temperatures and reduced chemical and meteorological activity, a higher ratio of scattering to condensate opacity at small optical depths, or a relatively permanent and uniform high-altitude haze which could be CH_4 condensation, as indicated by one of Kuiper's models (ref. 77). Alexander (ref. 40) describes in detail the characteristics of Saturn's cloud markings as recorded in photographs and drawings by numerous observers. The principal features are stripes parallel to the equator of which up to six belts (usually dark) and three zones (usually light) are discernible throughout the 200 year history of telescopic observations of disk detail. The equatorial (often brightest) zone is frequently described as yellowish and the belts as reddish brown. Color differences are real, but the usually subdued colors make precise description of the differences difficult. Standard nomenclature for the belts and zones is presented by Alexander (ref. 40), but it serves only as a rough guide to planetary features because the latitudes and contrast of feature edges are variable.

Spots are sometimes observed on Saturn, but apparently none are both permanent and readily identifiable. They have lifetimes up to a few months, may be light or dark with respect to the local background, appear within 60° of the equator, and are seen usually at marginal contrast and resolution. They typically extend a few tenths of a second of arc which corresponds to a few thousand km at mean opposition. They may be comparable to major terrestrial weather systems.

Although only H_2 and CH_4 are indicated in spectra of Saturn (ref. 49), it is reasonable to expect that the major condensates are those of H_2O and NH_3 molecules in the approximate

solar composition adopted in section 2.8.1. In this case, analysis similar to that applied to Jupiter's clouds by Lewis (ref. 140) is appropriate for Saturn's troposphere and particularly for condensation in convective cells undergoing upward, adiabatic expansion. Although the cloud property formulas given in appendix B-1 describe only crudely some of the cloud formation physics involved, they have been applied to the model atmospheres described in sections 2.8.3 and 3.8 with pure liquid H_2O condensation parameters. The results, shown in tables XXII, XXIII, XXIV, and figure 1 suggest that NH_3-H_2O solution clouds occur in the pressure range from a few to 140 atmospheres, solid H_2O ice clouds from a few to 50 atmospheres, and solid NH_3 ice clouds from a few tenths to 6 atmospheres. Composition and other differences influence cloud formation strongly even in this simplified approach, and therefore CH_4 clouds, although not predicted in any of the models, are possible just below the tropopause. Additional minor condensates, particularly NH_4SH, are possible as well and could be responsible for cloud contrast and coloration.

2.9.2 Atmospheric Motions

Motions of Saturn's atmosphere are inferred from repeated observations of individual spots (section 2.9.1), from repeated observations of other features such as serrated boundaries between belts and zones, and from Doppler shifts of line features in spectra of Saturn. For convenience, these motions are classified here as rotation and winds.

2.9.2.1 Rotation

Those spots whose positions have been carefully measured apparently have rotation periods longer than ten hours. An individual well-defined spot observed over a several-month interval can have a rotation period consistent within a few seconds, but other spots, even those appearing at the same time and latitude (but with different longitudes), can yield periods which differ by a few minutes. Spots observed within a few degrees of the equator generally have rotation periods between $10^h\ 12^m$ and $10^h\ 16^m$, but occasionally that range is exceeded. Most spots from 36 to 60° north and 36 to 50° south latitude yield rotation periods between $10^h\ 37^m$ and $10^h\ 41^m$. No spots have been observed poleward of 60° latitude, and the few observed at tropical latitudes do not show whether the period increase from the equator to temperate latitudes is gradual or abrupt. No longitude specification system has been generally accepted for Saturn (ref. 40).

Observation of the serrated edges of the belts and zones have led to periods agreeing with those of the spots. Some of the spectroscopic period results, however, are different from those of the spots and serrated edges by more than their uncertainties. For instance, the period $10^h\ 2^m \pm 5^m$ was obtained by Moore (ref. 145) near the equator (reflected solar Fraunhofer lines near 4500 Å) and the period of $10^h\ 52^m \pm 15^m$ was obtained by Rosino and Stagni (ref. 75) near latitude 45° (reflected solar Fraunhofer lines near 4000 Å). Nevertheless, because the spectroscopic results are considered less accurate, the period adopted here includes only the great majority of the spot measurements and is specified by $T_o = 10^h\ 26^m \pm 14^m$. The corresponding rotational angular velocity is $\omega_o = (1.67 \pm 0.04) \times 10^{-4}$ radian sec^{-1}.

2.9.2.2 Winds

Winds are defined here as all atmospheric motions relative to body rotation at the nominal period T_o and angular velocity ω_o. They can be inferred quantitatively only from the spot motions (sections 2.9.1 and 2.9.2.1) on scales greater than a few thousand km. The spot rotation periods cited in section 2.9.2.1 correspond to westerly (in the direction of rotation) prevailing winds near 250 m/sec at equatorial latitudes and easterly ones (opposing the rotation) near 180 m/sec at temperate latitudes. These subsonic winds winds reflect the motion of major systems; smaller scale velocities and wind shear cannot be inferred directly from Saturn observations. If, however, the results of Chapman (ref. 146) for Jupiter are scaled to Saturn by the ratio of the prevailing wind speeds, local winds of order of magnitude up to 30 m/sec with respect to the prevailing winds would occur.

3. CRITERIA

This section provides descriptions of the environment of Saturn intended for use in the design of spacecraft operating near that planet. The preceding State-of-the-Art section contains a discussion of the investigation used to arrive at the recommended values. The uncertainties, ranges, or limits given herein represent the extreme possible design values. Despite this intent, the environment of Saturn can be expected to contain surprises.

3.1 General Physical Properties

The mass of Saturn, its gravitational constant, radius, mean density, rotation rate, rotational pole location, and several orbital parameters are given in table IX. The planet flattens towards the poles and can be taken as a oblate spheroid. The radius at any chronocentric latitude can be obtained from:

$$R_o(\phi) = R_s\,[1-0.105\,(\sin\phi)^2]$$

where R_s is the equatorial radius, ϕ is the chronocentric latitude and $R_o(\phi)$ is the radius which defines the limb in visual observations and is to be associated with the NH_3 cloud bottoms given in the atmospheric models (section 3.8). No solid surface has been identified, and one is not expected at pressures less than 10^3 atm, the high pressure limit of the model atmospheres of section 3.8.

3.2 Gravitational Field

Parameters related to the gravitational field of Saturn are presented in table X. The range of gravitational acceleration g includes the equator to pole variation. Minimum values are to be associated with the equator, maximum values with the poles. The possibility of spacecraft orbit perturbation by natural satellites can be determined from the information in section 3.5.

TABLE IX

PHYSICAL PROPERTIES OF SATURN

Range of Distance from the Sun	$R_{s\odot}$ = 9.0 to 10.1 AU
Mean Distance from the Sun	$R_{s\odot}$ = 9.5388 AU
Heliocentric Orbital Speed	9.1 to 10.2 km sec^{-1}
Period of Revolution about the Sun	29.458 years
Inclination of Orbital Plane to Ecliptic Plane	$2^\circ.490$
Inclination of Equatorial Plane to Orbital Plane	$26^\circ.7$
Right Ascension of North Rotational Pole	$\alpha_p = 39^\circ.5586 + 1^\circ.180 \times 10^{-4}$ (Julian Date - 2443000.5)
Declination of North Rotational Pole (JD is Julian Date of Interest)	$\delta_p = 83^\circ.4255 + 1^\circ.182 \times 10^{-5}$ (Julian Date - 2443000.5)
Mass of Saturn	$M_s = (5.683 \pm 0.004) \times 10^{29}$ grams
Mass of Saturn and Satellites	$M_{ss} = (5.685 \pm 0.004) \times 10^{29}$ grams
Gravitational Constant of Saturn	$GM_s = (3.7925 \pm 0.0016) \times 10^{22}$ cm^3 sec^{-2}
Equatorial Radius	R_s = 59,800 ± 350 km
Polar Radius	R_p = 53,500 ± 350 km
Mean Density	$\bar{\rho}$ = 0.71 ± 0.01 g cm^{-3}
Optical Flattening or Oblateness	ϵ = 0.105 ± 0.008
Period of Rotation	$T_o = 10^h\ 26^m \pm 14^m$
Angular Rotation Rate	$\omega_o = (1.67 \pm 0.04) \times 10^{-4}$ radians sec^{-1}

TABLE X

GRAVITATIONAL FIELD PARAMETERS

Gravitational Potential at Distance R from Saturn in a Coordinate System Not Rotating with the Planet	$U = -(634 \pm 12)\,(R_s/R)\ \mathrm{km^2\ sec^{-2}}$
Escape Velocity at Distance R from Planet. (from potential above)	$V_{esc} = (35.6 \pm 0.4)\,(R_s/R)^{1/2}\ \mathrm{km\ sec^{-1}}$
Orbital Velocity at Distance R with Semi-major Axis a	$V_{orb} = (25.2 \pm 0.2)\,[2(R_s/R) - (R_s/a)]^{1/2}\ \mathrm{km\ sec^{-1}}$
Period of Object in Orbit with Semi-major Axis a	$P_{orb} = 4.14\,(a/R_s)^{3/2}$ hours
Range of Gravitational Acceleration at Zero of Altitude, i.e., $R = R_o$, in a Coordinate System Corotating with the Planet at Angular Rate ω_o	$g = (1050 \pm 200)\ \mathrm{cm\ sec^{-2}}$
Difference between Chronographic Latitude ϕ' and Chronocentric Latitude ϕ at Chronocentric Latitude ϕ	$\phi' - \phi = (6^\circ.0 \pm 0^\circ.5)\sin 2\phi$

3.3 Magnetic and Electric Fields

The general magnetic field of Saturn is estimated to be dipole in character with a dipole moment between 0 and 10^{29} A m^2 (0 and 10^{32} gauss cm^3). The inclination of the dipole axis is not known and any inclination should be considered with preference given to inclinations less than 20° from the rotational axis. In view of the range given for the dipole moment, a simple geometrically-centered dipole should be assumed. The magnetic flux density $\mathcal{B}$ in (T) and the dipole moment M in (A m^2) are related by

$$\mathcal{B} = (10^{-7})\,\frac{M}{R^3}\,(1 + 3\sin^2\phi_m)^{1/2}$$

where ϕ_m is the magnetic latitude measured with reference to a plane perpendicular to the dipole axis. The magnetic flux density at one equatorial radius from the dipole center should be taken in the range 0 to 4.7×10^{-2} T (0 to 470 gauss) on the basis of a magnetic moment range of 0 to 10^{29} A m^2 (0 to 10^{32} gauss cm^3) and $\phi_m = 0$.

At distances from the planet greater than the level R_u (ϕ), the static electric field ϵ should be taken as $\xi \leq 470\,(R_s/R)^2$ volts meter^{-1}. Below the reference level, fields 10^4 to 10^5 volts meter^{-1} extending over several kilometers and local fields up to 10^6 volts meter^{-1} over centimeters are possible in convective cloud-forming regions.

3.4 Electromagnetic Radiation

Above the tropopause (altitudes $z = 80 \pm 50$ km), the formulas in table XI specify the ranges of intensity, flux, and temperature associated with electromagnetic radiation near Saturn under conditions of maximum illumination. For conditions of partial illumination, total shadowing, or eclipse, the range lies between zero and the uppermost value specified. No day-night difference is expected in Saturn's emission of thermal radiation.

Below the tropopause, the maximum solar and synchrotron contributions are identical to those specified in table XI. In this region, the thermal contribution can be computed by the formulas of table XII. The possibility of lightning discharge may require the protection of light-sensitive surfaces.

When Saturn's rings occult an electromagnetic source, the intensity and flux may be reduced by the factor $\exp - \tau(R)/\sin B_{ob}$. The optical thickness $\tau(R)$ is obtained from figure 8 of section 3.6 at the radial distance where a line from the spacecraft to the source intersects the ring plane and B_{ob} is the elevation angle of this line above the ring plane.

The formulas in tables XV and XVI specify maximum values for the intensity and flux (solar reflected and thermal) of electromagnetic radiation from Saturn's rings. The fourth column of these tables should be used initially to determine whether further computation is justified. For passage within a few minutes of arc of the ring plane, the contribution from the "edge" of the ring system may be greater than that of the ring area (A_R) of interest. For exterior passage, an upper limit to the flux from the "edge" should be computed by assuming a thickness of 5 km, an intensity equal to that given for ring B (for solar reflected), an infinite optical thickness (for thermal radiation), and location of the edge at 2.29 R_s from the center of Saturn. For observation from greater than 5 R_s, the flux (solar reflected or thermal) from the "edge" will not approach the total from the A and B rings unless the spacecraft is within one arc minute of the ring plane. The reflected solar contribution from ring regions shadowed by the planet should be taken as zero.

The visual magnitude (M_v) of Saturn under conditions of maximum illumination ($\Psi = 0°$) is given by

$$M_v = (V_v \pm 0.2) + 5 \log (R_{s\odot} R)$$

where the absolute visual magnitude (V_v) is to be taken from table XIII, whereas $R_{s\odot}$ and R must be in AU. The color indexes for the planet are given in table XIII. The variation of visual magnitude with phase is not known and is likely less than 0.04 magnitudes per degree.

For $\Psi \leq 6°$, $B'_\odot$ and B_o within 3° of one another, and the observer and Sun on the same side of the ring plane, the visual magnitude of Saturn and rings is given by

$$M_v = (V_v \pm 0.3) + 5 \log (R_{s\odot} R) - 2.60 \sin B_o + 1.25 \sin^2 B_o + 0.044 \Psi$$

with $R_{s\odot}$ and R in AU and Ψ in degrees.

Reflected solar and thermal radiation from Saturn's satellites will be insignificant compared to that of Saturn except for close approach to a satellite. The satellite positions can be found in the appropriate year of the *American Ephemeris and Nautical Almanac* and their visual magnitudes and colors are specified by

$$M_v = (V_v \pm 0.3) + 5 \log (R_{s\odot} \Delta) + (0.03 + 0.02) \Psi$$

and the values in table XIV where $R_{s\odot}$ and Δ are in AU and Ψ is in degrees. The foregoing uncertainity of ± 0.3 for V_v should be increased to ± 0.5 for Mimas and ± 1.0 for Janus and Phoebe.

The maximum thermal from any satellite (1 μm $< \lambda <$ 3 meters) is specified by

$$I_\lambda = B_\lambda (128°K)$$

$$F_\lambda = \frac{\pi B_\lambda (128°K)}{(\Delta/R_{sat})^2}$$

$$F = \frac{15}{(\Delta/R_{sat})^2} \text{ watts m}^{-2}$$

where B_λ can be found in Allen (ref. 25) and R_{sat} is given in table XVII. Approaches to 1.5 R_s of any Saturn satellite may be made before its maximum thermal contribution can exceeded that of Saturn itself.

The field strengths associated with electromagnetic radiation for wavelengths longer than 100 cm are not known. When possible, equipment sensitive to such fields should be avoided.

TABLE XI

ELECTROMAGNETIC RADIATION NEAR SATURN UNDER CONDITIONS OF MAXIMUM ILLUMINATION

	Sun*	Saturn Reflected Sunlight*	Saturn Thermal**	Saturn Synchrotron***
Wavelength	$1\ \text{Å} < \lambda < 100$ cm	$1\ \text{Å} < \lambda < 10\mu$	$6\ \mu\text{m} < \lambda < 100$ cm	$1\ \text{cm} < \lambda < 100$ cm
Intensity-power/(area-wavelength-solid angle)	$I_\lambda = 1.5 \times 10^{-6} H_\lambda$ (steradian)$^{-1}$	$I_\lambda = \dfrac{p_\lambda H_\lambda}{(286 \pm 35)}$	$I_\lambda = B_\lambda(T_D)$	
power/(area-frequency-solid angle)			$I_\nu = B_\nu(T_D)$	$I_\nu = \dfrac{2kT_{sy}}{\lambda^2}$
Spectral Flux-power/(area-wavelength)	$F_\lambda = \dfrac{H_\lambda}{S^2}$	$F_\lambda = \dfrac{p_\lambda H_\lambda}{(91 \pm 11)(R/R_s)^2}$	$F_\lambda = \dfrac{\pi B_\lambda(T_D)}{(R/R_s)^2}$	
power/(area-frequency)			$F_\nu = \dfrac{\pi B_\nu(T_D)}{(R/R_s)^2}$	$F_\nu = \dfrac{(1.6 \pm 1.6) \times 10^{-19}}{9 + (R/R_s)^2}$ watts m^{-2} Hz^{-1}
Integrated flux-[power/area]	$F = \dfrac{(1.35 \pm 0.02) \times 10^3}{S^2}$ watts m^{-2}	$F = \dfrac{5.5 \pm 0.8}{(R/R_s)^2}$ watts m^{-2}	$F = \dfrac{5.0 \pm 1.5}{(R/R_s)^2}$ watts m^{-2}	$F = \dfrac{(5 \pm 5) \times 10^{-11}}{9 + (R/R_s)^2}$ watts m^{-2}
Effective Temperature	–	–	$T_e = 97 \pm 6°K$	$T_{sy} = (0.2 \pm 0.2)\lambda^2$ (°K) (λ in cm)

*Solar spectral irradiance H_λ from NASA SP-8005, revised (ref. 31). Geometric albedo p_λ from figure 6. The distance S from Sun to spacecraft in AU only.

**Planck function B_λ, B_ν from Allen (ref. 25) or elsewhere (intensity units). The disk brightness temperature T_D from figures 4 and 5.

***Spectral flux computed using T_{sy} must not exceed F_ν.

TABLE XII

FORMULAS FOR THERMAL RADIATION FROM SATURN BELOW THE TROPOPAUSE FOR 6 μm $< \lambda <$ 100 cm*

Parameter	Formula
Intensity (omnidirectional) – power/(area-wavelength-solid angle)	$I_\lambda = \begin{cases} B_\lambda\ (T_D) \text{ for } T < T_D \\ B_\lambda\ (T) \quad \text{for } T > T_D \end{cases}$
power/(area-frequency-solid angle)	$I_\nu = \begin{cases} B_\nu\ (T_D) \text{ for } T < T_D \\ B_\nu\ (T) \quad \text{for } T > T_D \end{cases}$
Spectral Flux (omnidirectional) – power/(area-wavelength)	$F_\lambda = \begin{cases} \pi B_\lambda\ (T_D) \text{ for } T < T_D \\ \pi B_\lambda\ (T) \quad \text{for } T > T_D \end{cases}$
power/(area-frequency)	$F_\nu = \begin{cases} \pi B_\nu\ (T_D) \text{ for } T < T_D \\ \pi B_\nu\ (T) \quad \text{for } T > T_D \end{cases}$
Integrated Flux – power/area	$F = \begin{cases} 5.0 \pm 1.5 \text{ watts m}^{-2} \text{ for } T < 97^\circ\text{K} \\ \left(\frac{T}{97}\right)^4 \text{ X } (5.0 \pm 1.5) \text{ watts m}^{-2} \text{ for } T > 97^\circ\text{K} \end{cases}$

*Planck function B_λ, B_ν from Allen (ref. 25) or elsewhere.
The local temperature T from tables XXII, XXIII and XXIV.
The disk brightness temperature T_D from figures 4 and 5.

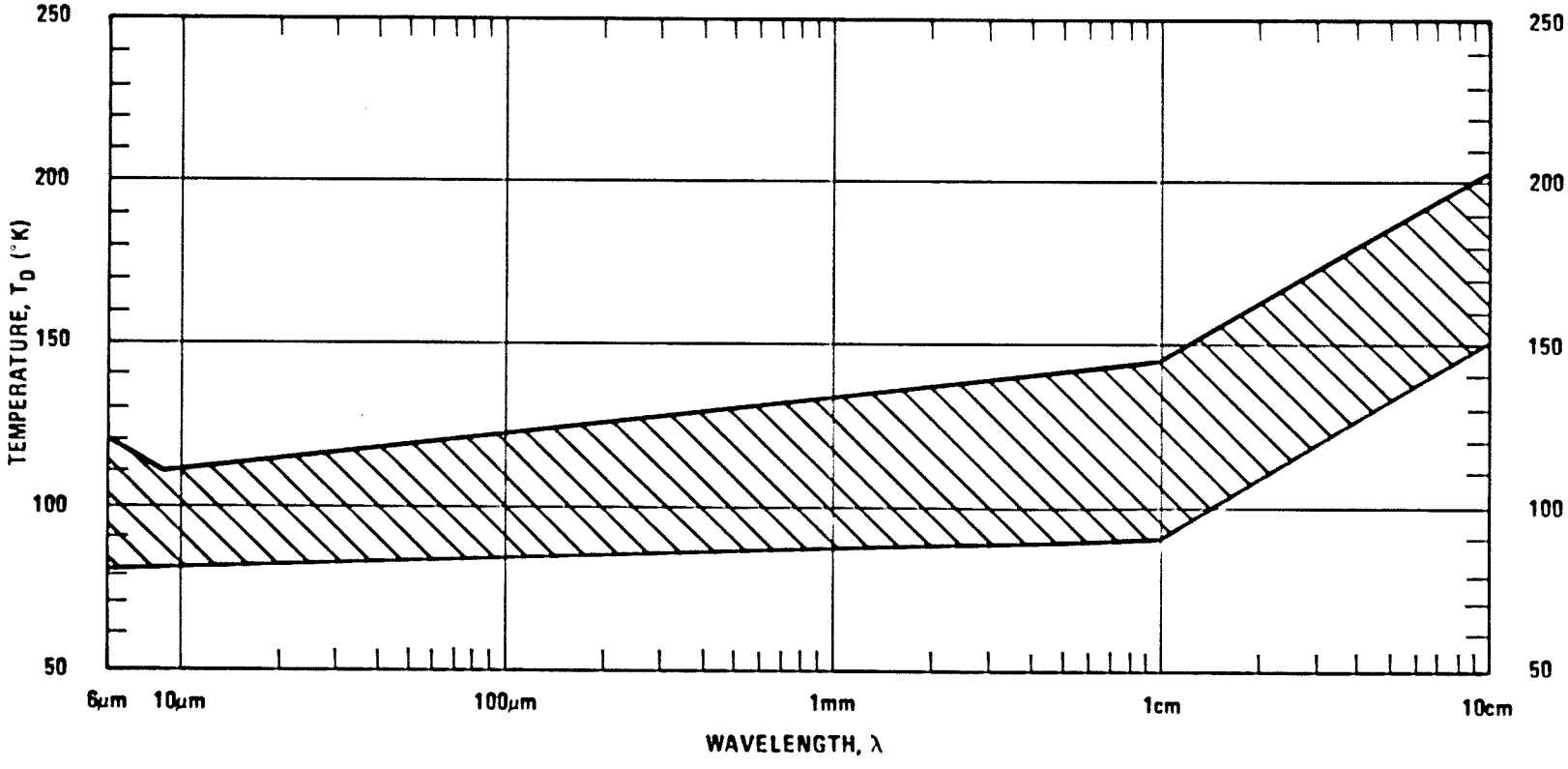

Figure 4.—Range of disk brightness temperature vs wavelength (6 μm to 10 cm).

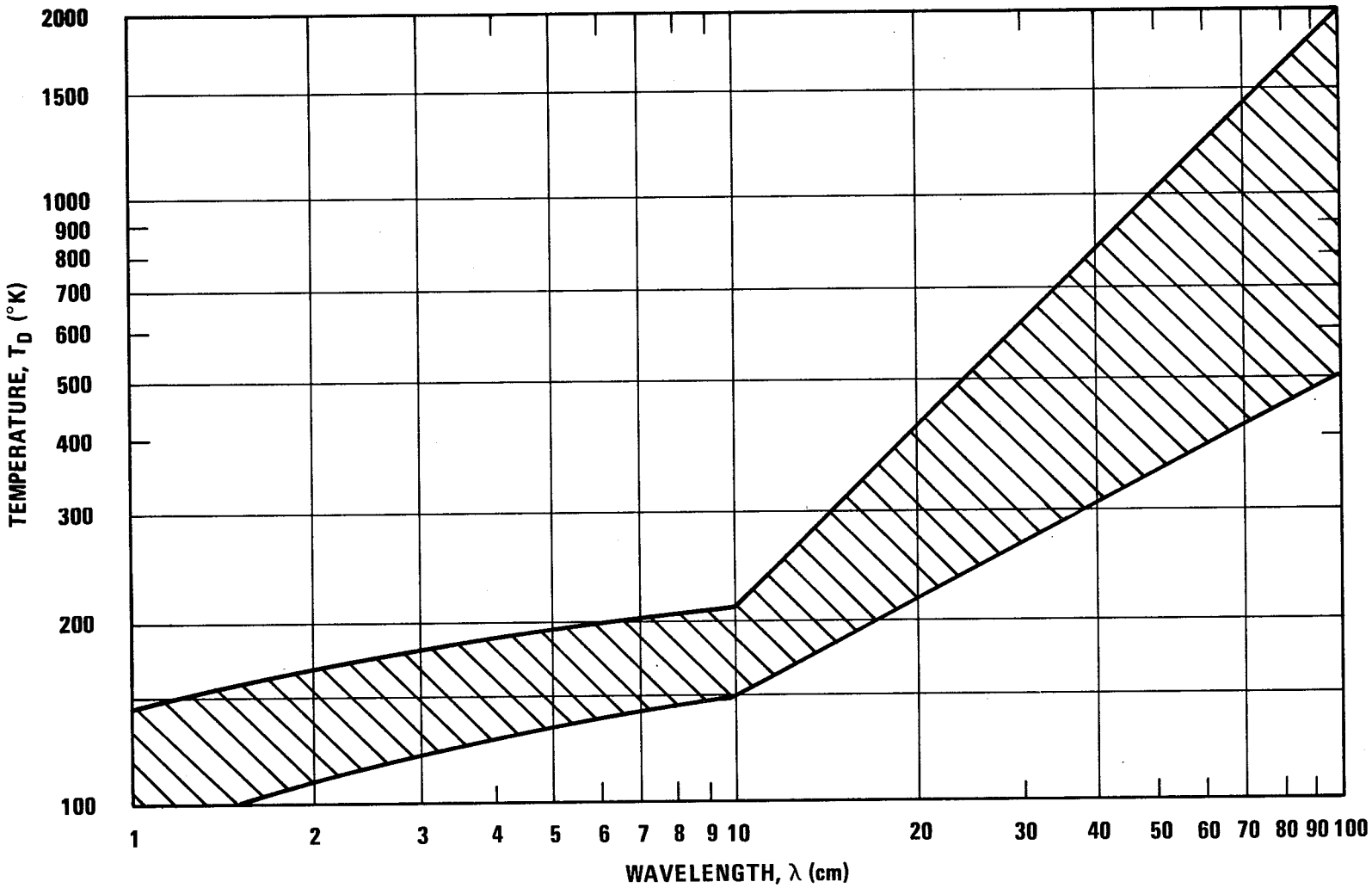

Figure 5.—Range of disk brightness temperature vs wavelength (1 to 100cm).

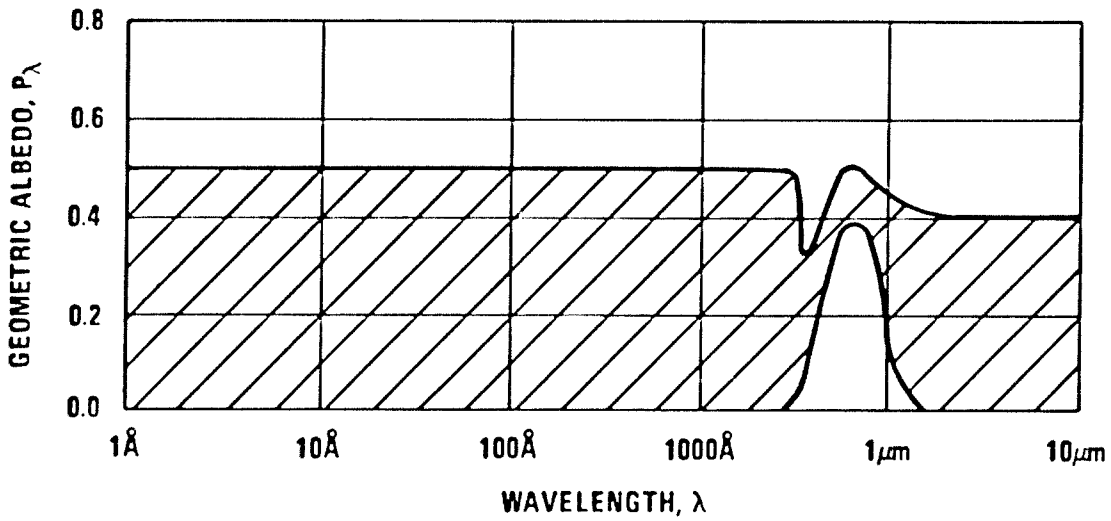

Figure 6.—Range of geometric albedo vs wavelength.

TABLE XIII

ABSOLUTE VISUAL MAGNITUDE AND COLORS FOR SATURN

Absolute Visual Magnitude*	Brightness Differences between Photometric Passbands					
V_v	U-B	B-V	V-W	V-X	V-Y	V-Z
−8.88	+0.58	+1.04	+0.46	−0.26	−0.15	−1.47

*For photometric definitions see appendix C and Newburn and Gulkis (1971), TR 32-1529, JPL.

3.5 Satellites and Meteoroids

Orbital and physical properties of Saturn's ten satellites are contained in table XVII. The visual magnitude and color indexes of these satellites are given in section 3.4. Some of the orbital elements for these satellites are functions of time. Information permitting the location of all the satellites except Janus can be found in the appropriate year of the *American Ephemeris and Nautical Almanac*. For Janus, the period and corresponding semi-major axis

TABLE XIV

ABSOLUTE VISUAL MAGNITUDE AND COLOR*
OF SATURN'S SATELLITES

Satellite	Absolute Visual Magnitude*	Brightness Differences between Photometric Passbands*			
	V_v	U-B	B-V	V-R	R-I
Janus	+4.5	–	–	–	–
Mimas	+2.6	–	–	–	–
Enceladus	+2.22	–	0.62	–	–
Tethys	+0.72	0.34	0.73	–	–
Dione	+0.89	0.30	0.71	0.48	0.31
Rhea	+0.21	0.35	0.76	0.61	0.26
Titan	–1.16	0.75	1.30	0.88	0.11
Hyperion	+4.61	0.42	0.69	–	–
Iapetus	+0.7 to +2.8	0.28	0.71	–	–
Phoebe	+6.9	–	–	–	–

*For photometric definitions see appendix C and Newburn and Gulkis (1971), TR 32-1529, JPL.

are not well established so the region in which Janus moves is defined with broad limits, but its location at any given time cannot be predicted.

Within 600 R_s of Saturn, the number of meteoroids S_c with mass greater than mass m in the mass range 10^{-6} to 10^2 grams is given by

$$\log S_c = -24.6 \pm 2 - 1.2 \log m$$

where S_c is in units of cm^{-3}. The mass density of these particles should be taken as $\rho_c = 0.5 \times 3^{\pm 1}$ grams cm^{-3} and the flux F_c through a plane surface can be computed from

TABLE XV

LIMITING VALUES OF SOLAR RADIATION REFLECTED FROM SATURN'S RINGS FOR WAVELENGTHS 1 Å < λ < 10 μm*

Parameter	Distance of Interest		
	$R > R_s$	$R > 5\ R_s$**	Directly above outermost (brightest) one third of B ring
Intensity – power/(area-wavelength-solid angle)	$I_\lambda = k_R H_\lambda$	$I_\lambda = k_R H_\lambda$	$I_\lambda = (1.9 \pm 0.6) \times 10^{-3} H_\lambda$ (steradian)$^{-1}$
Spectral Flux – power/(area-wavelength)	$F_\lambda = H_\lambda \int_{\Omega_R} k_R \cos\theta \, d\Omega$	$F_\lambda = \frac{H_\lambda k_R A_R \sin B_o}{R^2}$	$F_\lambda = (6 \pm 2) \times 10^{-3} H_\lambda$
Integrated Flux – power/area	$F = 1.4 \times 10^3 \int_{\Omega_R} k_R \cos\theta \, d\Omega$ (watts m^{-2})	$F = \frac{1.4 \times 10^3 k_R A_R \sin B_o}{R^2}$ (watts m^{-2})	$F = (3 \pm 1)$ watts m^{-2}

*Solar spectral irradiance H_λ from NASA SP-8005, revised (ref. 31).
Integral is over the ring segment of interest.
k_R from figure 7.
θ is the angle formed by the normal to the spacecraft area of interest and the direction of incident reflected radiation.
**A_R is the area of ring segment of interest.

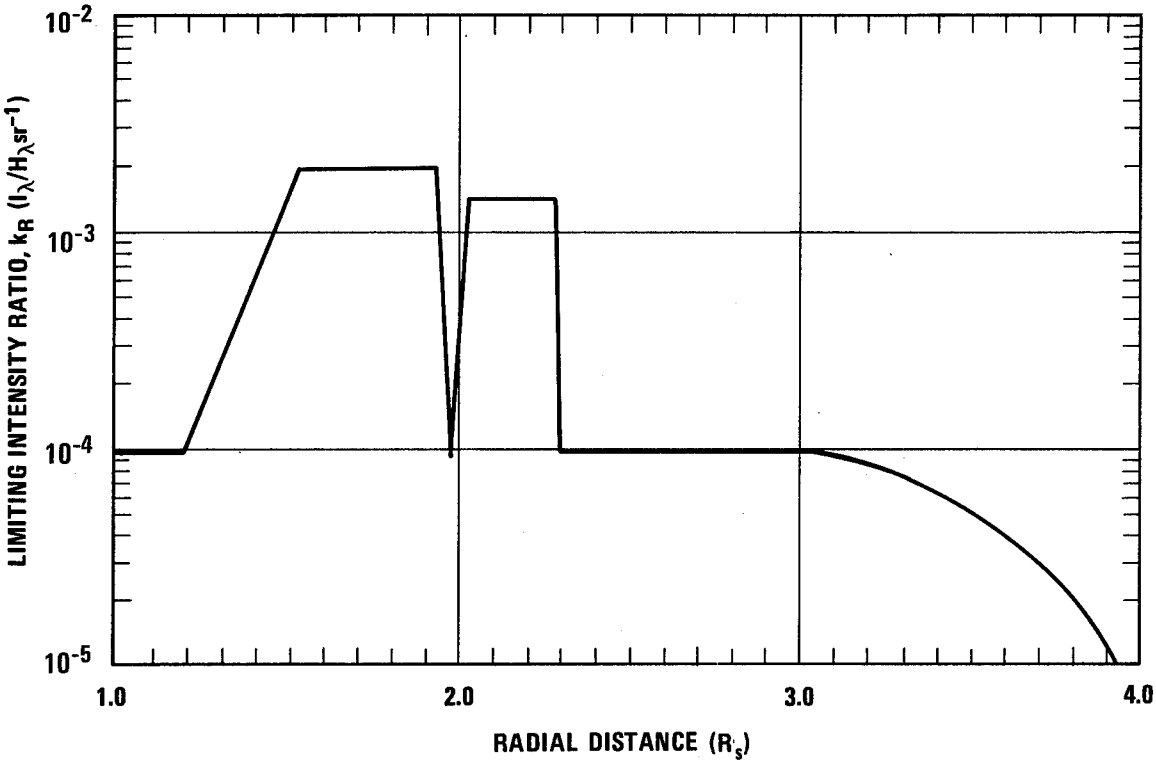

Figure 7.—Limiting intensity ratio vs radial distance from planet's center for Saturn's Rings.

$$F_c = \frac{S_c (V_s^2 + V_c^2)^{1/2}}{4}$$

where V_s is the speed of the spacecraft and V_c is the speed of the meteoroids, both with respect to Saturn. V_c may be approximated by $V_c = 36 (R_s/R)^{1/2}$ km sec^{-1}. For spacecraft crossing the equatorial plane inside the orbit of Enceladus, ring particles (section 3.6) are expected to dominate.

3.6 Saturn's Ring System

3.6.1 Dimensions

The dimensions of Saturn's five rings and associated uncertainties are presented in table XVIII. The dimensions in kilometers are of primary importance. The ratio (R/R_s) is used for convenience only and implies conversion with R_s = 59,800 km. In figures where R/R_s is

TABLE XVI

LIMITING VALUES OF THERMAL RADIATION FROM SATURN'S RINGS FOR WAVELENGTHS 10 $\mu m < \lambda < 100$ cm*

Parameter	Distance of Interest		
	$R > R_s$	$R > 5\ R_s$**	Directly above outermost one third of B ring
Intensity – power/(area-wavelength-solid angle)	$I_\lambda = B_\lambda\ (91^\circ K)\ [1-e^{-\tau(R)/\sin B_R}]$	$I_\lambda = B_\lambda\ (91^\circ K)\ [1-e^{-\tau/\sin B_o}]$	$I_\lambda = B_\lambda\ (91^\circ K)$
Spectral Flux – power/(area-wavelength)	$F_\lambda = \int_{\Omega_R} I_\lambda \cos\theta\ d\Omega$	$F_\lambda = \dfrac{I_\lambda A_R \sin B_o}{R^2}$	$F_\lambda = \pi B_\lambda\ (91^\circ K)$
Integrated Flux – power/area	$F = 4 \times \int_{\Omega_R} [1-e^{-\tau(R)/\sin B_R}] \cos\theta\ d\Omega$ (watts m^{-2})	$F = \dfrac{4 \times A_R \sin B_o\ [1-e^{-\tau/\sin B_o}]}{R^2}$ (watts m^{-2})	$F = 4$ (watts m^{-2})

*Frequency units may be obtained by substituting B_ν for B_λ. Planck function B_ν and B_λ from Allen (ref. 25) or elsewhere. Integral is over the ring segment of interest. $\tau(R)$ from figure 8. θ is the angle formed by the normal to spacecraft area of interest and the direction of incident energy.

**A_R is the area of ring segment of interest. $\bar{\tau}$ is the average τ over A_R.

TABLE XVII

ORBITAL AND PHYSICAL PROPERTIES OF SATURN'S SATELLITES

Satellite	Range of Distance from Saturn's Center (km)	Ratio of Mean Distance to Saturn's Equatorial Radius	Orbital Period (days)	Orbital Speed (km/sec)	Range of Chronocentric Latitude (degrees)	Radius (km)	Mass (g)
Janus*	$(169^{+3}_{-12}) \times 10^3$	2.82	$0.82^{+0.02}_{-0.08}$	15	±5	$150 \times 2^{\pm 1}$	$< 4 \times 10^{22}$
Mimas	$(186 \pm 4) \times 10^3$	3.10	0.9424	14	±1.6	250 ± 100	$(3.8 \pm 0.1) \times 10^{22}$
Enceladus	$(238 \pm 2) \times 10^3$	3.98	1.370	13	±0.005	300 ± 100	$(8 \pm 3) \times 10^{22}$
Tethys	$(294.8 \pm 0.5) \times 10^3$	4.93	1.888	11	±1.1	510 ± 150	$(6.4 \pm 0.2) \times 10^{23}$
Dione	$(378 \pm 1) \times 10^3$	6.31	2.737	10	±0.02	450 ± 150	$(11.0 \pm 0.3) \times 10^{23}$
Rhea	$(527 \pm 1) \times 10^3$	8.82	4.518	8	±0.3	650 ± 150	$2.3 \times 10^{23\pm1}$
Titan	$(1222 \pm 40) \times 10^3$	20.4	15.95	6	±0.3	2400 ± 200	$(1.37 \pm 0.01) \times 10^{26}$
Hyperion	$(1483 \pm 160) \times 10^3$	24.8	21.28	5	±0.6	$150 \times 2^{\pm 1}$	$< 4 \times 10^{22}$
Iapetus	$(3560 \pm 110) \times 10^3$	59.5	79.33	3	±14.7	$600 \times 2^{\pm 1}$	$(22 \pm 8) \times 10^{23}$
Phoebe**	$(12950 \pm 2200) \times 10^3$	216.6	550.4	2	±30	$100 \times 2^{\pm 1}$	$< 4 \times 10^{22}$

*Period and corresponding semi-major axis are not well established.
**Phoebe's motion is retrograde, the motion of all other satellites is direct.

used as an abscissa, the uncertainty in the location of key features such as the outer boundary of ring A should be obtained from table XVIII.

3.6.2 Composition

Water ice has been identified as a ring particle constituent and the presence of other unspecified compounds has been suggested. It is not known whether water ice covers the ring particles as a frost or forms the majority constituent. A particle density of $1 \times 4^{\pm 1}$ gram cm^3 should be used.

3.6.3 Thickness and Particle Orbits

The majority of ring particles are confined to the equatorial plane in a layer less than 5 km in thickness. The particle orbits are circular with their period and speed as given in table X. Where the optical thickness (τ) of the rings is less than 0.1 (figure 8) and near ring

TABLE XVIII

SATURN RING DIMENSIONS

Rings	Feature/Ring Boundary	Distance from Planetary Center (km)	Nominal Distance in Equatorial Radii (R/R_s)
Ring D	Saturn Equatorial Radius	59,800 ± 350	1.00
	Inner C Boundary	72,000 ± 3,500	1.21
Ring C			
Ring B	Inner B Boundary	91,400 ± 700	1.53
	Outer B Boundary	116,700 ± 700	1.95
	Width of Cassini's Division	4,800 $^{+1,400}_{-2,800}$	
Ring A	Inner A Boundary	121,600 ± 700	2.03
	Outer A Boundary	137,100 ± 700	2.29
Ring D'	Outer limit to possible D' Ring	239,200	4.00

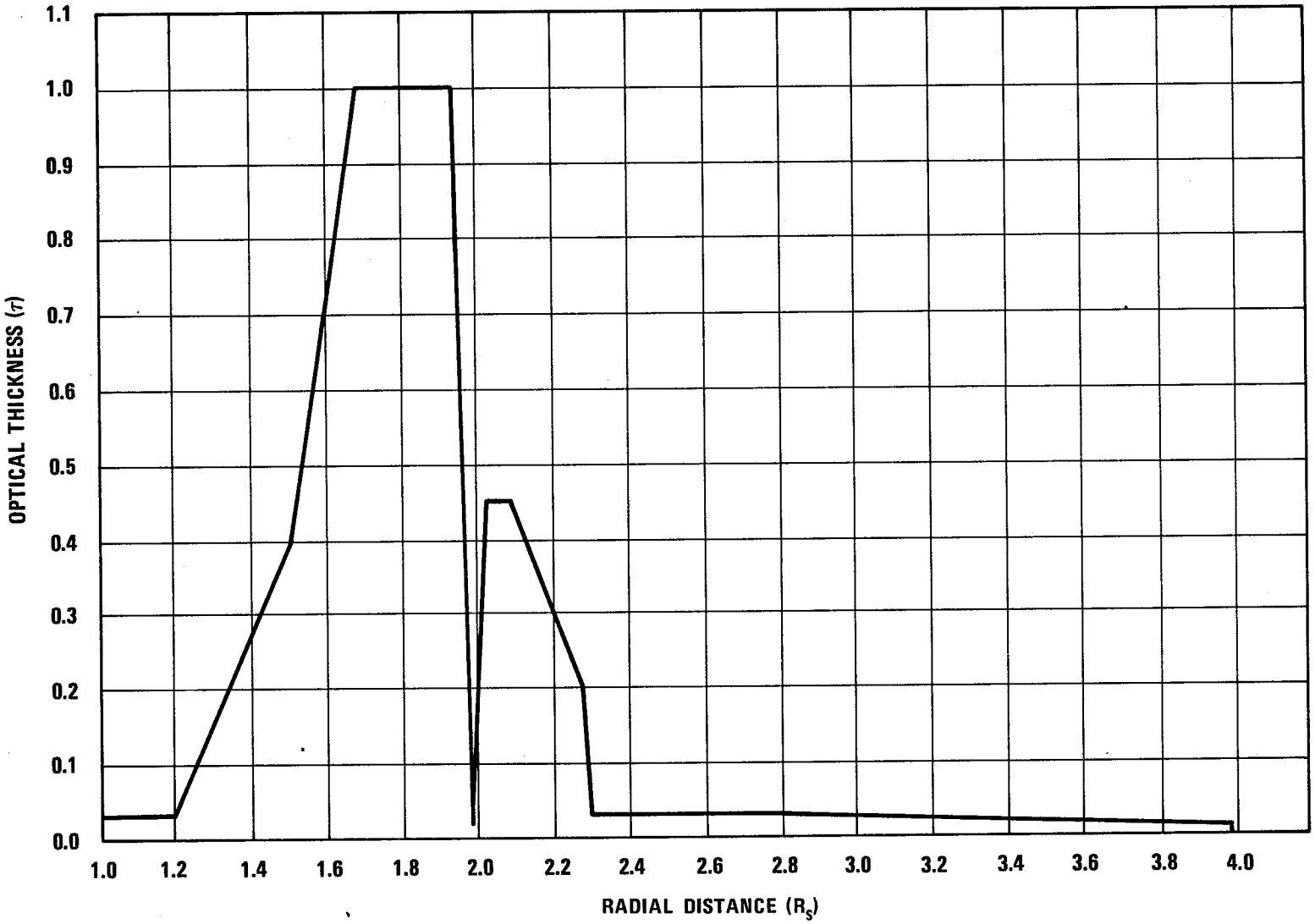

Figure 8.—Limiting ring optical thickness vs distance from the planet's center.

boundaries, particles at greater distance than 2.5 km from the equatorial plane may be found.

3.6.4 Particles

3.6.4.1 Size and Density

Present uncertainty in ring particle size and number density permit only an upper limit estimate of the cumulative mass number density S_m (number of particles per unit ring area with mass greater than mass m) as a function of distance from Saturn. Ring particles can be expected from $R_s = 1$ to $R_s = 4$ which includes the region of D and D′ rings as well as A, B, and C rings.

$$S_m(m > m_i) = k_1(R)\underbrace{3.16 \times 10^{-2}\left\{2.05\left(\frac{\rho_P}{m_i}\right)^{1/2} - 3.16 \times 10^{-8}\right\}}_{①}$$

$$+ k_2(R)\underbrace{3.17 \times 10^{5}\left\{2.05\left(\frac{\rho_P}{m_i}\right)^{1/2} - 31.6\right\}}_{②}$$

$$r_i(m_i) = (3\, m_i / 4\, \pi\, \rho_P)^{1/3}$$

The expression ① is set equal to one when $r_i(m_i)$ is < 0.1 cm and the expression ② is set equal to zero when $r_i(m_i) > 0.1$ cm. The particle density and mass must be in the same units, and the intermediate constants $k_1(R)$, $k_2(R)$ (cm^{-2}) are presented in table XIX. Linear interpolation should be used between consecutive entries. This model contains only particles with radii between 0.1 cm and 1 km in rings A, B, and D′ The C and D rings contain both small (0.001 cm $< r <$ 0.1 cm) and large (0.1 cm $< r < 10^5$ cm) particles with the small particles dominant by number. Particles with radii outside these ranges are not considered.

3.6.4.2 Computation of Impacts

For the purpose of computing the number of impacts in a given mass range, the ring particles should be taken as lying in the equatorial or ring plane. The ring area swept out by a spacecraft in crossing this plane is given by, $\left|(\vec{A}_s \cdot \vec{V}_{rel})/V_{sz}\right|$. In this expression, $\vec{A}_s$ is the spacecraft area of interest (with direction established by the outward normal to this area); $\vec{V}_{rel}$ is the relative velocity of the ring particles (with respect to the spacecraft); and V_{sz} is the component of the spacecraft velocity normal to the ring plane. The vector product $\vec{A}_s \cdot \vec{V}_{rel}$ must be negative.

TABLE XIX

SATURN RING MODEL PARAMETERS FOR COMPUTATION OF CUMULATIVE MASS NUMBER DENSITY

Radial Distance (R_s)	Optical Thickness $\tau(R)$	f*	$k_1(R)$** (cm^{-2})	$k_2(R)$** (cm^{-2})
1.00	0.030	0.1	3.14×10^{-5}	3.13×10^{2}
1.10	0.030	0.1	3.14×10^{-5}	3.13×10^{2}
1.20	0.030	0.1	3.14×10^{-5}	3.13×10^{2}
1.30	0.144	0.1	1.42×10^{-4}	1.42×10^{3}
1.40	0.261	0.1	2.44×10^{-4}	2.44×10^{3}
1.50	0.375	0.1	3.32×10^{-4}	3.30×10^{3}
1.53	0.400	1.0	3.50×10^{-3}	0.0
1.60	0.666	1.0	5.16×10^{-3}	0.0
1.70	1.000	1.0	6.71×10^{-3}	0.0
1.80	1.000	1.0	6.71×10^{-3}	0.0
1.90	1.000	1.0	6.71×10^{-3}	0.0
1.95	1.000	1.0	6.71×10^{-3}	0.0
1.99	0.020	1.0	2.10×10^{-4}	0.0
2.00	0.128	1.0	1.27×10^{-3}	0.0
2.03	0.450	1.0	3.84×10^{-3}	0.0
2.10	0.450	1.0	3.84×10^{-3}	0.0
2.20	0.310	1.0	2.83×10^{-3}	0.0
2.29	0.200	1.0	1.92×10^{-3}	0.0
2.30	0.030	1.0	3.14×10^{-4}	0.0
2.40	0.030	1.0	3.14×10^{-4}	0.0
2.50	0.030	1.0	3.14×10^{-4}	0.0
2.60	0.030	1.0	3.14×10^{-4}	0.0
2.70	0.030	1.0	3.14×10^{-4}	0.0
2.80	0.030	1.0	3.14×10^{-4}	0.0
2.90	0.028	1.0	2.93×10^{-4}	0.0
3.00	0.027	1.0	2.83×10^{-4}	0.0
3.10	0.025	1.0	2.62×10^{-4}	0.0
3.20	0.023	1.0	2.41×10^{-4}	0.0
3.30	0.022	1.0	2.31×10^{-4}	0.0
3.40	0.020	1.0	2.10×10^{-4}	0.0
3.50	0.018	1.0	1.89×10^{-4}	0.0
3.60	0.017	1.0	1.79×10^{-4}	0.0
3.70	0.015	1.0	1.58×10^{-4}	0.0
3.80	0.013	1.0	1.37×10^{-4}	0.0
3.90	0.012	1.0	1.27×10^{-4}	0.0
4.00	0.010	1.0	1.06×10^{-4}	0.0

*See section 2.6.3
**See equations in section 3.6

3.7 Charged Particles

Table XX gives values and formulas which specify the ranges of positions, fluxes, concentrations, energies, and temperatures for charged particles near Saturn. Limits on the electromagnetic radiation which could arise from trapped electrons are given in section 3.4.

It is not known whether the solar-interplanetary magnetic field boundary occurs inside or beyond Saturn's orbit. The sunward boundary of the magnetosphere could be as near to the planet as the ionosphere (associated with a small magnetic field and peak solar wind) or as far away as 240 R_s (associated with an upper limit magnetic field and nominal solar wind). Parameters for the interplanetary magnetic field near Saturn but beyond the influence of any Saturn magnetosphere are given in table VI.

3.8 Atmospheric Composition and Structure

Table XXIII gives the expected or nominal model atmosphere of Saturn in the pressure range 10^{-7} to 10^3 atmospheres. Cool and warm model atmospheres are given in tables XXII and XXIV. The cool and warm models are to provide the range of the physical parameters which reflect the uncertainties in the composition and structure of the nominal model as well as the expected variation with chronocentric latitude and longitude. Table XXI gives the composition used in each model without the effect of NH_3 and H_2O condensation. The zero of altitude in each model is taken at a pressure of one atmosphere. This reference level should be taken as equal, within 100 km, to the distance R_o which corresponds to the visual limb of the planet. The formulas in appendix B-1 can be used to interpolate between tabulated values. The radial distance R from the center of the planet can be related to the altitude z by

$$R = R_s [1 + (z - z_o)/R_s - 0.105 (\sin\phi)^2]$$

where z_o is the altitude of the NH_3 cloud bottom for each model atmosphere. The uncertainty in atmospheric quantities plotted as a function of radial distance is primarily the result of the ±350 km uncertainty in the equatorial radius of Saturn. The range permitted by the model atmospheres in density, pressure, and temperature, as a function of radial distance, is shown in figures 9, 10, 11. For latitudes other than the equator (ϕ=o), 62.79 sin ϕ^2 km should be subtracted from the ordinate in these figures.

3.9 Clouds and Atmospheric Motions

Ranges of altitude and concentration of clouds of water, ammonia ices, and solutions are suggested in tables XXII, XXIII, and XXIV. Additional minor cloud constituents (particularly CH_4 just below the tropopause and NH_4SH below the NH_3 clouds) and trace coloring agents are possible but cannot be specified quantitatively. Condensates are common in the bright zones (rising gas) and infrequent in the dark belts (descending gas). Because clouds are associated with complex weather phenomena, their positions, opacity, color, and brightness cannot be predicted. Hazards to spacecraft from possible corrosive cloud properties and from occasional water and ammonia rain, hail, snow, thunder, and lightning are anticipated.

TABLE XX

PARAMETERS OF CHARGED PARTICLES NEAR SATURN

Particle	Location	Temperature, Energy, or Velocity	Number Density, Flux, or Flux Parameter
Galactic Cosmic Rays	Everywhere	$0.1 < E < 10^{10}$ GeV (GeV/nucleon for alphas)	$\Phi_E = K(E + m_o c^2)^{-1.5}$ for E in units of of adjacent column Electrons: $0 \leqslant K \leqslant 0.02$ cm^{-2} sec^{-1} Protons: $0 \leqslant K \leqslant 2.5$ cm^{-2} sec^{-1} Alphas: $0 \leqslant K \leqslant 0.25$ cm^{-2} sec^{-1}
Solar Cosmic Rays (Protons)	Everywhere	$10 < E < 10^4$ MeV	Sporadic, with fluxes between 0 and 1.0 times those specified in NASA TR R-169 (ref. 121)
Solar Wind (Electrons and Protons)	Beyond Magnetosphere	V = 320 km/sec (up to 960 km/sec at peak solar activity)	$N_o = 0.09$ cm^{-3} (up to 0.9 cm^{-3} at peak solar activity)
Trapped Radiation (Electrons)	$L < 2.3$ $L \geqslant 2.3$	$E_o = (0.51) \times$ $\left[(1377/L^3 + 1)^{1/2} - 1\right]$Mev	$\Phi_o = 0$ $\Phi_o = 1.7 \times 10^{10}/L^6 (1377/L^3 + 1)^{-1/2}$ cm^{-2} sec^{-1}
Trapped Radiation (Protons)	$L < 2.3$ $L \geqslant 2.3$	$E_o = 497/L^3$ MeV	$\Phi_o = 0$ $\Phi_o = 4.7 \times 10^8/L^6 (1.06/L^3 + 1)^{-1/2}$ cm^{-2} sec^{-1}
Trapped Radiation Distribution with Energy (Electrons and Protons)	Within Magnetosphere		$0 \leqslant \Phi_E < \Phi_o \ (1 + E/E_o) \exp(-E/E_o)$
Trapped Radiation (Electrons and Protons)	Within Magnetosphere	$10 < E < 10^6$ eV	$0 < N_E < \dfrac{5.5 \times 10^{15}}{[E + (0.52)L^2]\ L^6}$ cm^{-3} and $N_E < 10^7$ cm^{-3}
Magnetospheric Plasma (Electrons and Protons)	Within Magnetosphere	$100 < T < 10^5$ °K	$0 < N_o < \dfrac{10^{16}}{L^8}$ cm^{-3} and $N_o < 10^7$ cm^{-3}
Ionosphere (Electrons and Protons)	$z > z_1$ where $z_1 = 450 \pm 200$ km	$T = 150 \pm 50$°K	$N_o = (10^{6\pm1}$ cm$^{-3})\exp - \left(\dfrac{z - z_1}{250 \text{ km}}\right)$

TABLE XXI

COMPOSITION FOR SATURN MODEL ATMOSPHERES

Parameter		Cool Model	Nominal Model	Warm Model
Fraction by Mass	H_2	0.55279	0.73514	0.89550
	He	0.39474	0.19737	0.09868
	H_2O	0.02484	0.00828	0.00276
	CH_4	0.01332	0.00444	0.00148
	N_e	0.00360	0.00120	0.00040
	NH_3	0.00339	0.00113	0.00037
	Others	0.00732	0.00244	0.00081
		1.00000	1.00000	1.00000
Fraction by Number	H_2	0.72996	0.88572	0.94679
	H_e	0.26251	0.11213	0.05254
	H_2O	0.00367	0.00105	0.00033
	CH_4	0.00221	0.00063	0.00020
	N_e	0.00047	0.00013	0.00004
	NH_3	0.00053	0.00015	0.00005
	Others	0.00065	0.00019	0.00005
		1.00000	1.00000	1.00000
Mean Molecular Weight grams/mole		2.66	2.27	2.13

The planetary rotation underlying the atmosphere is prograde at an angular velocity $\omega_o = (1.67 \pm 0.04) \times 10^{-4}$ radian/sec, corresponding to the period $T_o = 10^h 26^m \pm 14^m$. Within the convective troposphere (altitudes below 80 ± 50 km), there exist subsonic prevailing zonal winds, westerly near 250 m/sec at the equator and easterly near 180 m/sec at latitude 45° and beyond, with intermediate speeds elsewhere. In the convective troposphere, subsonic turbulence (local horizontal and vertical winds) of order of magnitude up to 30 m/sec occurs randomly with respect to the prevailing winds. Within the stratosphere and beyond (altitudes above 85 ± 50 km), the same description applies except that vertical turbulence is an order of magnitude smaller. The magnitude of possible wind shear cannot be reliably estimated.

TABLE XXII

VALUES AT SELECTED PRESSURES FOR COOL SATURN MODEL ATMOSPHERE

P (atm)	T (°K)	ρ (g cm^{-3})	z (km)	β	dT/dz (°K/km)	Hp (km)	Hρ (km)	w (mg/liter)	Comments
1.00×10^{-7}	72.0	4.50×10^{-11}	297.0	0.0	0.0	18.0	18.0		
3.00×10^{-7}	72.0	1.35×10^{-10}	277.2	0.0	0.0	18.0	18.0		
1.00×10^{-7}	72.0	4.50×10^{-10}	255.5	0.0	0.0	18.0	18.0		
3.00×10^{-6}	72.0	1.35×10^{-9}	235.8	0.0	0.0	18.0	18.0		
1.00×10^{-5}	72.0	4.50×10^{-9}	214.1	0.0	0.0	18.0	18.0		
3.00×10^{-5}	72.0	1.35×10^{-8}	194.3	0.0	0.0	18.0	18.0		
1.00×10^{-4}	72.0	4.50×10^{-8}	172.6	0.0	0.0	18.0	18.0		
3.00×10^{-4}	72.0	1.35×10^{-7}	152.8	0.0	0.0	18.0	18.0		
1.00×10^{-3}	72.0	4.50×10^{-7}	131.1	0.0	0.0	18.0	18.0		
3.00×10^{-3}	72.0	1.35×10^{-6}	111.3	0.0	0.0	18.0	18.0		
1.00×10^{-2}	72.0	4.50×10^{-6}	89.7	0.0	0.0	18.0	18.0		
3.00×10^{-2}	72.0	1.35×10^{-5}	69.9	0.0	0.0	18.0	18.0		
1.00×10^{-1}	72.0	4.50×10^{-5}	48.2	0.0	0.0	18.0	18.0		
0.204	72.0	9.19×10^{-5}	35.3	0.0		18.0	18.0		Tropopause
0.300	79.5	1.22×10^{-4}	28.1	0.258	−1.03	19.9	26.8		
0.600	95.0	2.05×10^{-4}	13.0	0.254	−1.02	23.8	31.9		Correspondence Level
1.00	108.1	3.00×10^{-4}	0.0	0.252	−1.01	27.0	36.2		Zero of Altitude
3.00	142.2	6.84×10^{-4}	−34.2	0.247	−0.987	35.6	47.2	0.0423	
4.85	160.0	9.82×10^{-4}	−52.3	0.245	−0.979	40.0	53.0	0.776	
6.34	170.8	1.20×10^{-3}	−63.4	0.244	−0.974	42.7	56.5	3.34	NH_3 Cloud Base
10.0	190.8	1.70×10^{-3}	−84.0	0.242	−0.967	47.7	63.0		
30.0	248.3	3.92×10^{-3}	−144.0	0.238	−0.951	62.1	81.5	0.464	
46.1	275.0	5.44×10^{-3}	−172.1	0.237	−0.946	68.8	90.1	4.54	Solid H_2O
66.7	300.0	7.20×10^{-3}	−198.6	0.235	−0.941	75.0	98.1	26.3	
87.8	320.0	8.89×10^{-3}	−219.9	0.235	−0.938	80.0	104.6	49.8	
100.0	329.9	9.82×10^{-3}	−230.5	0.234	−0.937	82.5	107.8	77.9	
138.2	355.9	1.26×10^{-2}	−258.3	0.233	−0.933	89.0	116.1	221.1	Solution H_2O-NH_3 Cloud Base
300.0	426.1	2.28×10^{-2}	−339.9	0.232	−0.926	106.6	138.7		
1000.0	526.2	5.76×10^{-2}	−481.8	0.229	−0.916	140.6	182.4		

TABLE XXIII

VALUES AT SELECTED PRESSURES FOR NOMINAL SATURN MODEL ATMOSPHERE

P (atm)	T (°K)	ρ (g cm^{-3})	z (km)	β	dT/dz (°K/km)	Hp (km)	Hρ (km)	w (mg/liter)	Comments
1.00×10^{-7}	119.0	2.32×10^{-11}	536.1	-0.0353	+0.101	41.5	40.1		
3.00×10^{-7}	114.5	7.25×10^{-11}	491.4	-0.0353	+0.101	39.9	38.6		
1.00×10^{-6}	109.7	2.52×10^{-10}	444.3	-0.0353	+0.101	38.3	37.0		
3.00×10^{-6}	105.5	7.86×10^{-10}	403.0	-0.0353	+0.101	36.8	35.6		
1.00×10^{-5}	101.1	2.73×10^{-9}	359.6	-0.0353	+0.101	35.3	34.1		
3.00×10^{-5}	97.3	8.53×10^{-9}	321.6	-0.0353	+0.101	34.0	32.8		
1.00×10^{-4}	93.3	2.97×10^{-8}	281.6	-0.0353	+0.101	32.5	31.4		
3.00×10^{-4}	89.7	9.25×10^{-8}	246.5	-0.0353	+0.101	31.3	30.2		
1.00×10^{-3}	86.0	3.21×10^{-7}	209.6	-0.0353	+0.101	30.0	29.0		
3.00×10^{-3}	82.7	1.00×10^{-6}	177.3	-0.0353	+0.101	28.9	27.9		
1.00×10^{-2}	79.3	3.49×10^{-6}	143.2	-0.0353	+0.101	27.7	26.7		
2.27×10^{-2}	77.0	8.17×10^{-6}	120.8	-0.0353		26.9	26.9		Upper Boundary to Stratosphere
3.00×10^{-2}	77.0	1.07×10^{-5}	113.4	0.0	0.0	26.9	26.9		
0.100	77.0	3.59×10^{-5}	81.1	0.0	0.0	26.9	26.9		
0.168	77.0	6.04×10^{-5}	67.1	0.0		26.9	26.9		Tropopause
0.300	95.0	8.37×10^{-5}	49.8	0.359	-1.03	33.1	51.7		Correspondence Level
0.727	130.0	1.55×10^{-4}	15.3	0.349	-0.999	45.4	69.7	0.00377	
1.00	145.2	1.91×10^{-4}	0.0	0.345	-0.988	50.7	77.3	0.0762	Zero of Altitude
1.12	151.0	2.05×10^{-4}	-5.9	0.343	-0.983	52.7	80.2	0.205	NH_3 Cloud Base
3.00	210.0	3.95×10^{-4}	-67.5	0.330	-0.946	73.4	109.5		
3.94	230.0	4.74×10^{-4}	-88.4	0.326	-0.935	80.3	119.1	0.0743	
5.10	250.0	5.64×10^{-4}	-109.9	0.323	-0.925	87.2	128.0	0.574	Solid H_2O
6.92	275.9	6.94×10^{-4}	-138.1	0.319	-0.913	96.3	141.3	4.82	Solution H_2O-NH_3 Cloud Base
10.0	309.9	8.93×10^{-4}	-175.5	0.314	-0.899	108.1	157.6		
30.0	434.1	1.91×10^{-3}	-317.0	0.300	-0.860	151.5	216.4		
100.0	617.8	4.48×10^{-3}	-536.0	0.287	-0.821	215.6	302.1		
300.0	841.3	9.99×10^{-3}	-813.7	0.276	-0.791	293.6	405.5		
1000.0	1166.2	2.37×10^{-2}	-1232.1	0.267	-0.764	406.9	554.9		

TABLE XXIV

VALUES AT SELECTED PRESSURES FOR WARM SATURN MODEL ATMOSPHERE

P (atm)	T (°K)	ρ (g cm^{-3})	z (km)	β	dT/dz (°K/km)	Hp (km)	Hρ (km)	w (mg/liter)	Comments
1.00×10^{-7}	196.7	1.32×10^{-11}	968.5	−0.0632	+0.138	90.3	85.0		
3.00×10^{-7}	183.5	4.24×10^{-11}	872.7	−0.0632	+0.138	84.3	79.3		
1.00×10^{-6}	170.0	1.53×10^{-10}	775.0	−0.0632	+0.138	78.1	73.4		
3.00×10^{-6}	158.6	4.91×10^{-10}	692.1	−0.0632	+0.138	72.9	68.5		
1.00×10^{-5}	147.0	1.77×10^{-9}	607.6	−0.0632	+0.138	67.5	63.5		
3.00×10^{-5}	137.1	5.68×10^{-9}	536.0	−0.0632	+0.138	63.0	59.2		
1.00×10^{-4}	127.0	2.04×10^{-8}	463.0	−0.0632	+0.138	58.4	54.9		
3.00×10^{-4}	118.5	6.57×10^{-8}	401.0	−0.0632	+0.138	54.4	51.2		
1.00×10^{-3}	109.8	2.36×10^{-7}	337.9	−0.0632	+0.138	50.5	47.4		
3.00×10^{-3}	102.5	7.60×10^{-7}	284.4	−0.0632	+0.138	47.1	44.2		
1.00×10^{-2}	94.9	2.73×10^{-6}	229.8	−0.0632	+0.138	43.6	41.0		
3.00×10^{-2}	88.6	8.79×10^{-6}	183.5	−0.0632	+0.138	40.7	38.3		
0.100	82.1	3.16×10^{-5}	136.4	−0.0632	+0.138	37.7	35.5		
0.101	82.0	3.21×10^{-5}	135.8	−0.0632		37.7	35.4		Tropopause
0.150	95.0	4.10×10^{-5}	119.9	0.375	−0.815	43.6	69.8		Correspondence Level
0.275	119.0	5.99×10^{-5}	90.3	0.370	−0.805	54.7	86.8	0.000262	
0.300	122.9	6.33×10^{-5}	85.4	0.369	−0.804	56.5	89.5		
0.335	128.0	6.79×10^{-5}	79.1	0.368	−0.802	58.8	93.1	0.00241	
0.425	139.8	7.90×10^{-5}	64.4	0.366	−0.797	64.2	101.3	0.0286	NH_3 Cloud Base
1.00	190.5	1.36×10^{-4}	0.0	0.359	−0.780	87.5	136.5		Zero of Altitude
1.29	209.0	1.61×10^{-4}	−23.7	0.356	−0.775	96.0	149.1	0.00568	
1.63	227.0	1.87×10^{-4}	−47.0	0.354	−0.770	104.3	161.4	0.0535	
2.13	249.0	2.21×10^{-4}	−75.7	0.351	−0.765	114.4	176.4	0.528	Solid H_2O Cloud Base
3.00	280.9	2.77×10^{-4}	−117.6	0.348	−0.758	129.6	197.9		
10.0	424.1	6.12×10^{-4}	−310.1	0.337	−0.733	194.8	293.6		
30.0	610.5	1.28×10^{-3}	−568.5	0.327	−0.711	280.5	416.0		
100.0	899.7	2.88×10^{-3}	−981.4	0.318	−0.691	413.3	605.7		
300.0	1270.5	6.13×10^{-3}	−1524.0	0.311	−0.676	583.6	846.8		
1000.0	1840.1	1.41×10^{-2}	−2375.0	0.305	−0.663	845.3	1215.8		

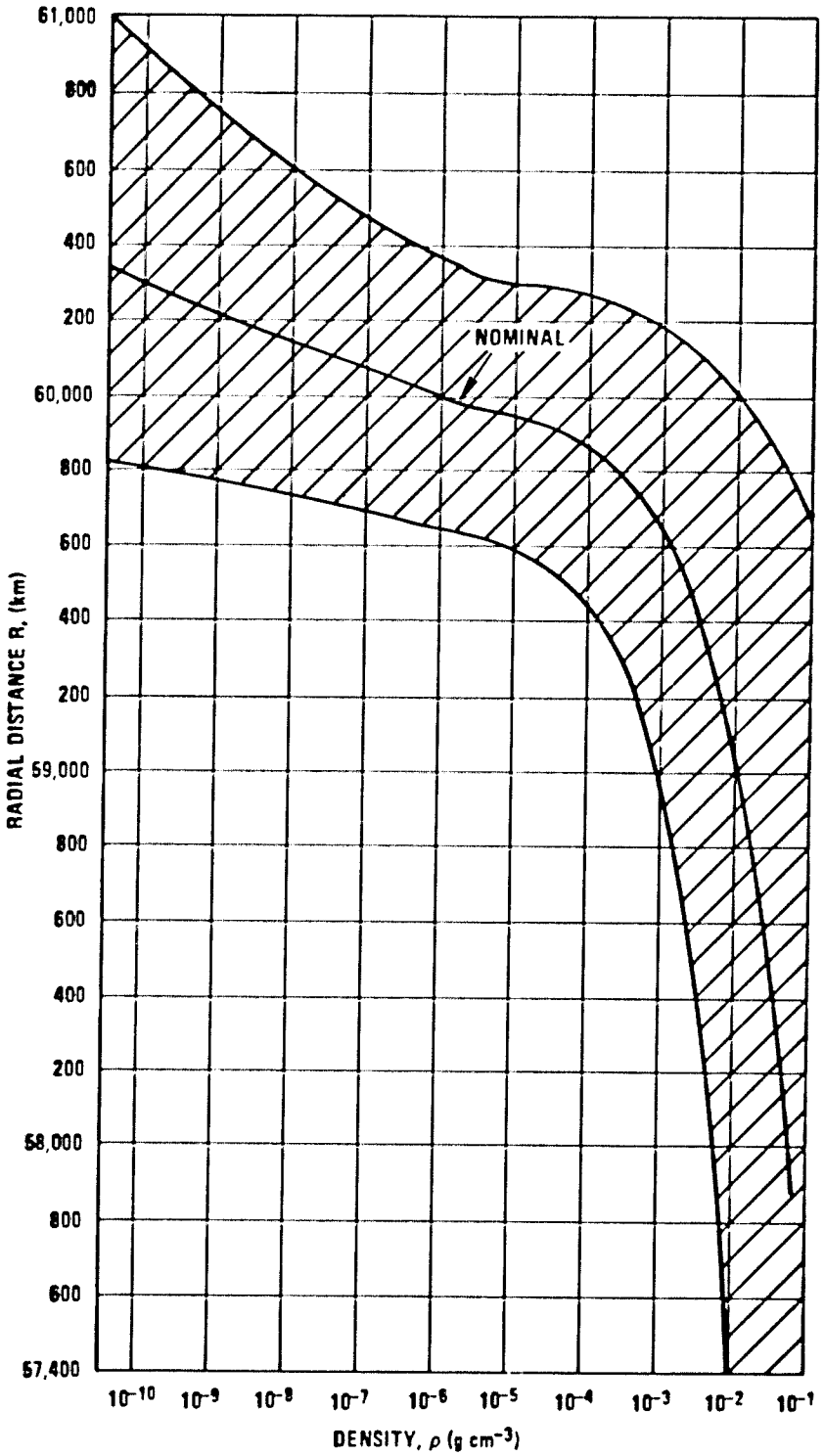

Figure 9.—Range of density vs radial distance at the equator permitted by the model atmospheres, including ± 350 km uncertainty in the equatorial radius of Saturn.

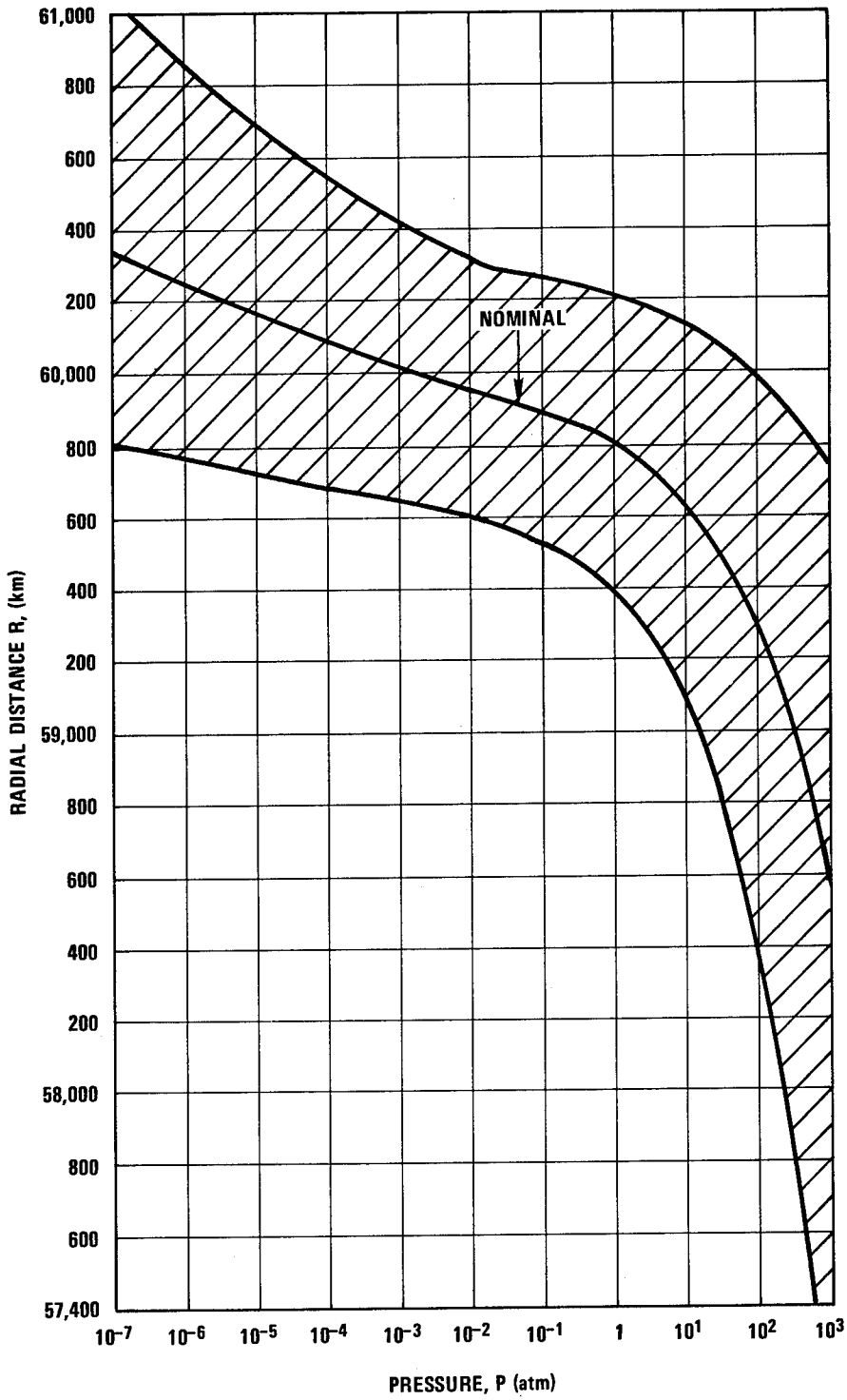

Figure 10.—Range of pressure vs radial distance at the equator permitted by the model atmospheres, including ± 350 km uncertainty in the equatorial radius of Saturn.

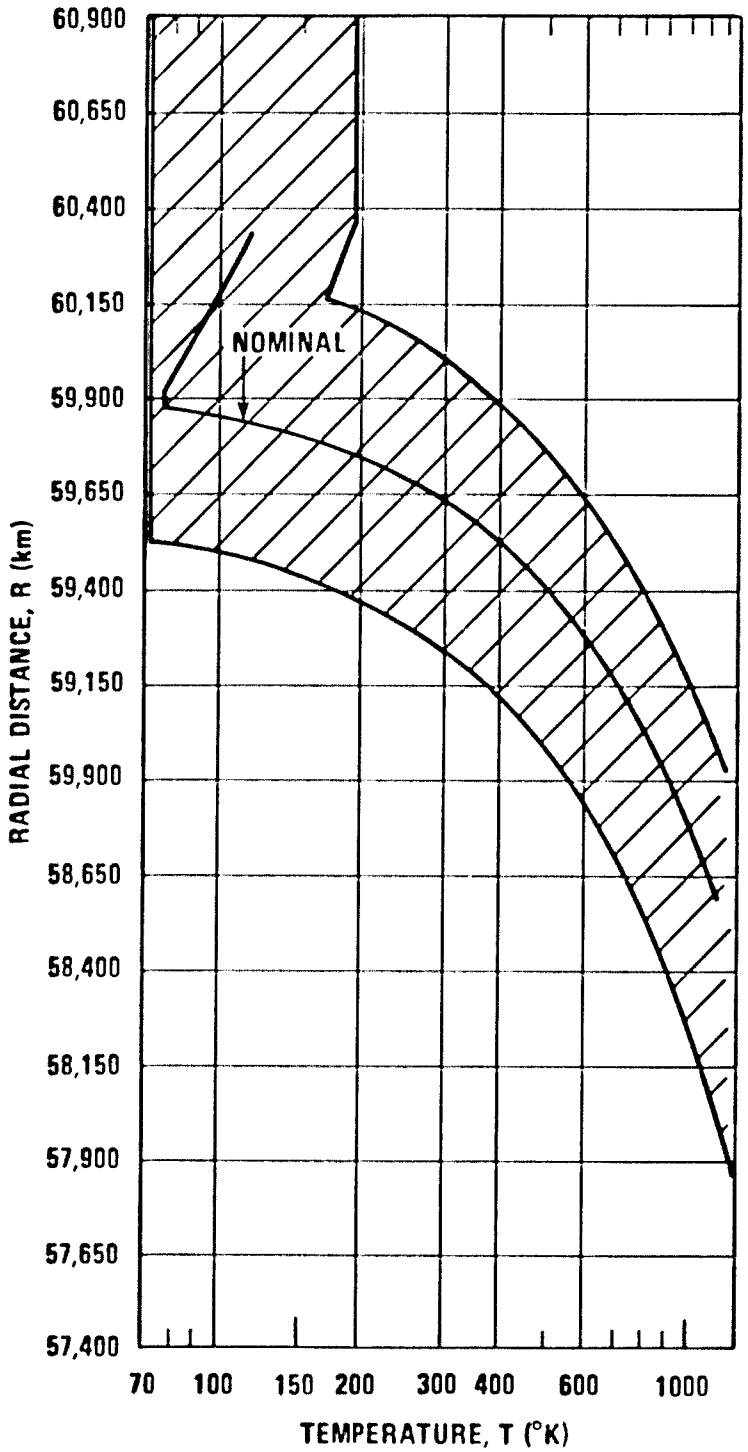

Figure 11.—Range of temperature vs radial distance at the equator permitted by the model atmospheres, including ± 350 km uncertainty in the equatorial radius of Saturn.

REFERENCES

1. Melbourne, W. G.; Mulholland, J. D.; Sjogren, W. L.; and Sturms, F. M. Jr.: Constants And Related Information For Astrodynamic Calculations, 1968. Tech. Rep. 32-1306, Jet Propulsion Lab., Pasadena, Calif., 1968.

2. Sturms, F. M. Jr.: Polynomial Expressions For Planetary Equations And Orbit Elements With Respect To The Mean 1950.0 Coordinate System. JPL, TR 32-1508, 1971.

3. Kelpczynski, W. J.; Seidelmann, P. K.; and Duncombe, R. L.: The Masses Of Saturn And Uranus. Astronomical J., vol. 75, no. 6, 1970, pp. 739-742.

4. Marsden, B. G.: The Orbit Of Hildago. Bull. Of The Amer. Astron. Soc., vol. 2, no. 3, 1970, p. 249, abstract.

5. Klepczynski, W. J.; Seidelmann, P. K.; and Duncombe, R. L.: The Masses Of The Principal Planets. Paper presented at I.A.U. Colloquium, no. 9, Heidelberg, Aug 1970.

6. Lieske, J. H.; Melbourne, W. G.; O'Handley, D. A.; Holdridge, D. B.; Johnson, D. E.; and Sinclair, W. S.: Simultaneous Solution For The Masses Of The Principal Planets From Analysis Of Optical, Radar, And Radio Tracking Date. Paper presented at I.A.U. Colloquium, no. 9, Heidelberg, Aug. 1970.

7. Kovalevsky, J.: Determination Of The Masses Of The Planets. Paper presented at I.A.U. Colloquium, no. 9, Heidelberg, Aug. 1970.

8. Jeffreys, H. Second-Order Terms In The Figure Of Saturn. Royal Astron. Soc. Monthly Notices, vol. 114, no. 4, 1954, pp. 433-436.

9. Mechtly, E. A.: The International System Of Units – Physical Constants And Conversion Factors, Revised. NASA SP-7012, 1969.

10. Cook, A. F.; Franklin, F. A.; and Palluconi, F. D.: Saturn's Rings – A Survey. JPL TM 33-488, 1970, 48 pp.

11. Gurnette, B. L.; and Woolley, R.v.d.R: Explanatory Supplement To The Astronomical Ephemeris And The American Ephemeris And Nautical Almanac. Her Majesty's Stationery Office, London, 1961.

12. Kozai, Y.: On The Astronomical Constants Of The Saturnian Satellites System. Annals Of The Tokyo Astronomical Observatory, 2nd Series, vol. 5, no. 2, 1957/58, pp. 73-106.

13. Carr, T. D.; and Gulkis, S.: The Magnetosphere Of Jupiter. Annual Review Of Astronomy and Astrophysics, vol. 7, 1969, pp. 577-618.

14. Warwick, J. W.: Particles And Fields Near Jupiter. NASA Contractor Rep. CR - 1685, 1970.

15. Smith, A. G.; Lebo, G. R.; Six, N. F.; Carr, T. D.; Bollhagen, H., May J.; and Levy, J.: Decameter-Wavelength Observations Of Jupiter – The Apparitions Of 1961 And 1962. Astrophys. J., vol. 141, no. 2, 1965, pp. 457-477.

16. Smith, A. G.: Studies Of Sporadic Radio Frequency Emission From The Planets. Univ. of Florida, Physics & Astron. Dept., DA-31-124-AROD-G903, Final Rep., 1969.

17. Drake, F. D.: Research In Ionospheric Physics. Cornell Univ., Ithaca, N.Y., Center for Radiophysics and Space Research, 1968.

18. Warwick, J. W.: Private communication, 1970.

19. Rose, W. K.; Bolgna, J. M.; and Sloanaker, R. M.: Linear Polarization Of The 3200 – Mc/sec. Radiation From Saturn. Phys. Rev. Letters, vol. 10, 1963, pp. 123-125.

20. Davies, R. D.; Beard, M.; and Cooper, B.F.C.: Observation Of Saturn At 11.3 Centimeters. Phys. Rev. Let., vol. 13, no. 10, 1964, pp. 325-327.

21. Kellermann, K. I.: The Thermal Radio Emission From Mercury, Venus, Mars, Saturn, And Uranus. Icarus, vol. 5, 1966, pp. 478-490.

22. Berge, G. L.; and Read, R. B.: The Microwave Emission Of Saturn. Astrophys. J., vol. 152, 1968, pp. 755-764.

23. Berge, G. L.: Recent Observations Of Saturn, Uranus, and Neptune At 3.12 Cm. Astrophys. Letters, vol. 2, 1968, pp. 127-131.

24. Gerard, E.: Observations Of Saturn, Uranus, And Neptune At 11.13 cm. Astronomy and Astrophys., vol. 2, 1969, pp. 246-248.

25. Allen, C. W.: Astrophysical Quantities, 2nd Ed., Univ. of London, The Athlone Press, 1963.

26. Roberts, J.A.; and Ekers, R. D.: The Position Of Jupiter's Van Allen Belt. Icarus, vol. 5, no. 2, 1966, pp. 149-153.

27. Zheleznyakov, V. V.: Configuration Of The Magnetic Field Of Saturn. Soviet Astronomy – AJ, vol. 8, no. 5, 1965, pp. 765–770.

28. Zlotnik, E. Ya: The Influence Of Saturn's Rings On Its Exosphere And Magnetic Field. Soviet Astronomy AJ, vol. 11, no. 3, 1967, pp. 462–470.

29. Goldreich, P.; and Lynden-Bell, D.: Io, A Jovian Unipolar Inductor. Astrophys. J., vol. 156, no. 1, 1969, pp. 59–78.

30. Fleagle, R. G.; and Businger, J. A.: An Introduction To Atmospheric Physics. Academic Press, N.Y., 1963.

31. Anon.: Solar Electromagnetic Radiation.NASA SP-8005, revised 1971.

32. Franklin, F. A.; and Cook, A. F.: Optical Properties Of Saturn's Rings. II. Two-Color Phase Curves Of The Two Bright Rings. Astronomical J., vol. 70, no. 9, 1965, pp. 704-720.

33. Bobrov, M. S.: Optics and Geometry Of The Matter Of Saturn's Rings, Physics of Planets. Proc. 11th Int. Astrophys. Sym., Liege, Belgium, July 9-12, 1962, p. 516-521.

34. Bless, R. C.; Code, A. D.; and Taylor, D. J.: Filter Photometry Of Saturn In the spectral Region λλ2950-2450. Astrophys. J., vol. 154, no. 3, 1968, pp. 1151-1153.

35. Harris, D. L.: Photometry And Colorimetry Of Planets And Satellites, Solar Systems. Kuiper, G. P. and Middlehurst, B. M., eds., Univ. of Chicago Press, vol. 3, chap. 8, 1961, pp. 272-342.

36. Walker, R. G.: Infrared Photometry of Stars And Planets, Doctoral Thesis, Harvard Univ. Press, Cambridge, Mass. 1966.

37. Focas, J. H.; and Dollfus, A.: Results About Major Planets. II. Final Scientific Report Vol. 2, U.S.A.F. Cambridge Research Laboratories, Report No. AFCRL – 69 – 0530 (II), 1969.

38. Hämeen – Anttila, K. A.: A Model Of Saturn's Rings. Results About Major Planets II, Final Sci. Rep., U.S.A.F. Cambridge Res. Lab., Rep No. AFCRL – 69 – 0530 (I), vol. 2, Part 5, 1969.

39. Lumme, K.: On Photometric Properties Of Saturn's Rings. Astrophys. & Space Sci., vol. 8, no. 1, 1970, pp. 90-101.

40. Alexander, A.F. O'D.: The Planet Saturn. MacMillan Co., N. Y., 1962.

41. Dollfus, A.: Visual And Photographic Studies Of Planets At The Pic Du Midi, Planets and Satellites. Kuiper, G. P., and Middlehurst, B.M. eds., Univ. of Chicago Press, 1961, pp. 534-570.

42. Guerin, P.: The New Ring Of Saturn. Sky and Telescope, vol. 40, no. 2, 1970, p. 88.

43. Feibelman, W. A.: Concerning The "D" Ring Of Saturn. Nature, vol. 214, 1967, pp. 793-794.

44. Sharonov, V. V.: The Nature Of The Planets. Gosudarstvennoe izdatel'stro Fiziko-matematicheskoi Literatury Moskva 1958, Transl., Jerusalem, 1964, available from Off. Tech. Services, Wash. D.C..

45. Low, F. J.; and Davidson, A. W.: The Thermal Emission Of Jupiter And Saturn. Bulletin American Astronomical Society, vol. 1, 1969, p. 200, abstract.

46. Murray, B. C.; and Wildey, R. L.: Stellar And Planetary Observations At 10 Microns. Astrophys. J., vol. 137, no. 2, 1963, pp. 692-693.

47. Low, F. J.: Infrared Brightness Temperature Of Saturn. Astronomical J., vol. 69, 1964, pp. 550-551.

48. Low, F. J.: Planetary Radiation At Infrared And Millimeter Wavelengths. Lowell Obs. Bull. No. 128, vol. 6, no. 9, 1965, pp. 184-187.

49. McElroy, M. B.: Atmospheric Composition Of The Jovian Planets. J. Atmos. Sci., vol. 26, 1969, pp. 798-812.

50. Low, F. J.: Observations Of Venus, Jupiter, And Saturn At λ 20μ. Astronomical J., vol. 71, 1966, p. 391.

51. Aumann, H. H.; Gillespie, C. M., Jr.; and Low, F. J.: The Internal Powers And Effective Temperatures Of Jupiter And Saturn. Astrophys. J. Let., vol. 157, 1969, pp. L69-L72.

52. Low, F. J.; and Davidson, A. W.: Lunar Observations At A Wavelength Of 1 – mm. Astrophys. J., vol. 142, 1965, p. 1278.

53. Tolbert, C. W.: Observed Millimeter Wavelength Brightness Temperatures Of Mars, Jupiter, And Saturn. Astronomical Journal, vol. 71, 1966, pp. 30-32.

54. Epstein, E. E.; Dworetsky, M. M.; Montgomery, J. W.; Fogarty, W. G.; and Schorn, R. A.: Mars, Jupiter, Saturn And Uranus: 3.3 -mm Brightness Temperatures And A Search For Variations With Time Or Phase Angle. Icarus, vol. 13, 1970, pp. 276-281.

55. Epstein, E. E.: Mars, Jupiter, And Saturn – 3.4mm Brightness Temperatures. Astrophys. J. Letters, vol. 151, 1968, pp. L149-L152.

56. Kellermann, K. I.: The Thermal Radio Emission From The Major Planets. J. Res. Radio Science, vol. 5, 1970, pp. 487-493.

57. Kutuza, B. G.; Losovskii, B. Ya; and Solomonovich, A. E.: Radio Emission Of Saturn At 8-mm Wavelength. Soviet Physics – Doklady, vol. 10, no. 4, 1965, pp. 277-278.

58. Wrixon, G. T., and Welch, W. J.: The Millimeter Wave Spectrum Of Saturn, Icarus, Vol. 13, 1970, pp. 163-172.

59. Braun, L. D.; and Yen, J. L.: Some Radio Observations At 35 GHz. Astronomical J. vol. 73, no. 10, 1968, p. S-168, abstract.

60. Welch, W. J.; Thornton, D. D.; and Lohman, R.: Observations Of Jupiter, Saturn, and Mercury At 1.53 cm. Astrophys. J., vol. 146, no. 3, 1966, pp. 799-809.

61. Kellerman, K. I.; and Pauling - Toth, I.I.K.: Observations Of The Radio Emission Of Uranus And Neptune And Other Planets At 1.9 Cm", Astrophys. J., vol. 145, no. 3, 1966, pp. 954-957.

62. Cook, J. J.; Cross, L. G.; Bair, M. E.; and Arnold, C. B.: Radio Detection Of The Planet Saturn. Nature, vol. 188, no. 4748, 1960, pp. 393-394.

63. Seling, T. V.: Observations Of Saturn At λ 3.75 cm. Astronomical J., vol. 75, no. 1, 1970, pp. 67-68.

64. Hughes, M. P.: Planetary Observations At A Wavelength of 6-cm. Planetary and Space Science, vol. 14, 1966, pp. 1017-1022.

65. Drake, F. D.: Microwave Spectrum Of Saturn. Nature, vol. 195, No. 4484, 1962, pp. 893-894.

66. Davies, R. D.; and Williams, D.: Observations Of The Continuum Emmision From Venus, Mars, Jupiter, And Saturn At 21.2 Cm Wavelength. Planet. Space Sci., vol. 14, 1966, pp. 15-32.

67. Gulkis, S.; McDonough, T. R.; and Craft, H.: The Microwave Spectrum Of Saturn. Icarus, vol. 10, no. 3, 1969, pp. 421-427.

68. McAdam, W. B.: Observations Of Emission From Saturn At 408 MHz. Astronomical Soc. of Australia, Proc., vol. 1, 1969, pp. 199-201.

69. Berge, G. L.: An Interferometric Study Of Jupiter's Decimeter Radio Emission. Astrophys. J., vol. 146, no. 3, 1966, pp. 767-798.

70. Branson, N. J. B. A.: High Resolution Radio Observations Of The Planet Jupiter. Royal Astronomical Soc. Monthly Notices, vol. 139, no. 2, 1968, pp. 155-162.

71. Kuiper, G. P.; Cruikshank, D. P.; and Fink, U.: The Composition Of Saturn's Rings. Bull. Amer. Astronomical Soc., vol. 2, no. 3, 1970, pp. 335-336.

72. Lebofsky, L. A.; and McCord, T. B.: Nature And Composition Of Saturn's Rings. American Geophysical Union, vol. 51, no. 4, 1970, p. 339.

73. Kuiper, G. P.: Limits Of Completeness. Planets and Satellites. Kuiper, G. P. and Middlehurst, B. M., eds., Univ, Chicago Press, Chicago, chap. 18, 1961, pp. 575-591.

74. Dollfus, A.: The Discovery Of The Tenth Satellite Of Saturn. L'Astronomie, 1968, pp. 253-262.

75. Rosino, L.; and Stagni, R.: Observations Of Saturn During The Period Of Theoretical Disappearance Of The Ring. (October 29 – December 18, 1966). Societa Astronomica Italiana Memorie, vol. 40, 1969, pp. 191-204.

76. Kozai, Y.: Titan and Rhea-Saturnian Satellites 1927-1947. Annals of the Tokyo Astronomical Observatory, 2nd Series, vol. 5, no. 2, 1957/58, pp. 107-127.

77. Kuiper, G. P.: The Atmospheres Of The Earth And Planets. Univ. Chicago Press, Chicago, 1952.

78. Brouwer, D.; and Clemence, G. M.: Orbits and Masses Of Planets And Satellites. Solar System. Kuiper, G. P., and Middlehurst, B. M., eds., Univ. of Chicago Press, vol. 3, chap. 3, 1961, pp. 31-94.

79. Texereau, J.: Observing Saturn's Edgewise Rings, October 1966. Sky and Telescope, vol. 33, 1967, pp. 226-227.

80. Walker, R. L.: A Tenth Satellite Of Saturn?. An anonymous article in Sky and Telescope referencing Walker, P. 71 and p. 93, Feb. 1967.

81. Belton, M. J. S.: An Estimate Of The Abundance And The Rotational Temperature Of CH_4 On Jupiter. Astrophys. J., vol. 157, 1969, pp. 469-477.

82. Cook, A. F.; and Franklin, F. A.: Optical Properties Of Saturn's Rings. I. Transmission. Smithsonian Contributions to Astrophysics, vol. 2, no. 13, 1958, pp. 377-383.

83. Anon: Meteoroid Environment Model – 1970 (Interplanetary and Planetary). Oct. 1970, NASA SP 8038.

84. Cook, A. F.; and Franklin, F. A.: The Effect Of Meteoroidal Bombardment On Saturn's Rings. Astronomical J., vol. 75, 1970, pp. 195-205.

85. Dollfus, A.: New Optical Measurements Of The Diameters Of Jupiter, Saturn, Uranus, And Neptune. Icarus, vol. 12, 1970, pp. 101-117.

86. Dollfus, A.: Results About Major Planets. I. Final Scientific Report, vol. 1, U.S.A.F., Cambridge Res. Lab., Rep. No. AFCRL – 69 – 0530 (I), 1969.

87. See, T. J. J.: Researches On The Equatorial Diameter Of Saturn, And On The Dimensions Of His System Of Rings. Astronomische Nachrichten, vol. 154, 1901, pp. 269-286.

88. See T. J. J.: Micrometrical Measures Of The Equatorial Diameter Of Saturn And His System Of Rings. Astronomische Nachrichten, vol. 157, 1902, pp. 389-400.

89. Lowell, P.: and Slipher, E. C.: Measures of Saturn-Ball, Rings, and Satellites. Lowell Observatory Bulletin 66, 1915, pp. 73-80.

90. Lowell, P.; and Slipher, E. C.: Saturn's Rings, Lowell Observatory Bulletin 68, 1915, pp. 85-115.

91. Focas, J. H.; and Dollfus, A: Propriétés Optiques et Épaisseur des Anneaux de Saturne Observes par la Tranche en 1966. Astron. & Astrophys., vol. 2, 1969, pp. 251-265.

92. Kiladze, R. I.: The Photographic Observations Of The Saturn Rings At The Transit Of The Earth Through Their Plane. Astron. Circ. (Russian), Publ. Off. Astron. Com., USSR Academy of Science, no. 439, 1967.

93. Cook, A. F.; and Franklin, F. A.: Rediscussion Of Maxwell's Adams Prize Essay On The Stability Of Saturn's Rings. Astronomical J., vol. 69, no. 2, 1964, pp. 173-200.

94. Cook, A. F.; and Franklin, F. A.: Rediscussion Of Maxwell's Adams Prize Essay On The Stability Of Saturn's Rings. II. Astronomical J. vol. 71, no. 1, 1966, pp. 10-19.

95. Jeffreys, H.: The Effects Of Collisions On Saturn's Rings. Royal Astron. Soc. Monthly Notices, vol. 107, 1947, pp. 263-267.

96. Bobrov, M. S.: On The Observation Of The Occultation Of Stars By Saturn's Rings. Soviet Astronomy–AJ, vol. 6, no. 4, 1962, pp. 525-531.

97. Moroz, V. I.: Physics Of Planets. NASA TT F-515, 1968, Transl. of Fizika Planet, Nauka. Press, Moscow.

98. Owen, T.: Saturn's Ring And The Satellites Of Jupiter: Interpretations Of Infrared Spectra, Science, vol. 149, 1965, pp. 974-975.

99. Kuiper, G. P.; Cruikshank, D. P.; and Fink, U.: The Composition Of Saturn's Rings. Sky and Telescope, Jan. 1970, p. 14.

100. Pilcher, C. B.; Chapman, C. R.; Lebofsky, L. A.; and Kieffer, H. H.: Saturn's Rings: Identification Of Water Frost. Science, vol. 167, no. 3923, 1970, pp. 1372-1373.

101. Bandermann, L. W.; and Wolstencroft, R. D.: The Erosion Of Particles In The Rings Of Saturn. Bull. Amer. Astron. Soc., vol. 1, 1969, p. 223, abstract.

102. Harrison, H.; and Schoen, R. I.: Evaporation Of Ice In Space: Saturn's Rings. Science, vol. 157, 1967, pp. 1175-1176.

103. Watson, K.; Murray, B. C.; and Brown, H.: The stability Of Volatiles In The Solar System. Icarus, vol. 1, 1963, pp. 317-327.

104. Alfven, H.: On The Structure Of The Saturnian Rings. Icarus, vol. 8, 1968, pp. 75-81.

105. Reiffenstein, J. M.: On The Formation Of The Rings Of Saturn. Planet. Space Sci., vol. 16, 1968, pp. 1511-1524.

106. Franklin, F. A.: and Colombo, G.: A Dynamical Model For The Radial Structure Of Saturn's Rings. Smithsonian Astrophysical Observatory Preprint, 1969.

107. Bobrov, M. S.: Current Status Of The Problem Of The Structure And Order Of Magnitude Of The Thickness Of The Saturn Rings. Fizika Planet (Teifel, V.G. ed.) Akad. Nauk. Kazakhskoi SSR, Astrofizicheskii Institut, Trudy, vol. 9, 1965, pp. 83-93, in Russian.

108. Bobrov, M. S.: Generalization Of The Theory Of The Shadow Effect On Saturn's Rings To The Case Of Particles Of Unequal Size. Soviet Astronomy – AJ, vol. 5, no. 4, 1961, pp. 508-516.

109. Bobrov, M. S.: Theoretical Phase Curves Of The Shadow Effect On Saturn's Rings I. Derivation Of Pertinent Formulas. Soviet Astronomy – AJ, vol. 4, 1960, pp. 288-297.

110. Bobrov, M. S.: Derivation Of The Theoretical Phase Function Of The Brightness Of Saturn's Rings And Its Comparison With Observations. Soviet Astronomy – AJ, vol. 3, no. 1, 1959, pp. 131-135.

111. Bobrov, M. S.: Concerning The Structure Of Saturn's Rings. I. The Degree of Pittedness And The Albedo Of The Particles Of Ring B. Astronomicheskii Zhurnal. Vol. 29, no. 3, 1952, p. 334, in Russian

112. Seelinger, H. von: Fur Theorie d. Beleuchtung d. Grossen Planeten, Insbesondere d. Saturn. Abhandlungen Bayer. Akad. Wisc., K1, II-16, 1887, p. 405.

113. Oetking, P.: Photometric Studies Of Diffusely Reflecting Surfaces With Applications To The Brightness Of The Moon. J. Geophys. Res., vol. 71, 1966, pp. 2505-2513.

114. Hapke, B: Comments On Paper By Philip Oetking, Photometric Studies Of Diffusity Reflecting Surfaces With Applications To The Brightness Of The Moon. J. of Geophys. Res., vol. 71, 1966, p. 2515.

115. Deirmendjian, D.: Electromagnetic Scattering On Spherical Polydispersions. Amer. Elsevier Publ. Co., N.Y., 1969.

116. Cragg, T. A.: Quoted in article in Sky and Telescope, vol. 13, 1954, p. 382.

117. Jeffreys, H.: The Relation Of Cohesion To Roche's Limit. Royal Astron. Soc. Monthly Notices, vol. 107, 1947, pp. 260-262.

118. Haffner, J. W.: Radiation Shielding In Space. Academic Press, N.Y., 1967.

119. Fanselow, J. L.: The Primary Cosmic – Ray Electron Spectrum Between 0.09 And 8.4 BeV In 1965. Astrophys. J., vol. 152, no. 3, 1968, pp. 783-798.

120. Burlaga, L. F.: Anisotropic Diffusion Of Solar Cosmic Rays. J. of Geophys. Res., vol. 27, no. 17, 1967, pp. 4449-4466.

121. McDonald, F. B.; ed.: Solar Proton Manual. NASA TR R-169, 1963.

122. Hundhausen, A. J.: Composition and Dynamics of the Solar Wind Plasma. Rev. Geophys. and Space Science, vol. 8, 1970, pp. 729-811.

123. Warwick, J. W.: Radio Astronomical Techniques For The Study Of Planetary Atmospheres, Radio Astronomical and Satellite Studies of the Atmosphere. Aarons, J., ed., North Am.-Holland Publ., Amsterdam, 1963, pp. 400-429.

124. Gulkis, S.: Lunar Occultation Observations Of Jupiter At 74 Cm And 128 Cm. J. Res. Radio Science, vol. 5, 1970, pp. 505-511.

125. Mayer, C. H.: Radio Emission From The Moon And Planets, Planets and Satellites. Kuiper, G. P. and Middlehurst, B. M., eds, Univ. Chicago Press, Chicago, chap. 12 1961, pp. 442-479.

126. Anon.: The Planet Jupiter (1970). NASA SP-8069, Dec. 1971.

127. Papadopoulos, K., And Lerche, I.: Collective Bremsstrahlung From Relativistic Electrons As A Possible Mechanism In Radio Sources. Astrophys. J., vol. 158, no. 3, 1969, pp. 981-986.

128. Gross, S. H.; and Rasool, S. I.: The Upper Atmosphere Of Jupiter. Icarus, vol. 3, 1964, pp. 311-322.

129. Hunten, D. M.: The Upper Atmosphere Of Jupiter. J. Atmos. Sci., vol. 26, 1969, pp. 826-834.

130. McGovern, W. E.; Exospheric Temperatures Of Jupiter And Saturn. J. of Geophys. Res., vol. 73, 1968, pp. 6361-6363.

131. Owen, T.: The Spectra Of Jupiter And Saturn In The Photographic Infrared. Icarus, vol. 10, 1969, pp. 355-364.

132. Spinrad, H.: Spectroscopic Research On The Major Planets. Applied Optics, vol. 3, 1964, pp. 181-186.

133. Giver, L. P.: High – Dispersion Spectrograms Of Jupiter And Saturn. Publs. Astron. Soc. Pacific, vol. 77, 1965, p. 128, abstract.

134. Moroz, V. I.: The Spectra Of Jupiter And Saturn In The 1.0-2.5 Micron Region. Soviet Astronomy AJ., vol. 10, no. 3, 1966, pp. 457-468.

135. Goody, R.: The Atmospheres Of The Major Planets. J. of Atmos. Sci., vol. 26, 1969, pp. 997-1001.

136. Lewis, J. S.: Observability Of Spectroscopically Active Compounds In The Atmosphere Of Jupiter. Icarus, vol. 10, no. 3, 1969, pp. 373-409.

137. Peebles, P. J. E.: The Structure And Composition Of Jupiter And Saturn. Astrophys. J., vol. 140, no. 1, 1964, pp. 328-347.

138. Hubbard, W. B.: Thermal Models Of Jupiter And Saturn. Astrophys. J. vol. 155, no. 1, 1969, pp. 333-344.

139. Slipher, E. C.: A Photographic Study Of The Brighter Planets. Pub. by Lowell Obs. and Nat'l Geo. Soc., 1964.

140. Lewis, J. S.: The Clouds Of Jupiter And The NH_3-H_2S Systems. Icarus, vol. 10, no. 3, 1969, pp. 365-378.

141. Gillet, F. C.; Low, F. J.; and Stein, W. A.: The 2.8 – 14 Micron Spectrum Of Jupiter. Astrophys. J., vol. 157, 1969, pp. 925-934.

142. Trafton, L. M.; and Münch, G.: The Structure Of The Atmospheres Of The Major Planets. J. Atmos. Sci., vol. 26, 1969, pp. 813-825.

143. Lewis, J. S.; and Prinn, R. G.: Chemistry And Photochemistry Of The Atmosphere Of Jupiter, to appear in Theory and Experiment in Exobiology, Schwartz, A.W., ed.

144. Trafton, L. M.: Model Atmospheres Of The Major Planets. Astrophys. J., vol. 147, no. 2, 1967, pp. 765-781.

145. Moore, J. H.: Spectroscopic Observations Of The Rotation Of Saturn. Pub. Astron. Soc. Pac., vol. 51, 1939, pp. 274-281.

146. Chapman, C. R.: Jupiter's Zonal Winds: Variation With Latitude. J. of Atmospheric Sciences, vol. 26, 1969, pp. 986-990.

147. Anon.: Magnetic Fields – Earth And Extraterrestrial. NASA SP-8017, 1969.

APPENDIX A
SYMBOLS *

A	second brightest of Saturn's five rings (2.6.1.1)
A_R	area of ring region of interest (2.4.2)
$\vec{A}_s$	spacecraft area (direction defined by outward normal) (2.6.3)
A_1	normalization constant (2.6.3)
A_2	normalization constant (2.6.3)
a	semi-major axis of particle orbiting Saturn (3.2)
α_p	right ascension of Saturn's north pole (2.1.3)
B	brightest of Saturn's five rings (2.6.1.1)
$\mathfrak{B}$	magnetic flux density (T) (2.3.1.2)
B_R	elevation angle of observer above ring plane with vertex at ring region of interest (2.4.6)
B_λ , B_ν	Plank function, intensity per unit wave length or frequency (3.4)
B_o	elevation angle of observer above ring plane (2.4.2)
$B'_\odot$	elevation angle of sun above ring plane (2.4.2)
β	atmospheric lapse rate (P/T)(dT/dP) (app. B-1)
β_o	lapse rate constant (app. B-1)
C	third brightest of Saturn's five rings (2.6.1.1)
C_p , C_v	specific heats at constant pressure or volume (app. B-1)
c	speed of light (3×10^{10} cm sec^{-1}) (2.7.1)
γ	ratio of specific heats (app. B-1)
D	innermost of Saturn's five rings (2.6.1.1)
D'	outermost of Saturn's five rings (2.6.1.1)
Δ	distance from object to observer (AU) (2.4.4)
δ_p	declination of Saturn's north pole (2.1.3)
E	charged particle kinetic energy (2.7.1)
E_o	local characteristic (kinetic) energy (MeV) (2.7.4.2)
$\mathcal{E}$	electric field strength (volts/meter) (2.3.2)
ϵ	planetary optical flattening (2.1.2)

*Numbers in parens give section where symbol used herein.

F	integrated flux of electromagnetic radiation (2.4.1)
F_c	flux of meteoroids with mass > m (2.5.2)
F_λ , F_ν	flux per unit wavelength or frequency (3.4)
f	parameter in ring particle models (2.6.3)
G	constant of gravitation (6.673×10^{-8} dyn cm^2/g^2) (2.1.1)
g	acceleration of gravity including rotation (2.2)
H_p	atmosphere pressure scale height (app. B-1)
H_ρ	atmosphere density scale height (app. B-1)
H_λ	solar spectral flux per unit wavelength (2.4.1)
$H_\odot$	solar constant (1.35×10^6 erg/cm^{-2} sec) (2.4.1)
θ	angle formed by the normal to spacefraft area of interest and direction of incident energy (tables XV and XVI)
I_λ , I_ν	intensity per unit wavelength or frequency (3.4)
J_2 , J_4	coefficients of gravitational potential (2.2)
K	constant (cosmic ray flux formula) (2.7.1)
K_1	lapse rate constant (°K) (app. B-1)
K_2	lapse rate constant (°K) (app. B-1)
k	Boltzmann's constant (1.38×10^{-16} erg/°K) (app. B-1)
k_R	ring intensity parameter (I_λ/H_λ) (2.4.2)
k_1 ,k_2	intermediate parameters in ring model (2.6.3)
L	magnetic shell parameter (2.7.4.2)
λ	wavelength of electromagnetic radiation (3.4)
M	magnetic dipole moment (A m^2) (2.3.1.2)
M_s	mass of Saturn system less mass of Titan (2.1.1)
M_{ss}	mass of Saturn system including planet, satellites, and rings (2.1.1)
M_T	mass of Titan (2.1.1)
M_V	apparent visual magnitude (2.4.3)
$M_\odot$	mass of the Sun (2.1.1)
m	mass of particle (2.6.3)
m_o	rest energy of particle (2.7.1)

μ	mean molecular weight (g/mole) (app. B-1)
N_E	number density, evaluated for charged particles of energy $\geqslant$ E (2.7.4.2)
N_o	characteristic number density (electrons and protons) (2.7.6)
dN_1, dN_2	relative number of ring particles with radius between r and r + dr (2.6.3)
ν	wave frequency (3.4)
P	atmospheric pressure (app. B-1)
P_{orb}	orbital period of object about Saturn (3.2)
P_2, P_4	Legendre polynomials (2.2)
p_λ	geometric albedo (wavelength dependent) (2.4.1)
p_g	integrated geometric albedo (2.4.1)
Ψ	phase angle (2.4.2)
R	distance from center of Saturn (2.4.1)
R_g	universal gas constant (82.082 cm^3 atm/mole °K) (app. B-1)
R_o	R evaluated at visible disk of Saturn (2.1.2)
R_p	polar radius of Saturn's visible disk (2.1.2)
R_s	equatorial radius of Saturn's visible disk (2.1.2)
R_{sat}	radius of a satellite (2.4.4)
$R_{s\odot}$	distance from Saturn to the Sun (2.4.1)
r	radius of ring particles (2.6.3)
ρ	atmospheric gas density (g/cm^3) (app. B-1)
$\overline{\rho}$	mean density of Saturn (2.1.2)
ρ_p	mass density of ring particles (2.6.3)
σ	coefficient of rotational term in gravitational potential (2.2)
S	observer to Sun distance (2.4.1)
S_c	number density of meteoroids with mass $\geqslant$ m (2.5.2)
S_m	areal number density of ring particles with mass $\geq$m (2.6.3)
T	physical temperature of atmosphere (°K) (app. B-1)
T_D	disk brightness temperature (°K) (2.4.5)
T_e	effective temperature of Saturn (°K) (2.8.2)

T_o	Saturn rotation period (2.9.2.1)
T_{sy}	Synchrotron source brightness temperature (2.4.5)
τ	normal, optical thickness (dimensionless) (2.4.1)
$\bar{\tau}$	τ averaged over area of interest (2.4.6)
U	gravitational potential function (2.2)
V_c	meteroid speed (2.5.2)
V_{esc}	escape speed for an object leaving Saturn (3.2)
V_{orb}	speed of an object in orbit about Saturn (3.2)
$\vec{V}_p$	velocity of ring particle (relative to Saturn) (2.6.3)
$\vec{V}_{rel}$	relative velocity between spacecraft and ring particle (2.6.3)
V_s	speed of spacecraft (relative to Saturn) (2.5.3)
$\vec{V}_s$	velocity of spacecraft (relative to Saturn) (2.6.3)
V_{sz}	speed of spacecraft normal to ring plane (2.6.3)
V_v	absolute visual magnitude (2.4.1)
w	amount of cloud material per unit volume of gas (app. B-1)
z	altitude above Saturn's visible disk (2.2)
z_o	altitude of NH_3 cloud base (2.8.3)
z_1	nominal ionosphere altitude (2.7.6)
Φ_E	flux of particles with energy $\geq$ E (2.7.1)
ϕ	Chronocentric latitude (2.1.2)
ϕ'	Chronographic latitude (2.2)
ϕ_m	magnetic latitude (2.3.1)
Ω	solid angle (2.4.2)
Ω_R	Ω subtended by ring region of interest (2.4.2)
Ω_e	Ω subtended by Sun at one AU (2.4.1)
ω_o	Saturn's angular rotation rate (2.9.2.1)

APPENDIX B

ATMOSPHERE AND CLOUDS (MATHEMATICAL BASIS)

In terms of the symbols defined in appendix A, the model atmospheres of sections 2.8 and 3.8 are governed, for each atmospheric region, by

(1) hydrostatic equilibrium $$\frac{dP}{dz} = -\rho g \tag{B1}$$

(2) the perfect gas law $$\rho = \mu P/R_g T \text{, and} \tag{B2}$$

(3) a temperature-dependent gradient $$\frac{d \log T}{d \log P} = \beta = \beta_o \frac{T + K_1}{T + K_2} \tag{B3}$$

where values of the constants K_1 and K_2 are restricted by $K_2 \geq 0$ in general, by $K_1 = K_2 = 0$ for regions of constant $\beta = \beta_o \neq 0$, and by $K_1 = -T_A$ and $K_2 = 0$ for regions of $\beta = 0$ (at constant temperature $T = T_A$). Values of K_1 and K_2 can be chosen to ensure that β approximates the adiabatic value $(\gamma-1)/\gamma$ for a real gas mixture whose specific heats are related by $\gamma = C_p/C_v$. (If C_p and C_v increase with temperature, $K_1 > K_2 > 0$ results.)

The solution of equations B1 through B3 requires that T and z at any value of P be related to those at T_A, z_A, and P_A in the same region by

$$\left(\frac{P}{P_A}\right)^{\beta_o} = \left(\frac{T}{T_A}\right)^{K_2/K_1} \left(\frac{T + K_1}{T_A + K_1}\right)^{(K_1-K_2)/K_1} \tag{B4}$$

$$z = z_A - \frac{R_g}{ug}\left(\frac{T - T_A}{\beta_o} - K_1 \ln\frac{P}{P_A} + \frac{K_2}{\beta_o} \ln\frac{T}{T_a}\right) \tag{B5}$$

The lapse rate and scale heights are given by

$$dT/dz = -\beta\mu g/R_g \tag{B6}$$

$$Hp = R_g T/\mu g$$

$$H\rho = H_p/(1-\beta) .$$

It is assumed that clouds are formed by condensation of a species j in convective regions moving upward to lower temperature and pressure when the saturation vapor pressure P_{js} is exceeded by the partial pressure. P_{js} is conventionally described by a form of the Clausius-Clapeyron equation

$$P_{js} = \exp [A_j - (\lambda_j / R_g T)] .$$

Here A_j and λ_j are constants, and λ_j is the latent heat of condensation. In this case P_{js} also specifies the partial pressure of the condensible gas in the cloud region above the lowest level of condensation, and the mass of the cloud per unit volume of gas is approximated by

$$W_j = \frac{\mu_j P_{js}}{R_g T} \left(\frac{\beta \lambda_j - R_g T}{\beta \lambda_j} \right). \tag{B7}$$

Here β is given by equation B3, and μ_j is the mean molecular weight of the condensate.

Table B-1 lists the four species actually used in computing cloud properties and the appropriate constants.

TABLE B-1.

PARAMETERS OF CONDENSATES

	Liquid H_2O	Solid H_2O Ice	Solid NH_3 Ice	Solid CH_4 Ice
μ_j (grams/mole)	18	18	17	16
A_j (for P_{js} in mm Hg)	20.592	24.055	23.744	18.651
λ_j (cal/mole)	10,350.67	12,230.27	7,740.64	2,537.18

In establishing the location of the cloud bases, condensation to a pure (one molecular species) solution or solid was assumed. For NH_3 - H_2O solutions as dilute as those likely in the nominal and warm models the liquid water constants were considered satisfactory approximations. For the cool model, the likely existence of NH_3 - H_2O solutions could result in the elimination of any solid H_2O phase.

APPENDIX C
GLOSSARY *

Adiabatic – Characteristic of processes in which heat is not transferred across system boundaries; in an atmosphere such a system is a hypothetically rising or falling parcel of gas, and the adiabatic requirement must be satisfied when the parcel reaches equilibrium with the local pressure, temperature, and density.

Apoapsis – That point in an orbit farthest from the center of attraction.

Astronomical Unit (AU) – The semi-major axis of the Earth's orbit about the Sun approximately; Gurnette and Woolley (ref. 11) provide a more precise definition; a modern value cited by Melbourne et al. (ref. 1) is 1 AU = $1.49597893 \times 10^8 \pm 5$ km.

Bandwidth – The range of frequencies (or wavelengths) within which electromagnetic radiation is emitted or detected; the power or response distributions need not be uniform within this range (ref. 35).

Bolometric – Characteristic of an infinite **bandwidth**, and including electromagnetic radiation at all frequencies (or wavelengths) and polarizations (ref. 25).

Brightness Temperature – The temperature at which a blackbody would radiate an intensity of electromagnetic radiation identical to that of the source for the **bandwidth** and polarization considered.

Chronocentric – Referenced to the center of Saturn (ref. 44).

Chronographic – Referenced to a line parallel to the direction of the **zenith** at Saturn.

Color – For a given light source, the difference in **magnitude** for two **bandwidths** centered on different wavelengths (ref. 35).

Decametric – Characteristic of electromagnetic radiation at those radio wavelengths between 10 and 100 meters; used here to cover a broader range extending perhaps to 7 meters.

Decimetric – Characteristic of electromagnetic radiation at those microwave wavelengths between 10 and 100 cm; used here synonymously with **UHF** to cover a broader range extending perhaps to 1 cm.

Declination – The celestial coordinate equal to the angle (north taken positive) between the direction of the item considered and the plane of the Earth's equator; the precession of the latter implies a slow variation of the declination even of fixed directions (ref. 11).

Disk Brightness Temperature (T_D) – The resulting **brightness temperature** when all radiation (excluding background sources) from a region surrounding an object is associated with the disk of that object; for Saturn the disk brightness temperature may include a contribution from the rings (thermal) and/or radiation belts (non-thermal).

Elevation Angle (B_o, B_{ob}, B_R, $B_\odot$) – The angular distance of a (intersecting) line above a plane; the Saturn equatorial (ring) plane is used exclusively.

---

*Bold face indicates cross references in glossary.

Effective Temperature (T_e) – The temperature at which a blackbody would radiate a bolometric intensity of electromagnetic radiation identical to that of the source (ref. 25).

Elongation – For a planetary satellite system, the configuration of planet and satellite which presents the largest angular displacement between the two as seen from the Earth.

Flattening (ϵ) – The positive difference between unity and the ratio of the polar to the equatorial diameter of a planetary disk (optical), or the value for the same quantity which would be derived on the basis of hydrodynamic theory and the gravitational potential inferred from observed satellite motions.

Flux, of Electromagnetic Radiation (F, F_ν, or F_λ) – The power per unit area crossing an imaginary plane surface from one side to the other, either per unit bandwidth or integrated over all frequencies.

Flux, of Charged Particles (ϕ_k) – The number of particles per unit area and per unit time crossing an imaginary plane surface with positive or negative (but not both) velocity components perpendicular to the surface.

Geometric Albedo (p_λ) – In the bandwidth considered, the ratio of the reflected flux (power per unit detector area) from an astronomical object (observed at distance Δ, zero phase angle) to the quotient of the solar power intercepted by the object divided by $\pi \Delta^2$. Here the flux, the power, and Δ must be expressed in consistent units, and Δ must be large compared to the dimensions of the object (refs. 25 and 35).

Intensity (I_ν or I_λ) – The flux of electromagnetic radiation per unit solid angle of the source for a defining imaginary surface whose normal intersects the source; intensity is independent of the source-surface separation.

Ionosphere – The atmospheric layer which includes the major maxima of electron and ion concentration.

Magnetopause – The outer boundary of the magnetosphere, where a planet's field interacts with external magnetic field and charged particle environments, particularly the solar wind (ref. 147).

Magnetosphere – The region surrounding a planet in which the local magnetic field is dominated by planet-associated fields rather than by external environments (ref. 147).

Magnitude (V_ν) – Five-halves times the common logarithm (base ten) of the ratio of the power received per unit area within some bandwidth for a standard object to that for an astronomical object. The base of this logarithmic scale is $x = 2.512$, such that an increase of one magnitude corresponds to a decrease in power by a factor x^{-1} or an increase in distance by a factor $x^{1/2}$. For solar system objects, absolute magnitudes V_ν are those assumed to occur in a standard geometrical configuration, namely Sun-object distance 1 AU, object-observer distance $\Delta = 1$ AU, and phase angle $\Psi = 0$. Standard objects are commonly defined on the UBVRI system of magnitudes, corresponding to specific wavelength-dependent response characteristic of the observing equipment (refs. 25 and 35).

Megahertz (MHz) – The frequency unit 10^6 cycles per second.

Optical Thickness (τ) – A parameter related to absorption and scattering of electromagnetic radiation. The ratio of the intensity of a source after (absorption and scattering) to that before is $\exp(-\tau)$ (ref. 32).

Phase Angle (Ψ) – The angle Sun-object-observer (ref. 35).

Photometric Passband – The range of wavelengths or frequencies within which electromagnetic radiation is detected. The response of a given device is rarely uniform within its passband. Photometric passbands may be narrow or broad and a number of photometric systems designated by letters such as U, B, V, etc. are in general use. See Newburn and Gulkis (1971), TR 32-1529, JPL and the references therein for a discussion of photometric systems.

Pitch Angle – The angle between the particle velocity vector and the external magnetic field vector evaluated at the position of the particle.

Plasma – A gas in which the concentration of charged particles has non-negligible effects on the properties of the gas.

Prograde – The sense of rotation or revolution common in the solar system in which the motion is counter-clockwise as viewed from the north.

Rayleigh Scattering – Scattering of electromagnetic radiation by particles whose characteristic size is small compared to the wavelength λ. In this case, the scattering center may be approximated by an oscillating electric dipole, whose scattering cross-section and opacity are proportional to λ^{-4}.

Right Ascension – The celestial coordinate equal to the angle (east taken positive) between the projection on the plane of the Earth's equator of the direction of the item considered and that of the **vernal equinox**; the precession of the Earth's rotation axis implies a slow variation of the right ascension even of fixed directions (ref. 11).

Scale Height (H_p, H_ρ) – A measure of the vertical gradient of a quantity x, e.g., pressure, electron concentration, such that if $H = x\,(dx/dz)^{-1}$ is constant with altitude z, the quantity x changes by a factor e within the altitude interval H.

Stratopause – The upper boundary of the **stratosphere**, characterized by a near-discontinuity in the temperature gradient.

Stratosphere – The atmospheric layer directly above the **troposphere** within which the temperature is constant or increases with altitude.

Trapped Radiation – Energetic charged particles whose trajectories in a planetary magnetic field are bounded in space. A particle travels nearly along the field line, "mirrors" at equal north and south magnetic latitudes, and drifts in longitude.

Tropopause – The upper boundary of the **troposphere** and the lower boundary of the **stratosphere**, characterized by a near-discontinuity in the temperature gradient.

Troposphere – The atmospheric layer within which major weather phenomena occur, characterized by decreasing temperature with altitude.

Ultra High Frequency (UHF) – Characteristic of electromagnetic radiation at those microwave frequencies between 300 and 3000 **MHz**, used here synonymously with **decimetric** to cover a broader range extending perhaps to 30,000 **MHz**.

Vernal Equinox – The direction from the center of the Earth to the center of the Sun at the time when the latter lies in the plane of the Earth's equator in March of each year (ref. 11).

Zenith – The direction opposite to that of the local acceleration of gravity (including the centrifugal terms) and perpendicular to the local horizon.

Zenith Angle – The angle between the directions to the zenith and to an object observed.

NASA SPACE VEHICLE DESIGN CRITERIA MONOGRAPHS

ENVIRONMENT

SP-8005	Solar Electromagnetic Radiation, revised May 1971
SP-8010	Models of Mars Atmosphere (1967), May 1968
SP-8011	Models of Venus Atmosphere (1968), December 1968
SP-9-13	Meteoroid Environment Model–1969 (Near Earth to Lunar Surface), March 1969
SP-8017	Magnetic Fields–Earth and Extraterrestrial, March 1969
SP-8020	Mars Surface Models (1968), May 1969
SP-8021	Models of Earth's Atmosphere (120 to 1000 km), May 1969
SP-8023	Lunar Surface Models, May 1969
SP-8037	Assessment and Control of Spacecraft Magnetic Fields, September 1970
SP-8038	Meteoroid Environment Model–1970 (Interplanetary and Planetary), October 1970
SP-8049	The Earth's Ionosphere, March 1971
SP-8067	Earth Albedo and Emitted Radiation, July 1971
SP-8069	The Planet Jupiter (1970), December 1971
SP-8084	Surface Atmospheric Extremes (Launch and Transportation Areas), May 1972
SP-8085	The Planet Mercury (1971), March 1972
SP-8092	Assessment and Control of Spacecraft Electromagnetic Interference, June 1972

STRUCTURES

SP-8001	Buffeting During Atmospheric Ascent, revised November 1970
SP-8002	Flight-Loads Measurements During Launch and Exit, December 1964
SP-8003	Flutter, Buzz, and Divergence, July 1964
SP-8004	Panel Flutter, July 1964
SP-8006	Local Steady Aerodynamic Loads During Launch and Exit, May 1965
SP-8007	Buckling of Thin-Walled Circular Cylinders, revised August 1968
SP-8008	Prelaunch Ground Wind Loads, November 1965
SP-8009	Propellant Slosh Loads, August 1968
SP-8012	Natural Vibration Modal Analysis, September 1968
SP-8014	Entry Thermal Protection, August 1968
SP-8019	Buckling of Thin-Walled Truncated Cones, September 1968

SP-8022	Staging Loads, February 1969
SP-8029	Aerodynamic and Rocket-Exhaust Heating During Launch and Ascent, May 1969
SP-8031	Slosh Suppression, May 1969
SP-8032	Buckling of Thin-Walled Doubly Curved Shells, August 1969
SP-8035	Wind Loads During Ascent, June 1970
SP-8040	Fracture Control of Metallic Pressure Vessels, May 1970
SP-8042	Meteoroid Damage Assessment, May 1970
SP-8043	Design–Development testing, May 1970
SP-8044	Qualification testing, May 1970
SP-8045	Acceptance testing, April 1970
SP-8046	Landing Impact Attenuation For Non-Surface-Planing Landers, April 1970
SP-8050	Structural Vibration Prediction, June 1970
SP-8053	Nuclear and Space Radiation Effects on Materials, June 1970
SP-8054	Space Radiation Protection, June 1970
SP-8055	Prevention of Coupled Structure-Propulsion Instability (Pogo), October 1970
SP-8056	Flight Separation Mechanisms, October 1970
SP-8057	Structural Design Criteria Applicable to a Space Shuttle, January 1971
SP-8060	Compartment Venting, November 1970
SP-8061	Interaction With Umbilicals and Launch Stand, August 1970
SP-8062	Entry Gasdynamic Heating, January 1971
SP-8063	Lubrication, Friction, and Wear, June 1971
SP-8066	Deployable Aerodynamic Deceleration Systems, June 1971
SP-8068	Buckling Strength of Structural Plates, June 1971
SP-8072	Acoustic Loads Generated by the Propulsion System, June 1971
SP-8077	Transportation and Handling Loads, September 1971

GUIDANCE AND CONTROL

SP-8015	Guidance and Navigation for Entry Vehicles, November 1968
SP-8016	Effects of Structural Flexibility on Spacecraft Control Systems, April 1969
SP-8018	Spacecraft Magnetic Torques, March 1969
SP-8024	Spacecraft Gravitational Torques, May 1969
SP-8026	Spacecraft Star Trackers, July 1970
SP-8027	Spacecraft Radiation Torques, October 1969
SP-8028	Entry Vehicle Control, November 1969

SP-8033	Spacecraft Earth Horizon Sensors, December 1969
SP-8034	Spacecraft Mass Expulsion Torques, December 1969
SP-8036	Effects of Structural Flexibility on Launch Vehicle Control Systems, February 1970
SP-8047	Spacecraft Sun Sensors, June 1970
SP-8058	Spacecraft Aerodynamic Torques, January 1971
SP-8059	Spacecraft Attitude Control During Thrusting Maneuvers, February 1971
SP-8065	Tubular Spacecraft Booms (Extendible, Reel Stored), February 1971
SP-8070	Spaceborne Digital Computer Systems, March 1971
SP-8071	Passive Gravity-Gradient Libration Dampers, February 1971
SP-8074	Spacecraft Solar Cell Arrays, May 1971
SP-8078	Spaceborne Electronic Imaging Systems, June 1971

CHEMICAL PROPULSION

SP-8025	Solid Rocket Motor Metal Cases, April 1970
SP-8041	Captive-Fired Testing of Solid Rocket Motors, March 1971
SP-8048	Liquid Rocket Engine Turbopump Bearings, March 1971
SP-8051	Solid Rocket Motor Igniters, March 1971

NASA-Langley, 1972 —— 30